AWARD NUMBER: W81XWH-21-1-0717

TITLE: Exploring Protein Quality Control Dysfunction in Dystonia

PRINCIPAL INVESTIGATOR: Christian Schlieker

CONTRACTING ORGANIZATION: Yale University, New Haven, CT

REPORT DATE: September 2022

TYPE OF REPORT: Annual

PREPARED FOR: U.S. Army Medical Research and Development Command
Fort Detrick, Maryland 21702-5012

REPORT DOCUMENTATION PAGE

Form Approved
OMB No. 0704-0188

1. REPORT DATE	2. REPORT TYPE	3. DATES COVERED
September 2022	Annual	15Aug2021-14Aug2022

4. TITLE AND SUBTITLE

Exploring Protein Quality Control Dysfunction in Dystonia

5a. CONTRACT NUMBER W81XWH-21-1-0717

5b. GRANT NUMBER PR200788

5c. PROGRAM ELEMENT NUMBER

6. AUTHOR(S)
Christian Schlieker, PI

E-Mail: christian.schlieker@yale.edu

5d. PROJECT NUMBER

5e. TASK NUMBER

5f. WORK UNIT NUMBER

7. PERFORMING ORGANIZATION NAME(S) AND ADDRESS(ES)

Yale University
105 Wall St
New Haven CT 06511-8917

8. PERFORMING ORGANIZATION REPORT NUMBER

9. SPONSORING / MONITORING AGENCY NAME(S) AND ADDRESS(ES)

U.S. Army Medical Research and Development Command
Fort Detrick, Maryland 21702-5012

10. SPONSOR/MONITOR'S ACRONYM(S)

11. SPONSOR/MONITOR'S REPORT NUMBER(S)

12. DISTRIBUTION / AVAILABILITY STATEMENT

Approved for Public Release; Distribution Unlimited

13. SUPPLEMENTARY NOTES
N/A

14. ABSTRACT
During the first year of this award, we made excellent progress towards defining cellular and molecular defects implicated in the congenital disorder DYT1 dystonia, the most severe form of dystonia that is characterized by spasms, twisted postures and involuntary muscle contractions. Starting from a tissue culture-based model, we identified the molecular signature of nuclear envelope abnormalities that are characteristic for many animal-based disease models of DYT1 dystonia. In doing so we defined robust biomarkers that are of immediate diagnostic utility for several forms of dystonia affecting veterans. In addition, we functionally investigated these molecules leading to the discovery of novel enzymatic activities that govern nuclear pore complex assembly which is perturbed in the disease state. Lastly, we developed novel methodology to show that nuclear envelope defects in dystonia profoundly perturb the cellular protein quality control system, critically informing the development of novel therapeutic avenues.

15. SUBJECT TERMS
Dystonia, movement disorders, DYT1 Dystonia, protein quality control

16. SECURITY CLASSIFICATION OF:			17. LIMITATION OF ABSTRACT	18. NUMBER OF PAGES	19a. NAME OF RESPONSIBLE PERSON USAMRDC
a. REPORT	b. ABSTRACT	c. THIS PAGE			19b. TELEPHONE NUMBER *(include area code)*
Unclassified	Unclassified	Unclassified	Unclassified	88	

Standard Form 298 (Rev. 8-98)
Prescribed by ANSI Std. Z39.18

TABLE OF CONTENTS

INTRODUCTION:

Dystonia is an incurable neurological disorder that is characterized by involuntary muscle contractions, severe spasms, and twisted postures. The most severe form of the disease is DYT1 dystonia, caused by mutation in the Torsin ATPase. We and other have previously demonstrated that nuclear envelope herniations (blebs) and defective nuclear pore assembly are the major phenotypic consequences of Torsin mutations, however it has been unclear if and how blebs contribute to disease onset. This proposal is designed to probe the hypothesis that blebs play a major role in disease etiology, starting from an identification of the molecular constituents of the blebs to define biomarkers, to functionally investigating their role in cells. Furthermore, we aim to test the hypothesis that blebs interfere with cellular protein homeostasis. In the future (second half of the award period), we plan to transition to concretely testing if pharmacological agents can rectify the defects identified in the first award period (ongoing/year 1 and 2), with the goal to put forward lead components for further pharmacological development towards treating dystonia, including both congenital and spontaneous/trauma-induced forms.

1. KEYWORDS:

Dystonia, movement disorders, DYT1 Dystonia, protein quality control

2. ACCOMPLISHMENTS:

What were the major goals of the project?

Specific Aim 1/Major Task 1 SOW: Define NPC assembly defects in relation to dystonia

Subtask 1: perform APEX/Mass spectrometry experiments in HeLa cells, bioinformatic analysis, cloning and validation of cellular factors in enriched in blebs in HeLa system – completed 100% - see appended manuscripts. This corresponds to the 1st SOW milestone (100% completed).

Subtask 2: functional characterization of the factors identified above-note originally planned for years 2 and 3 but already ~50% completed in year1.

Subtask 3: planned for year 3 and 4, 0% completed

Subtask 4: cloning, expression of above factors ~30% completed in year1.

Subtask 5: planned for year 3 and 4, 0% completed

Subtask 6: maintenance tasks-ongoing/25% completed.

Specific Aim 2/Major Task 2 SOW: Identification of the protein quality control defects that arise during congenital dystonia to enable pharmacological correction of cellular aberrations

Subtask 1: determine consequence of bleb sequestration - 30% completed

Subtask 2,3, still planned for later years as stated in SOW/0% completed

Subtask 4: note originally planned for later years but work in primary neurons started (<20% completed, see appended Nature Cell Biology manuscript)

Subtask 5: maintenance tasks: ongoing/25% completed

What was accomplished under these goals?

The following synopsis is brief as the appended manuscript (Prophet et al., accepted in Nature Cell Biology) and publication (Prophet et al. IJMS) provide an in-depth account of our completed work.

In the first year of this award, we made steep progress and have met and exceeded the milestones defined in the SOW. In brief, we successfully performed the mass spectrometry/proximity ligation-mediated identification of cellular factors residing in nuclear envelope blebs (Major Task 1-subtask 1). We have cloned the highest-ranking candidates, confirmed their localization, and generated an arsenal of plasmids and reagents to investigate their function in a cellular context. Based on these efforts and in vitro reconstitution after expression/purification of the players originally identified (HSPA1, DNAJB6, MLF2, NUP98) we found that blebs represent highly unusual, phase separated compartments arising from the aberrant accumulation of hydrophobic nucleoporins (NUPs) (e.g. NUP98)(Prophet et al, NCB). Importantly, we have also already validated these findings in primary neurons and neuronal cell lines, although this was originally planned for the 2nd/3d year of the award)(Prophet et al, NCB).

We have recently pushed this further by partially completing subtask 2, originally planned for years 2 and 3). We showed that HSPA1, DNAJB6, and MLF2 form a chaperone complex that prevents FG-NUP aggregation/amyloid formation both in cells and in our *in vitro* system (Prophet et al, NCB). Thus, we identified novel players that govern nuclear pore assembly, a poorly understood process still.

A second, major finding developed through Major task 2/subtask 1was that blebs sequester HSP70s and related co-chaperones with unparalleled efficacy when compared to "classical" inclusions linked to neurodegenerative diseases, e.g. PolyQ, causing cellular proteotoxicity. Critically, ubiquitylated proteins destined for degradation are also efficiently sequestered in the bleb phase, preventing their scheduled degradation (Prophet et al, NCB; Prophet et al., IJMS). Here we developed novel technology by engineering a model substrate (ORF10) derived from a viral protein that is now the first model substrate in the field to directly characterize proteotoxicity of nuclear envelope blebs that are observed in diverse experimental settings and disease states.

Thus, the major take home message is that previously understudied NE blebs exhibit an unusual type of severe proteotoxicity, revealing a critical contributor to disease onset.

What opportunities for training and professional development has the project provided?

Nothing to report.

How were the results disseminated to communities of interest?

Research highlights under this award were disseminated via twitter:
https://twitter.com/Schliekerlab/status/1517174987412676611
https://twitter.com/Schliekerlab/status/1453720900713336838

tweets also feed automatically into our homepage: https://medicine.yale.edu/lab/schlieker/

What do you plan to do during the next reporting period to accomplish the goals?

We do not anticipate major changes relative to the proposed activity/SOW. We will continue to validate and functionally investigate the remaining bleb constituents that were not part of the NCB publication and already have some promising leads here. We will continue to develop these and previously characterized ones into biomarkers, the rationale being that diagnostic markers for the most severe form of dystonia developed by us will be applicable also for spontaneous or trauma-induced forms of the disease.
Furthermore, we will determine the consequences of bleb sequestration on the interactomes of bleb-localizes chaperones, as stated in the SOW. Since we proceeded beyond the milestones in some areas (see above) and obtained highly encouraging data supporting the concept of perturbed proteostasis as driver for the disease, we will likely begin with major task2/subtask3 sooner than originally planned, already in the next year. In doing so we will exploit our momentum to explore the utility of pharmacological agents to rectify defects in proteostasis.

4. IMPACT:*:*

What was the impact on the development of the principal discipline(s) of the project?

Our data reported in the appended Nature Cell Biology manuscript represent a major breakthrough for our understanding of dystonia. Indeed, we consider the near-complete sequestration of essential chaperones in blebs as a more critical cellular perturbation than the relatively mild nuclear transport defects that are observed in a subset of disease models of DYT1 dystonia. This is a major shift in our understanding of this disease, which will profoundly influence the thinking in the field. Moreover, our findings reinforce our original motivation to focus on the protein quality control defects in the context of pharmacological correction down the road.

We also pioneered new biomarkers (MLF2, other Hsp40/70chaperones) and technology (ORF10 as model substrate) allowing for the first time a *functional* characterization of NE blebs (prior observations were purely morphological), which also arise outside of dystonia in various pathological states and are poorly understood due to the absence of suitable readouts. Thus, our tools will likely be useful outside of the specific context of dystonia.

What was the impact on other disciplines?

Apart from the aforementioned disease relevance, our identification and characterization of novel enzymatic activities that can stabilize cellular condensates has broad implications for cell biology and engineering. For example, it was previously not possible to maintain nucleoporin-based condensates in a functional state over longer periods of time *in vitro*. Our studies defined chaperones that can maintain condensates in a functional state over long periods of time, facilitating future research based on those in vitro systems.

What was the impact on technology transfer?

Nothing to report.

What was the impact on society beyond science and technology?

Nothing to Report.

5. CHANGES/PROBLEMS:

We do not plan any major changes relative to the proposed activity for the next award year.

Actual or anticipated problems or delays and actions or plans to resolve them

Nothing to report.

Changes that had a significant impact on expenditures

Nothing to report.

Significant changes in use or care of human subjects, vertebrate animals, biohazards, and/or select agents

Nothing to report in any of those categories.

6. PRODUCTS:

- **Publications, conference papers, and presentations**

Journal publications.

Prophet S, Rampello AJ, Niescier RF, Gentile JE, Mallik S, Koleske AJ, Schlieker C. (2022). Atypical nuclear envelope condensates linked to neurological disorders reveal nucleoporin-directed chaperone activities. Nature Cell Biology*, accepted/in press.*

Prophet, S.M., Naughton, B.S., and Schlieker, C. p97/UBXD1 generate ubiquitinated proteins that are sequestered into nuclear envelope herniations in Torsin-deficient cells. Int. J. Mol. Sci. 2022, 23(9):4627.

Books or other non-periodical, one-time publications.

Nothing to report.

Other publications, conference papers and presentations

Invited presentations at international meetings:

- "Genome Organization & Nuclear Function " CSHL meeting, Cold Spring Harbor Laboratory, NY (May 3-7, 2022)
- "Life on the Edge-The Nuclear Envelope and Nucleocytoplasmic Transport", German society for Cell Biology/DGZ, Potsdam, Germany (July 20-24, 2022)

Invited presentations at institutions:

- Max Planck Institute for Multidisciplinary Sciences, Goettingen, Germany (8/4/22)

- **Website(s) or other Internet site(s)**

Nothing to report.

- **Technologies or techniques**

As stated in the impact section we defined biomarkers and developed the model substrate ORF10 as a tool to better characterize cellular dysfunction in relation to nuclear envelope abnormalities. We freely share these plasmid-based tools with the scientific community upon request.

- **Inventions, patent applications, and/or licenses**

Nothing to report.

- **Other Products**

Plasmids

Construct	Vector
UBXD1-FLAG	pcDNA3.1+
FLAG-UBXD1ΔVIM	pcDNA3.1+
AIFM1-FLAG	pcDNA3.1+
KSHV ORF10-FLAG	pcDNA3.1+
KSHV ORF10-HA	pcDNA3.1+
Δ133 ORF10-HA	pcDNA3.1+
Δ133 ORF10-APEX-FLAG	pcDNA3.1+
polyQ-25-GFP	pcDNA3.1+
polyQ-72-GFP	pcDNA3.1+
polyQ-97-GFP	pcDNA3.1+
MLF2-APEX2-HA	pRetroX-Tight-Pur
NLS-APEX2-FLAG	pRetroX-Tight-Pur
MLF2-APEX2-HA	pcDNA3.1+
MLF2-LPXTG-His-FLAG	pcDNA3.1+
MLF2-LPXTG-His-FLAG	pFastBac1
MLF2 R/K-LPXTG-His-FLAG	pcDNA3.1+
MLF2 R/K-LPXTG-His-FLAG	pFastBac1
MLF2 R/K-M/A-LPXTG-His-FLAG	pcDNA3.1+
MLF2 R/K-M/A-LPXTG-His-FLAG	pFastBac1
Murine MLF2-FLAG	pcDNA3.1+
HA-DNAJB6b	pcDNA3.1+
HA-DNAJB6b-H31Q	pcDNA3.1+
mCherry-DNAJB6b-LPEXTG-His-FLAG	pET11a
DNAJB6b-LPXTG-His-FLAG	pET11a
HA-DNAJB6b-ΔG/F	pcDNA3.1+
HA-DNAJB6b-ΔG/F-S/T	pcDNA3.1+
HA-DNAJB6b F93L	pcDNA3.1+
HA-DNAJB6b ΔC10	pcDNA3.1+
Murine FLAG-DNAJB6b	pcDNA3.1+
HA-HSPA1A	pcDNA3.1+
His-HSPA1A	pET11a
$Nup98^{1-500}$-His	pET11a
OGT	pGEX-6P1

FLAG-DNAJB1	pcDNA3.1+
HA-DNAJB2	pcDNA3.1+
HA-DNAJB2 C321S	pcDNA3.1+
DNAJB12-HA	pcDNA3.1+
DNAJB12-HA H138Q	pcDNA3.1+
HSPA8-FLAG	pcDNA3.1+
FLAG-HSPH1	pcDNA3.1+
FLAG-HSPH2	pcDNA3.1+
EMC1-FLAG	pcDNA3.1+
EMC7-FLAG	pcDNA3.1+
HA-PPIA	pcDNA3.1+
FABP5-HA	pcDNA3.1+
ANXA2-HA	pcDNA3.1+
H2AC6-HA	pcDNA3.1+
BAG3-HA	pcDNA3.1+

Cell lines

Genetic background	**Parental cell line**
MLF2 KO	HeLa
TorsinKO/MLF2 KO	HeLa
+Dox MLF2-APEX-HA	HeLa
TorsinKO +Dox MLF2-APEX-HA	HeLa

7. PARTICIPANTS & OTHER COLLABORATING ORGANIZATIONS

What individuals have worked on the project?

Name:	Christian Schlieker
Project Role:	PD/PI
Research Identifier (e.g. ORCID ID):	0000-0002-1237-4267
Nearest person month worked:	7 person months
Contribution to Project:	Project planning, supervision, writing of manuscripts (all aims)
Funding Support:	N/A

Name:	Sunanda Mallik
Project Role:	Postdoctoral Associate
Research Identifier (e.g. ORCID ID):	0000-0002-3825-3527
Nearest person month worked:	9 person months
Contribution to Project:	(SOW major task 1, subtask 2, 4,6; major task 2 subtask 1, 4, 5)
Funding Support:	N/A

Name:	Sarah Margaret Prophet
Project Role:	Graduate Student
Research Identifier (e.g. ORCID ID):	0000-0002-4321-8144
Nearest person month worked:	8 person months
Contribution to Project:	(SOW major task 1 subtask 1-4 and major task 2 subtask 1)
Funding Support:	N/A

Name:	Pei-Ling Tsai
Project Role:	Associate Research Scientist
Research Identifier (e.g. ORCID ID):	0000-0002-5181-9441
Nearest person month worked:	12 person months
Contribution to Project:	training of Dr. Mallik and major task 1 subtask 6, major task 2 subtask 5)
Funding Support:	N/A

Has there been a change in the active other support of the PD/PI(s) or senior/key personnel since the last reporting period?

Nothing to report.

What other organizations were involved as partners?

Nothing to report

8. SPECIAL REPORTING REQUIREMENTS

Nothing to report.

9. APPENDICES:

One publication and one accepted manuscript are appended in the following order:

Prophet, S.M., Naughton, B.S., and Schlieker, C. p97/UBXD1 generate ubiquitinated proteins that are sequestered into nuclear envelope herniations in Torsin-deficient cells. Int. J. Mol. Sci. 2022, 23(9):4627.

Prophet S, Rampello AJ, Niescier RF, Gentile JE, Mallik S, Koleske AJ, Schlieker C. (2022). Atypical nuclear envelope condensates linked to neurological disorders reveal nucleoporin-directed chaperone activities. Nature Cell Biology*, accepted/in press.*

International Journal of
Molecular Sciences

MDPI

Article

p97/UBXD1 Generate Ubiquitylated Proteins That Are Sequestered into Nuclear Envelope Herniations in Torsin-Deficient Cells

Sarah M. Prophet [1], Brigitte S. Naughton [1] and Christian Schlieker [1,2,*]

[1] Department of Molecular Biophysics & Biochemistry, Yale University, New Haven, CT 06520, USA; sarah.prophet@yale.edu (S.M.P.); brigitte.naughton@yale.edu (B.S.N.)
[2] Department of Cell Biology, Yale School of Medicine, New Haven, CT 06520, USA
* Correspondence: christian.schlieker@yale.edu; Tel.: +1-(203)-432-5035

Abstract: DYT1 dystonia is a debilitating neurological movement disorder that arises upon Torsin ATPase deficiency. Nuclear envelope (NE) blebs that contain FG-nucleoporins (FG-Nups) and K48-linked ubiquitin are the hallmark phenotype of Torsin manipulation across disease models of DYT1 dystonia. While the aberrant deposition of FG-Nups is caused by defective nuclear pore complex assembly, the source of K48-ubiquitylated proteins inside NE blebs is not known. Here, we demonstrate that the characteristic K48-ubiquitin accumulation inside blebs requires p97 activity. This activity is highly dependent on the p97 adaptor UBXD1. We show that p97 does not significantly depend on the Ufd1/Npl4 heterodimer to generate the K48-ubiquitylated proteins inside blebs, nor does inhibiting translation affect the ubiquitin sequestration in blebs. However, stimulating global ubiquitylation by heat shock greatly increases the amount of K48-ubiquitin sequestered inside blebs. These results suggest that blebs have an extraordinarily high capacity for sequestering ubiquitylated protein generated in a p97-dependent manner. The p97/UBXD1 axis is thus a major factor contributing to cellular DYT1 dystonia pathology and its modulation represents an unexplored potential for therapeutic development.

Keywords: dystonia; DYT1; TorsinA; p97; UBXD1; YOD1; ubiquitin; ERAD; Ufd1/Npl4

Citation: Prophet, S.M.; Naughton, B.S.; Schlieker, C. p97/UBXD1 Generate Ubiquitylated Proteins That Are Sequestered into Nuclear Envelope Herniations in Torsin-Deficient Cells. *Int. J. Mol. Sci.* **2022**, *23*, 4627. https://doi.org/10.3390/ijms23094627

Academic Editor: Patrick R. Onck

Received: 26 February 2022
Accepted: 20 April 2022
Published: 21 April 2022

1. Introduction

Torsins are essential [1] AAA+ ATPases that localize within the endoplasmic reticulum (ER)/ nuclear envelope (NE) membrane system [2,3], where they carry out poorly understood functions. Torsins are unusual AAA+ ATPases as they strictly require interactions with one of two transmembrane activators to hydrolyze ATP [4–6]. The first of these activating proteins is lamina-associated polypeptide 1 (LAP1) and the second is luminal domain-like LAP1 (LULL1) [7]. Mutations within the C-terminal domain of TorsinA [8], one of the four Torsins encoded by the human genome [9], cause the neurological movement disorder DYT1 dystonia [2,10,11]. These DYT1 dystonia-causing mutations disrupt interactions between TorsinA and LAP1 or LULL1 [4,8,12], demonstrating the importance of the Torsin/activator complex during neurological development.

While the precise biological role of Torsins remains unknown, herniations of the NE are observed across all Torsin loss-of-function models ranging from *Caenorhabditis elegans* [13] to mouse neurons [1] (see schematic illustration, Figure 1A). These herniations, referred to as blebs, represent aberrant nuclear pore complex (NPC) biogenesis intermediates that are arrested prior to inner and outer nuclear membrane fusion [14–16]. Although blebs do not harbor mature NPCs, specific nucleoporins (Nups) associated with building multiple subcomplexes of the NPC are found inside these herniations [14,15,17,18]. In addition to Nups, the protein of unknown function myeloid leukemia factor 2 (MLF2) localizes to blebs [15,18] by a yet-to-be identified mechanism.

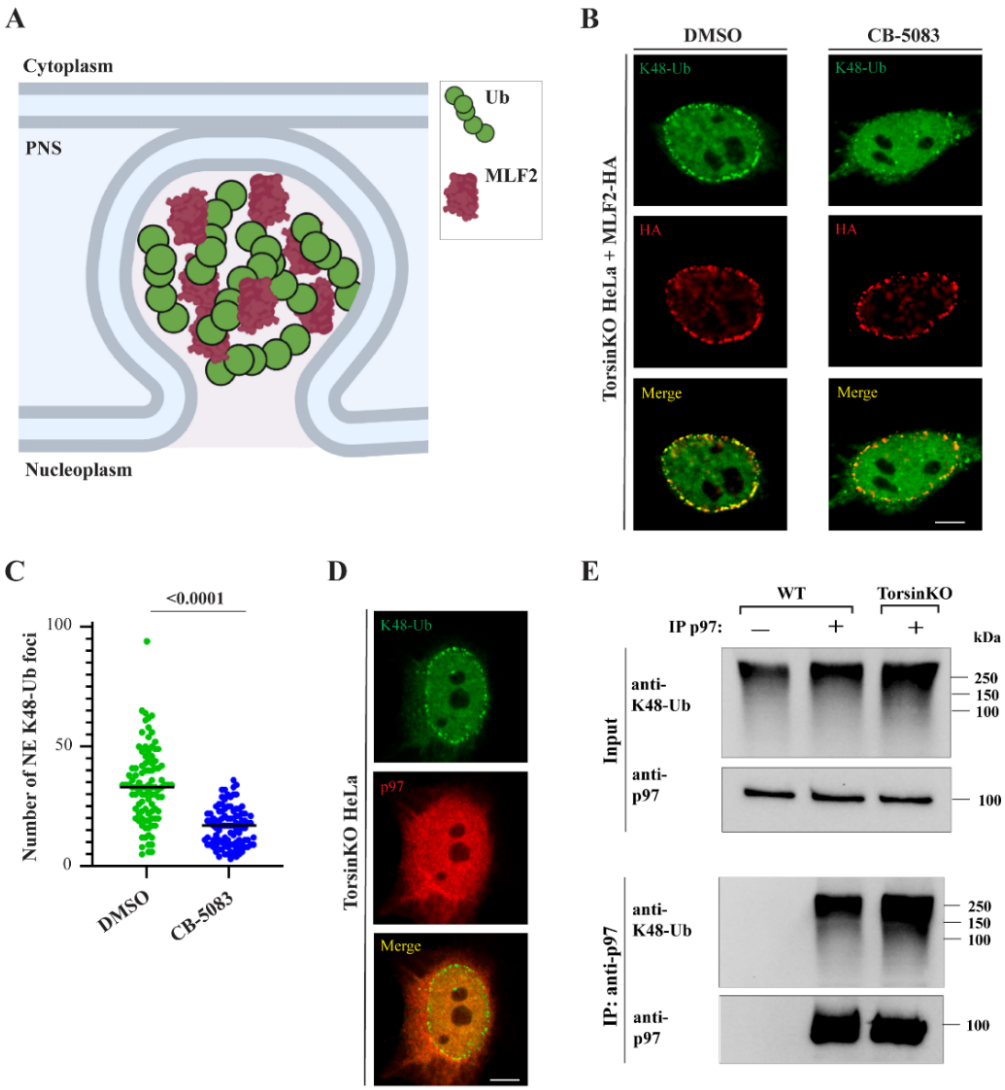

Figure 1. K48-Ub accumulation inside NE blebs of Torsin-deficient cells requires p97 activity. (**A**) Schematic diagram of a NE bleb. PNS, perinuclear space. Ub, ubiquitin. (**B**) Representative immunofluorescence (IF) images of TorsinKO HeLa cells overexpressing MLF2-HA under vehicle (DMSO) or p97 inhibition (CB-5083) conditions. Cells were treated with 5 µM CB-5083 for four hours before processing for IF, stained with K48-Ub and HA antibodies, and imaged by confocal microscopy. Scale bar, 5 µm. (**C**) The number of NE-associated K48-Ub foci in TorsinKO cells upon DMSO or CB-5083 treatment was quantified for 100 cells/condition. Statistical analysis was performed using a Mann–Whitney U test. (**D**) Representative IF image of p97 localization in TorsinKO cells. Cells were processed for IF and stained with p97 and K48-Ub antibodies. Scale bar, 5 µm. (**E**) An immunoprecipitation (IP) of endogenous p97 under native conditions from WT and TorsinKO cells. The IP was analyzed by immunoblot with antibodies against p97 and K48-Ub.

To inhibit p97, we treated TorsinKO cells with the p97 inhibitor CB-5083 [24,25]. As MLF2-HA localizes to blebs in a ubiquitin-independent manner [15], this construct was expressed to distinguish TorsinKO cells with blebs from those without. After four hours of p97 inhibition, the K48-Ub signal inside blebs was significantly depleted (Figure 1B,C) despite MLF2-HA remaining efficiently sequestered inside blebs (Figure 1B). To determine whether p97 is functioning directly within the bleb, we assessed its localization. Consistent with our previous observations [15,17], we found it was not stably enriched within blebs (Figure 1D) although we cannot exclude the formal possibility that p97 is present at levels below the detection limit of immunofluorescence (IF). While it is possible that p97 acts directly within the bleb lumen to generate the K48-Ub proteins, p97 activity

Beyond Ub and MLF2 [15,18], blebs are also highly enriched for components that suggest a protein quality control (PQC) defect exists in Torsin-deficient cells. First, blebs harbor K48-linked polyubiquitin (K48-Ub) chains [17,19] conjugated to proteins of unknown identity or origin. As K48-Ub is canonically associated with proteasome-mediated degradation [20], its enrichment inside blebs indicates that Torsin-deficient cells may have a compromised PQC mechanism. Secondly, blebs sequester a specific chaperone network composed of abundant HSP70 and HSP40 members [18]. The presence of HSP70s and HSP40s inside blebs along with K48-Ub suggests that a stress-related chaperone activ-

ity such as facilitating protein degradation [21] may also become dysregulated in Torsin loss-of-function models.

As neither the identity nor the origin of the K48-Ub protein inside blebs is known, the PQC pathway that becomes dysregulated upon Torsin deficiency remains poorly understood. Consequently, whether and how this PQC pathway contributes to DYT1 dystonia remains unknown. K48-Ub accumulation in blebs could indicate that proteins become ubiquitylated in response to Torsin dysfunction or that proteins fail to be degraded when Torsin function is compromised. While DYT1 dystonia is the most common congenital form of dystonia [10], no curative treatment has been reported and therapeutic options are only partially effective. Thus, a more accurate characterization of the PQC defect in Torsin-deficient cells may lead to the identification of yet unexplored pathways and define molecular players that might represent new targets for therapeutic intervention.

In this report, we employ a Torsin-deficient cell line as a model system to scrutinize the poorly understood process of K48-Ub accumulation widely observed in disease models of DYT1 dystonia. We demonstrate that p97 activity is required to generate K48-Ub accumulation inside blebs. We further show that K48-Ub conjugates inside blebs are unlikely to result from de novo synthesis or canonical ER-associated protein degradation (ERAD) as depleting components of the Hrd1–Ufd1/Npl4/p97 axis has little effect on K48-Ub deposition in blebs. A candidate approach aimed at the identification of alternative p97 cofactors revealed that the incompletely understood p97 adaptor UBXD1 and the deubiquitylating enzyme YOD1 are required for Ub accumulation. Stimulating an increase in global ubiquitylation by heat shock results in a stark increase in K48-Ub conjugates sequestered into blebs. This supports the idea that NE blebs have a remarkable capacity for sequestering misfolded, ubiquitylated species and preventing their degradation.

Taken together, our observations reveal that the p97/UBXD1 axis is a central player for the cellular pathology caused by defects in Torsin function. As p97 is a druggable target for a diverse set of diseases [22], its potential involvement in DYT1 dystonia reveals unexplored therapeutic opportunities to improve the lives of patients suffering from this debilitating disease.

2. Results

2.1. p97 Activity Is Required for K48-Ub Accumulation inside NE Blebs

The cellular processes that produce the K48-Ub conjugates found inside blebs (Figure 1A) have not been identified. One essential K48-Ub-directed enzyme in mammalian cells is the p97 ATPase (also called VCP in mammals and Cdc48 in yeast). While p97 activity functions in a number of diverse processes, its best characterized role is to mobilize ubiquitylated clients from membranes, interaction partners, or aggregates [23]. After extraction, these ubiquitylated proteins are often degraded by the proteasome. Because p97 is a major K48-Ub-directed enzyme, we investigated whether its activity was relevant for generating the K48-Ub conjugates inside blebs.

To inhibit p97, we treated TorsinKO cells with the p97 inhibitor CB-5083 [24,25]. As MLF2-HA localizes to blebs in a ubiquitin-independent manner [15], this construct was expressed to distinguish TorsinKO cells with blebs from those without. After four hours of p97 inhibition, the K48-Ub signal inside blebs was significantly depleted (Figure 1B,C) despite MLF2-HA remaining efficiently sequestered inside blebs (Figure 1B). To determine whether p97 is functioning directly within the bleb, we assessed its localization. Consistent with our previous observations [15,17], we found it was not stably enriched within blebs (Figure 1D) although we cannot exclude the formal possibility that p97 is present at levels below the detection limit of immunofluorescence (IF). While it is possible that p97 acts directly within the bleb lumen to generate the K48-Ub proteins, p97 activity at locations distinct from the bleb may also be required for K48-Ub accumulation in Torsin-deficient cells.

Int. J. Mol. Sci. **2022**, *23*, 4627 4 of 17

at locations distinct from the bleb may also be required for K48-Ub accumulation in Torsin-deficient cells.

2.2. p97 Associates with More K48-Ub in Torsin-Deficient Cells

Upon finding that p97 activity is important for accumulating K48-Ub conjugates inside blebs, we asked whether p97 is generally associated with more ubiquitin in TorsinKO cells compared to the wild type (WT). To address this, we prepared soluble detergent extracts and performed an immunoprecipitation (IP) under native conditions with an anti-p97 antibody. Upon immunoblotting the IP with an anti-K48-Ub antibody, we observe that endogenous p97 is associated with significantly more K48-Ub in TorsinKO cells compared to WT (Figure 1E). This suggests that cells with deficient Torsin ATPase activity have more ubiquitylated p97 clients than cells with functional Torsins.

Taken together, we demonstrate that p97 associates with K48-Ub to a greater extent in TorsinKO cells compared to WT and that p97 activity is required for these ubiquitylated proteins to localize within blebs.

2.3. p97 Does Not Require the Ufd1/Npl4 Heterodimer for the Majority of the K48-Ub Protein Deposition to Blebs

The increased association of p97 with K48-Ub in TorsinKO cells suggests that a process linked to p97 function becomes perturbed during Torsin deficiency. One major p97-dependent process is ERAD [26]. During ERAD, p97 interacts with the Ufd1/Npl4 heterodimer to extract ubiquitylated glycoproteins from the ER membrane [27]. To determine whether ERAD-directed adaptor proteins contribute to K48-Ub accumulation within blebs, we depleted the heterodimer by treating cells with Ufd1/Npl4-targeting siRNA for 48 h (Figures 2A,C and 3C). Knocking down Ufd1/Npl4 caused a minor decrease in the number of K48-Ub foci around the nuclear rim of TorsinKO cells (Figure 2A,B). However, this effect was far less pronounced compared to the K48-Ub depletion observed upon inhibiting p97 activity (Figure 1B,C). This suggests that a Ufd1/Npl4-independent p97 activity generates the majority of the K48-Ub protein inside blebs.

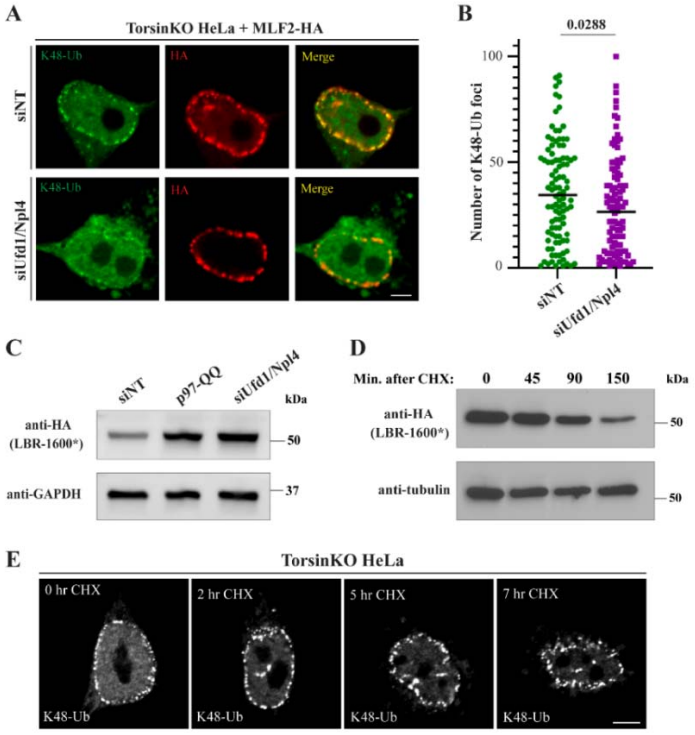

Figure 2. The K48-Ub proteins sequestered inside blebs do not result from canonical ERAD. (**A**) Representative IF images of TorsinKO cells overexpressing MLF2-HA under nontargeting (siNT) or Ufd1/Npl4 knockdown conditions. Cells were treated with 25 nM RNAi against both Ufd1 and Npl4 for 48 h before processing for IF. Cells were stained with antibodies against K48-Ub and HA. Scale bar, 5 µm. (**B**) The number of NE-associated K48-Ub foci in TorsinKO cells under nontargeting or

Ufd1/Npl4 knockdown conditions was quantified for 100 TorsinKO cells/condition. Statistical analysis was performed using a Mann–Whitney U test. (**C**) Representative immunoblot of the ERAD substrate LBR-1600* in TorsinKO cells under siNT, siUfd1/Npl4, or p97-QQ overexpression conditions. p97-QQ is a dominant-negative mutation that inhibits endogenous p97 activity. The Ufd1/Npl4 knockdown was conducted for 48 h while LBR-1600* and p97-QQ were expressed for 24 h prior to immunoblotting. (**D**) TorsinKO cells expressing the short-lived HA-LBR-1600* were treated with CHX for the indicated timepoints and processed for immunoblot. Cells were allowed to express HA-LBR-1600* for 24 h before treatment with 100 μg/mL CHX. (**E**) Representative IF images of TorsinKO cells treated with CHX for the indicated timepoints. Cells were treated with 100 μg/mL of CHX prior to processing for IF and stained with an K48-Ub antibody. Scale bar, 5 μm.

To validate that knocking down Ufd1/Npl4 resulted in measurable functional defects, i.e., stabilizing substrates destined for degradation, we expressed the short-lived protein LBR-1600* [28] (Figure 2C). LBR-1600* is a mutant of the ER- and inner nuclear membrane-localized lamin B receptor that is degraded in a p97- and proteasome-dependent manner [28,29]. Upon knocking down Ufd1/Npl4, LBR-1600* was strongly stabilized to the same extent as co-overexpressing a dominant-negative p97 construct, p97-QQ (Figure 2C). We therefore conclude that depleting the Ufd1/Npl4 heterodimer substantially stabilizes ERAD substrates but does not deplete blebs of K48-Ub conjugates to a similar extent as inhibiting p97.

2.4. Many Canonical ERAD-Associated E3 Ligases Do Not Significantly Contribute to the K48-Ub Protein inside Blebs

Prior to cytosolic degradation, ERAD substrates must be ubiquitylated and (in some cases) translocated across the lipid bilayer of the ER [26]. Ubiquitylation occurs on the cytosolic face of the ER and can be achieved by several E3 ligases embedded within the ER membrane. These E3 ligases not only ubiquitylate ERAD substrates but can also serve as dislocon channels within the ER membrane [30–32]. ERAD substrates are primed with ubiquitin by these E3 ligases so that the p97 machinery can recognize and extract these clients [27,33]. Depending on the nature of the ERAD substrate [34–36], the dislocon that enables passage out of the ER is canonically formed by either of the two highly conserved complexes composed of Hrd1 [30,37] or Doa10 [32] (MARCH6 in mammalian cells). While lower eukaryotic ERAD relies mostly on these two complexes, metazoans have alternative E3 ligases and mechanisms such as gp78 [26,36].

To investigate the involvement of the canonical E3 ligases in K48-Ub bleb accumulation, we depleted Hrd1, MARCH6, or gp78 from TorsinKO cells for 48 h (Figure S2A,B). None of these conditions significantly affected K48-Ub accumulation inside blebs to the extent achieved by p97 inhibition (compare Figure S2 and Figure 1B). Taken together with the minimal to modest effect of Ufd1/Npl4 depletion described above (Figure 2A, B), these data suggest that p97 does not require canonical ERAD machinery to generate the K48-Ub proteins sequestered inside blebs. These results further suggest that if ERAD substrates contribute to the K48-Ub inside blebs, they are likely retrotranslocated and ubiquitylated by a noncanonical mechanism largely independent of Hrd1, MARCH6, and gp78.

2.5. Newly Synthesized, Misfolded Proteins Do Not Account for the Majority of the K48-Ub Protein inside Blebs

An estimated 30% of all newly synthesized proteins are defective and degraded by the proteosome [38]. Newly synthesized misfolded proteins thus represent a constant threat to cellular proteostasis [39]. For this reason, cells have evolved multiple mechanisms to prevent translational errors and degrade aberrant proteins [40]. As the process of translation produces a significant number of ubiquitylated polypeptides, we determined whether newly synthesized ubiquitylated proteins contribute to the K48-Ub signal inside blebs. To this end, we monitored K48-Ub accumulation in blebs when translation was inhibited via cycloheximide (CHX) treatment. To confirm the efficacy of inhibiting translation, we

of translation produces a significant number of ubiquitylated polypeptides, we determined whether newly synthesized ubiquitylated proteins contribute to the K48-Ub signal inside blebs. To this end, we monitored K48-Ub accumulation in blebs when translation was inhibited via cycloheximide (CHX) treatment. To confirm the efficacy of inhibiting translation, we performed a CHX chase in WT HeLa cells expressing the short-lived protein HA-LBR 1600* [28]. As expected, CHX treatment resulted in a steady decline of HA-LBR 1600* over time, consistent with a blockage of de novo synthesis and concomitant proteasomal turnover (Figure 2D). When translation was inhibited in TorsinKO cells by CHX treatment for up to seven hours, we observed no change in the accumulation of K48-Ub protein within the bleb (Figure 2E). As a four-hour treatment with the p97 inhibitor CB-5083 results in a near-complete depletion of K48-Ub inside blebs (Figure 1B,C), this suggests that newly synthesized misfolded proteins are unlikely to significantly contribute to the K48-Ub cargo sequestered into blebs.

2.6. The Relevant p97 Activity for Accumulating K48-Ub Inside Blebs Depends on the Cofactors YOD1 and UBXD1

p97 is functionalized by at least 40 different interaction partners in mammalian cells [41] that direct its ATPase activity to distinct processes including ERAD, membrane fusion, and lysosome clearance [41,42]. To better understand what cellular process(es) requires p97 activity to produce the K48-Ub conjugates inside blebs, we determined the effect of depleting specific p97-interacting proteins.

While p97 interacts with many cofactors/adaptors, at least three major p97 complexes exist. These are the Ufd1/Npl4 heterodimer, p47, and UBXD1 [41]. The Ufd1/Npl4 dimer is canonically associated with recruiting p97 to the ER membrane during ERAD [43] whereas p47 recruits p97 during homotypic membrane fusion [44]. UBXD1, however, has been reported to contribute to a number of processes including trafficking events [45,46], autophagy [47], and ERAD [48]. Beyond these three complexes, p97 recruits the deubiquitinase (DUB) YOD1 to participate in a number of processes including ERAD [50] and lysosome clearance [47].

To interrogate the diverse processes to which p97 contributes, we depleted p47 and UBXD1 by RNAi in TorsinKO cells (Figure 3A–C). To monitor bleb formation, these cells expressed MLF2-HA (Figure 3A). To perturb YOD1 activity, we expressed WT or a dominant-negative YOD1 construct YOD1-CS-FLAG [50] in TorsinKO cells co-expressing MLF2-HA (Figure 3A,B).

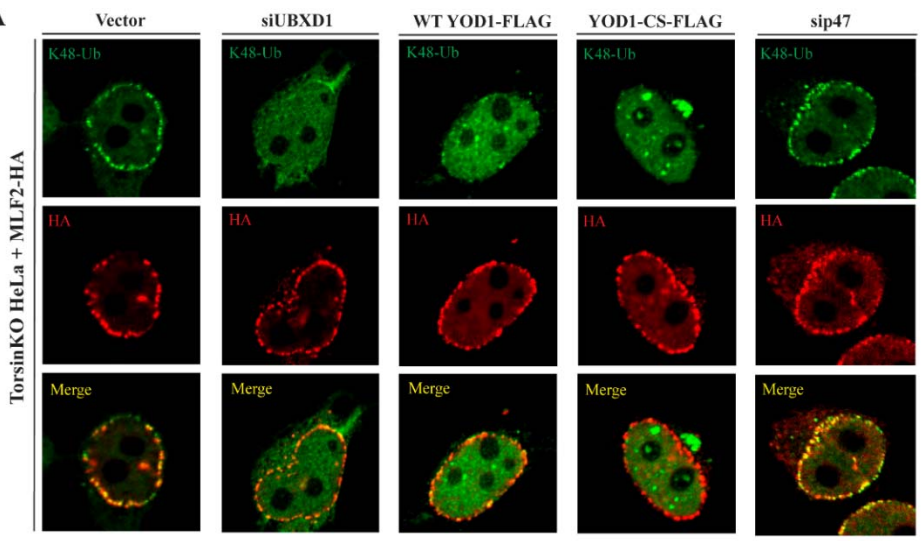

Figure 3. *Cont.*

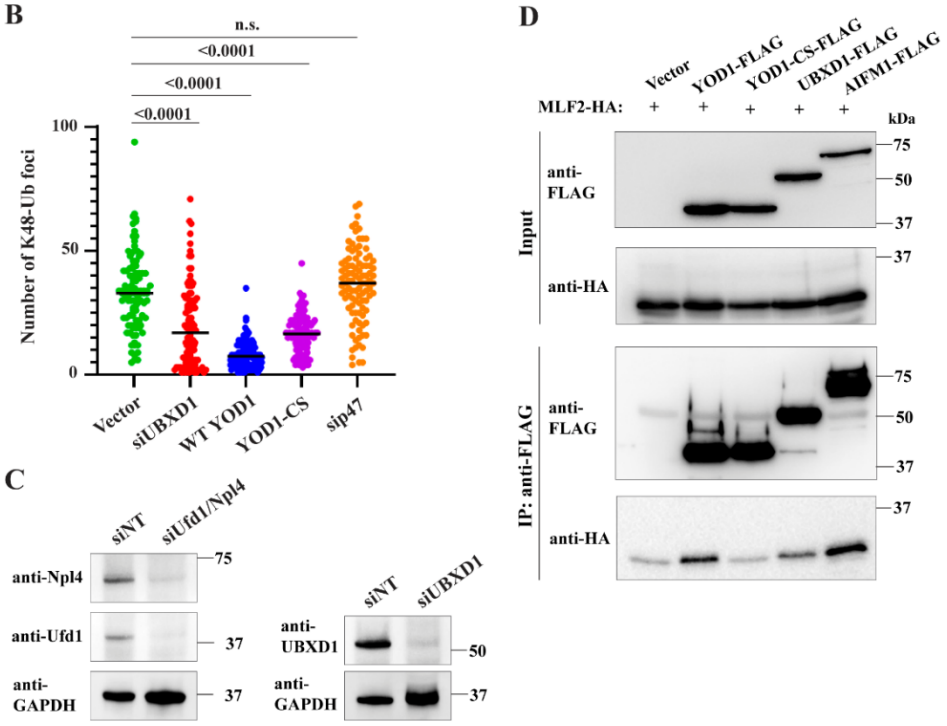

Figure 3. p97 depends on the cofactors YOD1 and UBXD1 to generate the K48-ubiquitinated proteins sequestered inside blebs. (**A**) Representative IF images of TorsinKO cells overexpressing MLF2-HA under conditions of normal or disrupted p97 activity. p97 activity was disrupted by knocking down UBXD1 or p47 or overexpressing the dominant-negative YOD1-CS-FLAG. UBXD1 and p47 were knocked down for 48 h and overexpressed constructs were overexpressed for 24 h prior to processing for IF. Cells were stained with antibodies against K48-Ub and HA. Note that WT YOD1-FLAG is an active deubiquitinase (DUB) that cleaves the K48-Ub chains off clients that are normally ubiquitylated and sequestered into blebs. Scale bar, 5 µm. (**B**) The number of K48-Ub foci was quantified for 100 TorsinKO cells/condition. Statistical analysis was performed using a Mann–Whitney U test. N.s., not significant. (**C**) An immunoblot confirming the effects of siRNA targeting Ufd1, Npl4 or UBXD1 in TorsinKO cells after 48 h of knockdown. (**D**) Anti-FLAG pulldowns (IP) from TorsinKO cells after 48 h of knockdown. (**D**) An IP of FLAG-tagged WT YOD1, YOD1-CS, UBXD1, or AIFM1 from TorsinKO cells expressing MLF2-HA. Cells were allowed to express the constructs for 24 h prior to harvesting. An IP of the FLAG tag for all samples was analyzed by immunoblot against the FLAG and HA tags. MLF2-HA specifically co-immunoprecipitates with WT YOD1, UBXD1, and AIFM1.

Upon depleting UBXD1 or perturbing YOD1 activity, the number of K48-Ub foci around the nuclear rim was significantly decreased (Figure 3A,B). This was not the case when p47 was depleted (Figure 3A,B). As WT YOD1 is an active DUB, expressing the WT construct also resulted in a significant decrease in the number of K48-Ub foci in TorsinKO cells (Figure 3A,B). This suggests that ubiquitylated proteins targeted by YOD1 localize to blebs as removing the ubiquitin modification by overexpressed WT YOD1 also depletes blebs of K48-Ub (Figure 3A,B). Taken together, these results suggest that the p97 interactors UBXD1 and YOD1, but not p47, participate in the process(es) that generate the K48-Ub proteinaceous blebs.

MLF2, a protein of unknown function, is highly enriched inside the lumen of blebs [15,18]. While UBXD1, YOD1, and some YOD1-CS are enriched inside blebs (Figure 3C), MLF2 may contribute to bleb formation by interacting with these p97 adaptors either directly or indirectly. To test this possibility, we conducted an IP with an anti-FLAG antibody from TorsinKO cells expressing FLAG-tagged WT YOD1, YOD1-CS, UBXD1, or AIFM1 (Figure 3D). AIFM1 is known MLF2-interacting protein [51,52] and therefore served as a positive co-IP control (Figure 3D). We found that MLF2-HA specifically co-immunoprecipitated with UBXD1 and WT but not dominant-negative YOD1 in TorsinKO cells (Figure 3D). While these interactions may be direct or indirect, MLF2 may function with specific

interactions may be direct or indirect, MLF2 may function with specific p97 complexes during the generation of ubiquitylated protein and rely on active YOD1 for recruitment to these sites.

2.7. Provoking an Increase in Global Ubiquitylation Causes More K48-Ub Conjugates to Become Sequestered inside Blebs

Whether blebs are enriched for specific K48-ubiquitylated proteins or sequester general ubiquitin cargo is not understood. While we have performed multiple mass spectrometry-based workflows in an attempt to identify the K48-Ub conjugates inside blebs [15,18], we have not observed the enrichment of a specific set of ubiquitylated proteins. This suggests that blebs may possess an extraordinarily high capacity for sequestering a wide variety of ubiquitylated species, and the enrichment of specific proteins may therefore be difficult to capture by mass spectrometry. Thus, to probe the capacity of blebs to sequester ubiquitylated protein, we subjected WT and TorsinKO cells to heat shock, a condition that is known to greatly increase the amount of ubiquitylated protein inside cells [53–55].

Upon subjecting TorsinKO cells to 42 °C for 16 h, the amount of K48-Ub inside blebs increased significantly (Figure 4A–D). This effect was observed by IF (Figure 4A,B) and by biochemical fractionation wherein cells were enriched for ER/NE fractions (Figure 4C,D). This enrichment involved isolating nuclei and membrane fractions by centrifugation through a sucrose gradient. ER/NE fractions were further enriched by centrifugation following DNase/heparin treatment. Successful fractionation was confirmed by immunoblot using antibodies against emerin (enriched in the ER/NE) and hnRNPA1 (enriched in the nucleoplasmic fraction) (Figure 4C). After validating successful fractionation, the ER/NE samples were subjected to immunoblot with an anti-K48-Ub antibody (Figure 4D). While WT HeLa cells had approximately the same amount of ER/NE-associated K48-Ub during unstressed (37 °C) and stressed (42 °C) conditions (Figure 4D), TorsinKO cells had significantly more ER/NE-associated K48-Ub upon heat shock (Figure 4D). Thus, when a global increase in ubiquitin is provoked, TorsinKO cells sequester more K48-Ub inside blebs.

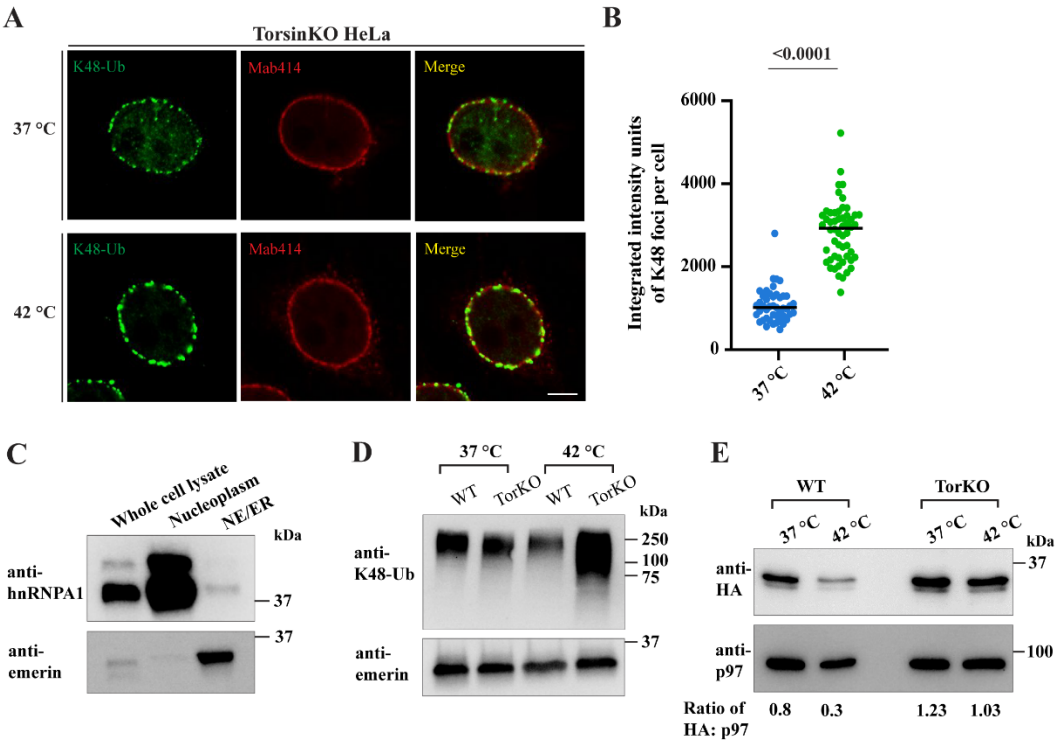

Figure 4. *Cont.*

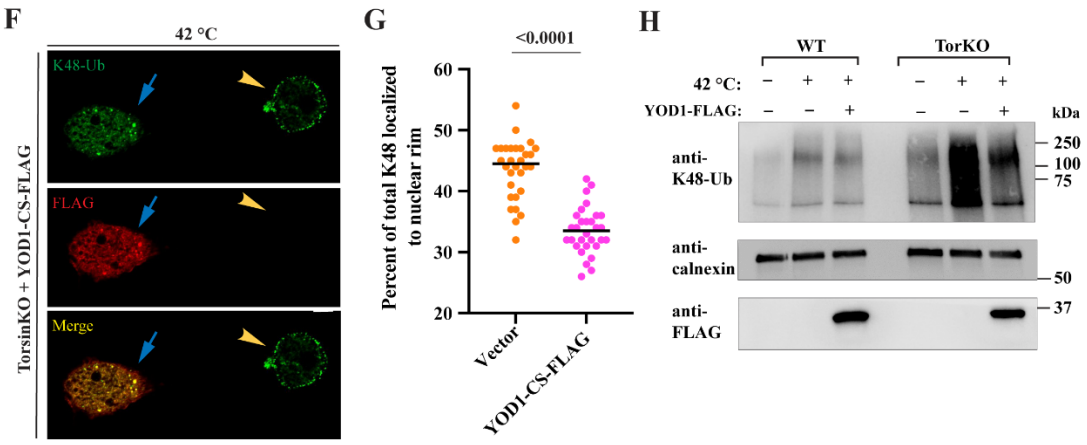

Figure 4. NE blebs in Torsin-deficient cells sequester ubiquitylated proteins that are produced by heat shock stress. (**A**) Representative IF images of NE-associated K48-Ub foci in TorsinKO cells upon heat shock. Cells were cultured at 37 °C or 42 °C for 16 h before processing for IF. Cells were stained with an antibody against K48-Ub and Mab414, which recognizes a subset of FG-nucleoporins. Scale bar, 5 µm. (**B**) Quantification of the average intensity of K48-Ub signal inside blebs from TorsinKO cells exposed to 37 °C or 42 °C for 16 h. This value was quantified for 50 TorsinKO cells/condition. Statistical analysis was performed using a Mann–Whitney U test. (**C**) An immunoblot demonstrating the subcellular fractionation of TorsinKO cells. Cells were enriched for NE/ER fractions (indicated by the emerin antibody) that were free from significant nucleoplasmic contamination (indicated by the anti-hnRNPA1 antibody). (**D**) NE/ER fractions from WT or TorsinKO HeLa cells under unstressed or heat shock stress conditions were analyzed by immunoblot with antibodies against K48-Ub and emerin. Cells were exposed to a 42 °C heat shock for 16 h before harvesting. (**E**) Unstressed or heat-shocked WT and TorsinKO cells overexpressing MLF2-HA for 24 h were fractionated into ER/NE enrichments. The fractions were analyzed by immunoblot using. Note that p97 controls for protein loading in this immunoblot. The ratio of HA to p97 density was calculated for each lane. (**F**) Representative IF images of TorsinKO cells expressing YOD1-CS-FLAG under heat shock stress as described in panel (**A**). Cells were transfected with YOD1-CS-FLAG eight hours prior to the beginning of heat shock. Blue arrow, transfected cell. Yellow arrowhead, untransfected cell. Scale bar, 5 µm. (**G**) Quantification of the percent of total K48-Ub signal that localize to the nuclear rim in TorsinKO cells upon 42 °C heat shock with or without YOD1-CS-FLAG overexpression. This value was obtained for 30 cells/condition. Statistical analysis was performed using a Mann–Whitney U test. (**H**) WT and TorsinKO cells expressing WT YOD1-FLAG for 24 h were subjected to heat shock stress and enriched for ER/NE fractions. These fractions were compared by immunoblot to unstressed or heat-shocked cells in the absence of overexpressed YOD1-FLAG.

Heat shock results in the ubiquitylation and degradation of many proteins that are otherwise relatively stable [55,56]. One possibility is that blebs stabilize proteins that are targeted for degradation, as we have demonstrated for the model substrate Δ133-ORF10 [18]. While MLF2 is not directly ubiquitylated inside blebs [15], we found that MLF2-HA undergoes degradation in WT cells exposed to heat shock (Figure 4E). Note that p97 is included as a loading control in this immunoblot (Figure 4E). In contrast to WT HeLa cells under stress, MLF2-HA is stabilized in TorsinKO cells under heat shock conditions with a steady state abundance that is relatively unchanged from unstressed to stressed conditions (Figure 4E).

To determine whether K48-Ub accumulation inside blebs upon heat shock also depends on YOD1 activity, we expressed the dominant-negative YOD1-CS-FLAG construct and exposed cells to heat shock (Figure 4F,G). In untransfected heat-shocked TorsinKO cells, an intense K48-Ub signal was detected within NE foci by IF (Figure 4F, yellow arrowhead). However, upon expression of YOD1-CS-FLAG, this NE accumulation was inhibited (Figure 4F, blue arrow). We quantified this effect by determining the percent of K48-Ub

foci that localize to the nuclear rim under heat shock with or without YOD1-CS-FLAG overexpression (Figure 4G). This analysis demonstrated that upon heat shock, TorsinKO cells overexpressing YOD1-CS developed significantly fewer NE-associated K48-Ub foci (Figure 4G).

As WT YOD1 overexpression also significantly reduced the amount of K48-Ub inside blebs (Figure 3A,B), we expressed WT YOD1-FLAG in WT and TorsinKO cells undergoing heat shock stress (Figure 4H). These cells were fractionated into ER/NE enrichments and analyzed by immunoblot with antibodies against K48-Ub, calnexin as a loading control, and FLAG (Figure 4H). As described above, untransfected TorsinKO cells accumulated a significant amount of ER/NE-associated K48-Ub upon heat shock (Figure 4H). However, when WT YOD1-FLAG was expressed, this heat shock-specific increase in K48-Ub was significantly reduced (Figure 4H). These results are consistent with a model wherein Torsin-deficient cells sequester ubiquitylated proteins that are—to a large extent—clients of the p97 machinery and heat labile.

3. Discussion

The conserved cellular phenotype observed across phylogenetically distinct Torsin ATPase loss-of-function models is NE blebs that are stalled nuclear pore complexes (Figure 1A). These blebs contain specific components including FG-nucleoporins [15,17], chaperones [18,57], MLF2 [15], and K48-Ub [14,17]. We report that cells devoid of Torsin function sequester K48-Ub protein in a p97-dependent manner (Figure 1B,C). The accumulation of ubiquitylated proteins inside blebs is only slightly decreased upon knockdown of the Ufd1/Npl4 heterodimer (Figure 2A,B), a major adaptor that recruits p97 to ubiquitylated substrates during ERAD. This suggests that the relevant p97 activity is not critically dependent on Ufd1/Npl4. Similarly, neither depletion of canonical Ub ligases implicated in ERAD (Figure S2A) nor a block of de novo protein synthesis (Figure 2E) significantly affects Ub deposition in NE blebs to the extent of p97 inhibition (Figure 1B,C). Unexpectedly, depletion of the p97 adaptor UBXD1, that has to our knowledge not been tied to nuclear processes, leads to a drastic reduction in Ub accumulation in NE blebs (Figure 3A,B).

We demonstrate that globally increasing the number of ubiquitylated proteins by heat shock causes significantly more K48-Ub to be trapped inside blebs (Figure 4). This finding may argue against a specific enrichment of K48-Ub proteins and suggest a more general degradation defect exists in Torsin-deficient cells. Another interpretation consistent with this result is that blebs harbor specific heat-labile proteins that become defective and ubiquitylated under heat shock conditions. Future studies are warranted to distinguish between these two possibilities.

Our findings reported herein are consistent with a model wherein Torsin-deficient cells fail to efficiently degrade ubiquitylated proteins and instead sequester this cargo into NE herniations. We have previously demonstrated that Δ133-ORF10, a short-lived virus-derived model substrate, is rapidly degraded in WT cells but is stabilized in TorsinKO cells where it is sequestered into blebs [18]. In the present study, we generalize this finding in the physiological context of heat shock. We demonstrate that endogenous, ubiquitylated cargo provoked by heat shock is sequestered into blebs. In further support of the concept that cargo are stabilized within blebs, we find that while MLF2 is turned over in WT cells exposed to heat shock, it is strongly stabilized in TorsinKO cells under heat shock (Figure 4E). As MLF2 and Δ133-ORF10 are tightly sequestered inside blebs in TorsinKO cells, these data are consistent with the idea that proteins normally efficiently degraded in WT cells are sequestered and consequently stabilized inside blebs in Torsin-deficient cells.

Given that DYT1 dystonia is a neurological disease, a general defect in the ability to turn over potentially aberrant proteins would disproportionally affect postmitotic neurons as this cell type is unable to dilute harmful species though cell division. As this cell type is particularly vulnerable to TorsinA mutation [19,58,59], this defect may at least partially explain why TorsinA mutation exclusively causes a neurological disease. Therefore, we pro-

pose that the p97/UBXD1 axis represents a potential therapeutic target for DYT1 dystonia as its inhibition reduces K48-Ub accumulation inside blebs.

As Torsin ATPases localize within the ER/NE system [3,60,61], the protein quality control defect arising upon Torsin loss of function may be related to ERAD. While the involvement of Torsin activity in ERAD has been investigated [14,62], it has not been found to play a critical role in processing many canonical ERAD model substrates. Furthermore, Torsin depletion is not consistently associated with causing general ER stress [14,17,63]. As we report herein, inhibiting translation (Figure 2E), depleting the Ufd1/Npl4 heterodimer (Figure 2A,B) or canonical Ub ligases required for ERAD (Figure S2A) fail to significantly reduce the amount of K48-Ub sequestered into blebs. Thus, if Torsin loss of function results in a PQC defect related to ERAD, it would likely affect clients of a distinct pathway that are retrotranslocated and ubiquitylated by a noncanonical mechanism. It is furthermore unlikely that these clients would be newly synthesized proteins given that CHX treatment has little impact on the K48-Ub cargo inside blebs (Figure 2E).

Our data suggest that the p97 interaction partners UBXD1 and YOD1 function in the PQC pathway that becomes dysregulated upon Torsin deficiency. While YOD1 is best characterized as participating in ERAD-related processes [50,64], it has also been reported to facilitate autophagy of damaged lysosomes [47]. Notably, this latter function is in conjunction with UBXD1 and the p97 adaptor PLAA [47]. While we did not find that knockdown of PLAA effected K48-Ub levels inside blebs (data not shown), UBXD1 has been reported to function in a wide range of processes including mitophagy [48] and trafficking [46]. Thus, it will be interesting for future endeavors to test whether UBXD1 and YOD1 contribute to the same p97-dependent process in Torsin-deficient cells or if these two adaptors function with p97 in distinct, dysregulated processes.

The small-molecule p97 inhibitor CB-5083 depletes the K48-Ub cargo inside blebs within four hours of treatment (Figure 1B). This relatively short treatment time reveals a previously unappreciated feature of blebs: K48-Ub cargo must undergo some dynamic exchange with the nucleoplasm. This dynamic feature of blebs has not been detected by previous workflows monitoring steady-state levels of K48-Ub sequestration [14,15,17,58]. It will be important to determine the fate of the K48-Ub protein once they are released from blebs under p97 depletion conditions. For example, this cargo could be degraded once inside the nucleoplasm or it could persist within the cell and pose an even greater proteotoxic threat, depending on the resident times in NE blebs versus the nucleoplasm. Efforts to uncover how p97 inhibition affects blebs may also reveal whether proteasome flux is impaired in models of DYT1 dystonia and the identity of K48-Ub conjugates. Answering these questions will not only advance therapeutic options but further our understanding of Torsin ATPases.

4. Materials and Methods

4.1. Antibodies

The following antibodies were used in this study (WB, Western blot (Bio-Rad [Hercules, CA, USA]). IF, immunofluorescence): K48 linkage-specific polyubiquitin (WB, 1:4000. IF, 1:500. MilliporeSigma [Burlington, MA, USA], Apu2), HA-peptide (WB, 1:2000. IF, 1:500. Roche, 3F10), p97 (WB, 1:7000. Abcam [Cambridge, England], ab109240), α-tubulin (WB, 1:5000. MilliporeSigma [Burlington, MA, USA], T5168), α-GAPDH (WB, 1:10,000. Proteintech [Rosemont, IL, USA], 60004-1-Ig), α-Ufd1 (WB, 1:1000. Cell Signaling [Danvers, MA, USA], 13789), α-Npl4 (WB, 1:1000. Cell Signaling, 13489), α-UBXD1 (WB, 1:500. Bethyl Laboratories [Montgomery, TX, USA], A302-931A), α-hnRNPA1 (WB, 1:2000. Abcam [Cambridge, England], ab5832), α-emerin (WB, 1:4000. Cell Signaling [Danvers, MA, USA], 30853S), α-calnexin (WB, 1:2000. Abcam [Cambridge, England], 75801), FLAG peptide (WB, 1:4000. IF, 1:500. MilliporeSigma [Burlington, MA, USA], F3165), rabbit IgG HRP conjugate (WB, 1:10,000. SouthernBiotech [Birmingham, AL, USA], 4030-05), mouse IgG HRP conjugate (WB, 1:20,000. SouthernBiotech [Birmingham, AL, USA], 1030-05), rabbit and mouse IgG Alexa488 conjugates (IF, 1:700. Invitrogen [Waltham, MA, USA], A11008

and A28175), and rabbit and mouse IgG Alexa568 (IF, 1:700. Invitrogen [Waltham, MA, USA], A-11011 and A-11004).

4.2. Cell Culture and Cell Lines

Torsin-deficient [17] and WT HeLa cells were maintained in Dulbecco's Modified Eagle's Medium (DMEM) supplemented with 10% fetal bovine serum (Thermo Fisher Scientific [Waltham, MA, USA]) and 100 units mL^{-1} of penicillin-streptomycin (Thermo Fischer Scientific [Waltham, MA, USA]). Cells were verified to be free of mycoplasma contamination through the absence of extranuclear Hoechst 33342 (Life Technologies [Carlsbad, CA, USA]) staining. Heat shock was achieved by incubating cells for 16 h at 42 °C.

4.3. Small-Molecule Treatment, Plasmids, and Transient Transfections

Inhibition of p97 was achieved using the small-molecule CB-5083 [24,25] (Apexbio Technology [Houston, TX, USA], 1542705-92-9). The compound was dissolved in DMSO to a stock concentration of 10 mM. The stock solution was diluted 1:2000 in DMEM completed as described above for a final concentration of 5 µM. Cells were exposed to media containing CB-5083 for four hours prior to harvesting for downstream applications.

The cDNA sequence encoding MLF2-HA was cloned into the pcDNA3.1+ vector as previously described [15] using standard PCR. WT YOD1-FLAG, YOD1-CS-FLAG, and p97-QQ constructs in pcDNA3.1+ were cloned as previously described [50]. HA-tagged and untagged LBR-1600* were cloned as previously described [28,29]. The cDNA encoding UBXD1 was amplified from HeLa cell cDNA and cloned into pcDNA3.1+ using NheI and XbaI with an N-terminal FLAG tag. pENTR-AIF (AIFM1) was a gift from Huda Zoghbi (Addgene plasmid #16182; http://n2t.net/addgene:16182, accessed on 20 January 2019; RRID: Addgene_16182) and was subcloned into pcDNA3.1+ with a C-terminal FLAG tag.

Transient plasmid transfections were performed using Lipfectamine 2000 (Invitrogen [Waltham, MA, USA]) according to the manufacturer's instructions. Constructs were allowed to express for 24 h prior to analyses.

4.4. siRNAs, Transient RNAi Knockdowns, and qPCR Validation

The following siRNAs [47] targeting UBXD1 were ordered from MilliporeSigma [Burlington, MA, USA]. Forward oligo 1: 5′-CCAGGUGAGAAAGGAACUU[dT][dT]-3′. Forward oligo 2: 5′-UCAGAUACCACGUUGGUCCC[dT][dT]-3′. Nontargeting and siRNAs targeting Ufd1, Npl4, p47, Hrd1, MARCH6, and gp78 were purchased from Horizon Discovery [Waterbeach, England] as SMARTpools.

RNAi knockdowns were performed with Lipfectamine RNAiMAX (Invitrogen [Waltham, MA, USA]) according to the manufacturer's instructions and allowed to knock targets down for 48 h before analyses.

Knockdown efficiency was validated by quantitative PCR (qPCR) using iQ SYBR Green (Bio-Rad [Hercules, CA, USA]) mix with a CFX Real-Time PCR 639 Detection System (Bio-Rad [Hercules, CA, USA]). Each knockdown was evaluated using the ΔΔCt method using the internal control transcript RPL32. Primer sequences used for qPCR were as follows: UBXD1 (FWD: TGGAGAGGCACAAGGAACAGC, REV: CCCGCTTGATCTC-CTCTGCT), Ufd1 [65] (FWD: GAGGGAAGATAATTATGCCAC, REV: CTTCCAAGAG-TAAGTTCTGC), Npl4 (FWD: GCTTGGCCACCTATTTGTCTCAGAA, REV: CATTGGT-GACCAGGAACAGCAAGA), Hrd1 [66] (FWD: GCGAGACATGATGGCATCTG, AACC-CCTGGGACAACAAGG, REV: GCGAGACATGATGGCATCTG), MARCH6 (FWD: AG-CATGCTCGAAATAACAACGCT, REV: GGCGGTAAGGCTGAAAGCCA), gp78 (FWD: CGTGTGCCACTGGACCTCAG, REV: CACCAGCATGCGCTGTCTCT), p47 (FWD: AG-TACCAGCTCTCCAGCCCAA, REV: CGCCGTCTGCAAGCCGAA). All primers were synthesized by Integrated DNA Technologies [Coralville, IA, USA].

4.5. Immunofluorescence and Confocal Microscopy

HeLa cells were grown on coverslips prior to processing for IF. Cells were fixed onto coverslips in 4% paraformaldehyde (Thermo Fisher Scientific [Waltham, MA, USA]) for 20 min at room temperature, then permeabilized in 0.1% Triton X-100 (MilliporeSigma [Burlington, MA, USA]) for 10 min. After blocking in 4% bovine serum albumin for 15 min, cells were incubated for 45 min with primary antibodies diluted 1:500 in blocking solution. After exhaustive washing in phosphate buffered saline (PBS), cells were incubated in fluorescent secondary antibodies diluted 1:700 in blocking solution. Prior to mounting onto slides, the cells were stained with Hoechst 33342 (Life Technologies [Carlsbad, CA, USA]) and adhered to slides with Fluoromount-G (Southern Biotech [Birmingham, AL, USA]).

Confocal images were collected on an LSM 880 laser scanning microscope (Zeiss [Jena, Germany]) with a C Plan-Apochromat 63×/1.40 oil DIC M27 objective using ZEN 2.1 software (Zeiss [Jena, Germany]). Image quantification and processing was performed in Fiji [67] or CellProfiler [68] as described below.

4.6. Immunoprecipitation and Immunoblot Analysis

All immunoprecipitation (IP) experiments were conducted under native conditions. Cells were transfected or exposed to relevant conditions 16–24 h prior to harvesting for IP, then lysed in NET buffer (150 mM NaCl, 50 mM Tris pH 7.4, 0.5% NP-40) supplemented with EDTA-free protease inhibitor cocktail (Roche [Basel, Switzerland]) and 5 mM NEM (MilliporeSigma [Burlington, MA, USA]). Equal amounts of protein were loaded onto protein A beads conjugated to 1 µg anti-p97 (Abcam [Cambridge, England], ab109240) or Anti-FLAG M2 Affinity Gel (MilliporeSigma, [Burlington, MA, USA], A2220). After incubating for three hours, the resin was washed extensively in NET buffer and protein was eluted in SDS reducing buffer for downstream immunoblot analyses.

Cell lysates were prepared for immunoblot in NET buffer plus protease inhibitors and 5 mM NEM as described above. Immunoblotting with IP eluates or cell lysates was performed with SDS-PAGE gels (Bio-Rad [Hercules, CA, USA]) and transferred onto PVDF membranes (Bio-Rad [Hercules, CA, USA]). Membranes were blocked in 5% w/v milk in PBS + 0.1% Tween-20 (MilliporeSigma [Burlington, MA, USA]). Primary and HRP-conjugated secondary antibodies were diluted in blocking buffer. Blots were visualized by chemiluminescence on a ChemiDoc Gel Imaging System (Bio-Rad [Hercules, CA, USA]).

4.7. Cycloheximide Chase

TorsinKO HeLa cells were plated in a 10 cm dish and transfected with HA-LBR 1600* [28], which was allowed to express for 24 h prior to harvesting cells. After 24 h, the cells were either trypsinized and split into two tubes for immunoblot or kept within the culture dish containing coverslips for IF. Tubes for immunoblot were incubated at 37 °C with gentle shaking and treated with either DMSO or 100 µg/mL CHX diluted in completed DMEM described above. Culture dishes for IF were treated with the same conditions and remained within the culturing incubator. Aliquots for immunoblot or coverslips were taken at zero, one, two, five, or seven hours post treatment. Cells were collected via centrifugation and subjected to immunoblot or fixed with 4% paraformaldehyde and processed for IF as described above.

4.8. NE Enrichment

NE fractions were enriched from whole-cell lysates as previously described [29]. Cells were collected by centrifugation and resuspended in buffer A (10 mM HEPES, pH 7.4, 250 mM sucrose, 2 mM MgCl2) supplemented with EDTA-free protease inhibitor cocktail (Roche [Basel, Switzerland]). Cell pellets were homogenized in 100 µL of buffer A by passing through a 25-gague needle and layered on top of 10 mL STM 0.9 buffer (50 mM Tris, pH 7.4, 0.9 M sucrose, 5 mM $MgCl_2$). The homogenates were centrifuged through the STM 0.9 layer at 1000× g for 10 min twice and a white pellet was observed at the bottom. This pellet, composed of the nuclei/ER and cell debris, was resuspended in TP buffer (10 mM

Tris, pH 8.0, 10 mM Na_2HPO_4, 2 mM $MgCl_2$) supplemented with heparin (2 mg/mL), benzonase nuclease (2 µL/mL), and protease inhibitor cocktail (Roche [Basel, Switzerland]) and rotated overnight at 4 °C. In the morning, the nuclei were spun at 15,000× *g* for 45 min to separate the ER/NE (pellet) from the nucleoplasm (supernatant). ER/NE enrichments were resuspended in 1% SDS and prepared for immunoblot analysis.

4.9. Image Processing and Statical Analysis

All image quantification was performed using Fiji [67] or CellProfiler [68] software. The number of NE-associated K48-Ub foci was determined with Fiji software by defining a region of interest (ROI) around the nucleus of individual cells and quantifying the number of K48-Ub foci using the "Find Maxima" function. In line with our previous publications [15,17,18], the prominence or noise tolerance was set to 10. All statistical analyses for quantifying NE-associated K48-Ub foci utilized the Mann–Whitney U test, which does not assume the distributions are normal.

The intensity of K48-Ub in TorsinKO cells at 37 and 42 °C was assessed using CellProfiler [68] software. Cells were processed for IF as described above and imaged for K48-Ub using identical exposure times for each condition. For comparative analysis of K48-Ub intensity at 37 and 42 °C, the integrated intensity units of K48-Ub foci at the nuclear rim of each cell were quantified in CellProfiler. For determination of the distribution of K48-Ub at 42 °C in the absence and presence of YOD1-CS-FLAG, CellProfiler was used to determine the fraction of total K48-Ub in the outer nuclear region for each cell. The populations were statistically analyzed using the Mann–Whitney U test, which does not require normal distributions.

Supplementary Materials: The following are available online at https://www.mdpi.com/article/10.3390/ijms23094627/s1.

Author Contributions: Conceptualization, S.M.P., B.S.N. and C.S.; methodology, S.M.P., B.S.N. and C.S.; validation, S.M.P., B.S.N. and C.S.; formal analysis, S.M.P., B.S.N. and C.S.; investigation, S.M.P., B.S.N. and C.S.; resources, S.M.P., B.S.N. and C.S.; writing—original draft preparation, S.M.P.; writing—review and editing, S.M.P., B.S.N. and C.S.; visualization, S.M.P., B.S.N. and C.S.; supervision, C.S.; funding acquisition, S.M.P. and C.S. All authors have read and agreed to the published version of the manuscript.

Funding: This work is supported by DOD PR200788 (C.S.), NIH 5T32GM007223-44 (S.M.P.), NIH F31NS120528 (S.M.P.).

Institutional Review Board Statement: Not applicable.

Informed Consent Statement: Not applicable.

Data Availability Statement: All raw data used to generate plots and original scans of immunoblots are available upon request.

Acknowledgments: We thank members of the Schlieker lab for helpful comments regarding experimental design and manuscript preparation.

Conflicts of Interest: The authors declare no conflict of interest.

References

1. Goodchild, R.E.; Kim, C.E.; Dauer, W.T. Loss of the dystonia-associated protein torsina selectively disrupts the neuronal nuclear envelope. *Neuron* **2005**, *48*, 923–932. [CrossRef]
2. Ozelius, L.J.; Hewett, J.W.; Page, C.E.; Bressman, S.B.; Kramer, P.L.; Shalish, C.; de Leon, D.; Brin, M.F.; Raymond, D.; Corey, D.P.; et al. The early-onset torsion dystonia gene (dyt1) encodes an atp-binding protein. *Nat. Genet.* **1997**, *17*, 40–48. [CrossRef] [PubMed]
3. Naismith, T.V.; Heuser, J.E.; Breakefield, X.O.; Hanson, P.I. Torsina in the nuclear envelope. *Proc. Natl. Acad. Sci. USA* **2004**, *101*, 7612–7617. [CrossRef] [PubMed]
4. Zhao, C.; Brown, R.S.; Chase, A.R.; Eisele, M.R.; Schlieker, C. Regulation of torsin atpases by lap1 and lull. *Proc. Natl. Acad. Sci. USA* **2013**, *110*, E1545–E1554. [CrossRef] [PubMed]

5. Brown, R.S.; Zhao, C.; Chase, A.R.; Wang, J.; Schlieker, C. The mechanism of torsin atpase activation. *Proc. Natl. Acad. Sci. USA* **2014**, *111*, E4822–E4831. [CrossRef]
6. Sosa, B.A.; Demircioglu, F.E.; Chen, J.Z.; Ingram, J.; Ploegh, H.L.; Schwartz, T.U. How lamina-associated polypeptide 1 (lap1) activates torsin. *eLife* **2014**, *3*, e03239. [CrossRef]
7. Goodchild, R.E.; Dauer, W.T. The aaa+ protein torsina interacts with a conserved domain present in lap1 and a novel er protein. *J. Cell Biol.* **2005**, *168*, 855–862. [CrossRef]
8. Demircioglu, F.E.; Sosa, B.A.; Ingram, J.; Ploegh, H.L.; Schwartz, T.U. Structures of torsina and its disease-mutant complexed with an activator reveal the molecular basis for primary dystonia. *eLife* **2016**, *5*, e17983. [CrossRef]
9. Rose, A.E.; Brown, R.S.; Schlieker, C. Torsins: Not your typical aaa+ atpases. *Crit. Rev. Biochem. Mol. Biol.* **2015**, *50*, 532–549. [CrossRef]
10. Gonzalez-Alegre, P. Advances in molecular and cell biology of dystonia: Focus on torsina. *Neurobiol. Dis.* **2019**, *127*, 233–241. [CrossRef]
11. Rampello, A.J.; Prophet, S.M.; Schlieker, C. The role of torsin aaa+ proteins in preserving nuclear envelope integrity and safeguarding against disease. *Biomolecules* **2020**, *10*, 468. [CrossRef] [PubMed]
12. Naismith, T.V.; Dalal, S.; Hanson, P.I. Interaction of torsina with its major binding partners is impaired by the dystonia-associated deltagag deletion. *J. Biol. Chem.* **2009**, *284*, 27866–27874. [CrossRef] [PubMed]
13. VanGompel, M.J.; Nguyen, K.C.; Hall, D.H.; Dauer, W.T.; Rose, L.S. A novel function for the caenorhabditis elegans torsin ooc-5 in nucleoporin localization and nuclear import. *Mol. Biol. Cell* **2015**, *26*, 1752–1763. [CrossRef] [PubMed]
14. Pappas, S.S.; Liang, C.C.; Kim, S.; Rivera, C.O.; Dauer, W.T. Torsina dysfunction causes persistent neuronal nuclear pore defects. *Hum. Mol. Genet.* **2018**, *27*, 407–420. [CrossRef] [PubMed]
15. Rampello, A.J.; Laudermilch, E.; Vishnoi, N.; Prophet, S.M.; Shao, L.; Zhao, C.; Lusk, C.P.; Schlieker, C. Torsin atpase deficiency leads to defects in nuclear pore biogenesis and sequestration of mlf. *J. Cell Biol.* **2020**, *219*, e201910185. [CrossRef]
16. Jacquemyn, J.; Foroozandeh, J.; Vints, K.; Swerts, J.; Verstreken, P.; Gounko, N.V.; Gallego, S.F.; Goodchild, R. Torsin and nep1r1-ctdnep1 phosphatase affect interphase nuclear pore complex insertion by lipid-dependent and lipid-independent mechanisms. *EMBO J.* **2021**, *40*, e106914. [CrossRef]
17. Laudermilch, E.; Tsai, P.L.; Graham, M.; Turner, E.; Zhao, C.; Schlieker, C. Dissecting torsin/cofactor function at the nuclear envelope: A genetic study. *Mol. Biol. Cell* **2016**, *27*, 3964–3971. [CrossRef]
18. Prophet, S.M.; Rampello, A.J.; Niescier, R.F.; Shaw, J.E.; Koleske, A.J.; Schlieker, C. Mlf2 modulates phase separated nuclear envelope condensates that provoke dual proteotoxicity. *bioRxiv* **2021**. [CrossRef]
19. Liang, C.C.; Tanabe, L.M.; Jou, S.; Chi, F.; Dauer, W.T. Torsina hypofunction causes abnormal twisting movements and sensorimotor circuit neurodegeneration. *J. Clin. Investig.* **2014**, *124*, 3080–3092. [CrossRef]
20. Lam, Y.A.; Lawson, T.G.; Velayutham, M.; Zweier, J.L.; Pickart, C.M. A proteasomal atpase subunit recognizes the polyubiquitin degradation signal. *Nature* **2002**, *416*, 763–767. [CrossRef]
21. Rosenzweig, R.; Nillegoda, N.B.; Mayer, M.P.; Bukau, B. The hsp70 chaperone network. *Nat. Rev. Mol. Cell Biol.* **2019**, *20*, 665–680. [CrossRef] [PubMed]
22. Huryn, D.M.; Kornfilt, D.J.P.; Wipf, P. P97: An emerging target for cancer, neurodegenerative diseases, and viral infections. *J. Med. Chem.* **2020**, *63*, 1892–1907. [CrossRef] [PubMed]
23. Van den Boom, J.; Meyer, H. Vcp/p97-mediated unfolding as a principle in protein homeostasis and signaling. *Mol. Cell* **2018**, *69*, 182–194. [CrossRef] [PubMed]
24. Zhou, H.J.; Wang, J.; Yao, B.; Wong, S.; Djakovic, S.; Kumar, B.; Rice, J.; Valle, E.; Soriano, F.; Menon, M.K.; et al. Discovery of a first-in-class, potent, selective, and orally bioavailable inhibitor of the p97 aaa atpase (cb-5083). *J. Med. Chem.* **2015**, *58*, 9480–9497. [CrossRef] [PubMed]
25. Anderson, D.J.; Le Moigne, R.; Djakovic, S.; Kumar, B.; Rice, J.; Wong, S.; Wang, J.; Yao, B.; Valle, E.; Kiss von Soly, S.; et al. Targeting the aaa atpase p97 as an approach to treat cancer through disruption of protein homeostasis. *Cancer Cell* **2015**, *28*, 653–665. [CrossRef]
26. Wu, X.; Rapoport, T.A. Mechanistic insights into er-associated protein degradation. *Curr. Opin. Cell Biol.* **2018**, *53*, 22–28. [CrossRef]
27. Ji, Z.; Li, H.; Peterle, D.; Paulo, J.A.; Ficarro, S.B.; Wales, T.E.; Marto, J.A.; Gygi, S.P.; Engen, J.R.; Rapoport, T.A. Translocation of polyubiquitinated protein substrates by the hexameric cdc48 atpase. *Mol. Cell* **2022**, *82*, 570–584.e578. [CrossRef]
28. Tsai, P.L.; Zhao, C.; Turner, E.; Schlieker, C. The lamin b receptor is essential for cholesterol synthesis and perturbed by disease-causing mutations. *eLife* **2016**, *5*, e16011. [CrossRef]
29. Tsai, P.L.; Zhao, C.; Schlieker, C. Methodologies to monitor protein turnover at the inner nuclear membrane. *Methods Enzymol.* **2019**, *619*, 47–69.
30. Wu, X.; Siggel, M.; Ovchinnikov, S.; Mi, W.; Svetlov, V.; Nudler, E.; Liao, M.; Hummer, G.; Rapoport, T.A. Structural basis of er-associated protein degradation mediated by the hrd1 ubiquitin ligase complex. *Science* **2020**, *368*, eaaz2449. [CrossRef]
31. Schoebel, S.; Mi, W.; Stein, A.; Ovchinnikov, S.; Pavlovicz, R.; DiMaio, F.; Baker, D.; Chambers, M.G.; Su, H.; Li, D.; et al. Cryo-em structure of the protein-conducting erad channel hrd1 in complex with hrd. *Nature* **2017**, *548*, 352–355. [CrossRef] [PubMed]
32. Schmidt, C.C.; Vasic, V.; Stein, A. Doa10 is a membrane protein retrotranslocase in er-associated protein degradation. *eLife* **2020**, *9*, e56945. [CrossRef] [PubMed]

33. Twomey, E.C.; Ji, Z.; Wales, T.E.; Bodnar, N.O.; Ficarro, S.B.; Marto, J.A.; Engen, J.R.; Rapoport, T.A. Substrate processing by the cdc48 atpase complex is initiated by ubiquitin unfolding. *Science* **2019**, *365*, eaax1033. [CrossRef] [PubMed]
34. Mehrtash, A.B.; Hochstrasser, M. Ubiquitin-dependent protein degradation at the endoplasmic reticulum and nuclear envelope. *Semin. Cell Dev. Biol.* **2019**, *93*, 111–124. [CrossRef]
35. Wu, X.; Rapoport, T.A. Translocation of proteins through a distorted lipid bilayer. *Trends Cell Biol.* **2021**, *31*, 473–484. [CrossRef]
36. Ferro-Novick, S.; Reggiori, F.; Brodsky, J.L. Er-phagy, er homeostasis, and er quality control: Implications for disease. *Trends Biochem. Sci.* **2021**, *46*, 630–639. [CrossRef]
37. Vasic, V.; Denkert, N.; Schmidt, C.C.; Riedel, D.; Stein, A.; Meinecke, M. Hrd1 forms the retrotranslocation pore regulated by auto-ubiquitination and binding of misfolded proteins. *Nat. Cell Biol.* **2020**, *22*, 274–281. [CrossRef]
38. Schubert, U.; Anton, L.C.; Gibbs, J.; Norbury, C.C.; Yewdell, J.W.; Bennink, J.R. Rapid degradation of a large fraction of newly synthesized proteins by proteasomes. *Nature* **2000**, *404*, 770–774. [CrossRef]
39. Wolff, S.; Weissman, J.S.; Dillin, A. Differential scales of protein quality control. *Cell* **2014**, *157*, 52–64. [CrossRef]
40. Gloge, F.; Becker, A.H.; Kramer, G.; Bukau, B. Co-translational mechanisms of protein maturation. *Curr. Opin. Struct. Biol.* **2014**, *24*, 24–33. [CrossRef]
41. Buchberger, A.; Schindelin, H.; Hanzelmann, P. Control of p97 function by cofactor binding. *FEBS Lett.* **2015**, *589*, 2578–2589. [CrossRef] [PubMed]
42. Ye, Y.; Tang, W.K.; Zhang, T.; Xia, D. A mighty "protein extractor" of the cell: Structure and function of the p97/cdc48 atpase. *Front. Mol. Biosci.* **2017**, *4*, 39. [CrossRef] [PubMed]
43. Ye, Y.; Meyer, H.H.; Rapoport, T.A. Function of the p97-ufd1-npl4 complex in retrotranslocation from the er to the cytosol: Dual recognition of nonubiquitinated polypeptide segments and polyubiquitin chains. *J. Cell Biol.* **2003**, *162*, 71–84. [CrossRef] [PubMed]
44. Kondo, H.; Rabouille, C.; Newman, R.; Levine, T.P.; Pappin, D.; Freemont, P.; Warren, G. P47 is a cofactor for p97-mediated membrane fusion. *Nature* **1997**, *388*, 75–78. [CrossRef]
45. Haines, D.S.; Lee, J.E.; Beauparlant, S.L.; Kyle, D.B.; den Besten, W.; Sweredoski, M.J.; Graham, R.L.; Hess, S.; Deshaies, R.J. Protein interaction profiling of the p97 adaptor ubxd1 points to a role for the complex in modulating ergic-53 trafficking. *Mol. Cell. Proteomics* **2012**, *11*, M111.016444. [CrossRef]
46. Ritz, D.; Vuk, M.; Kirchner, P.; Bug, M.; Schutz, S.; Hayer, A.; Bremer, S.; Lusk, C.; Baloh, R.H.; Lee, H.; et al. Endolysosomal sorting of ubiquitylated caveolin-1 is regulated by vcp and ubxd1 and impaired by vcp disease mutations. *Nat. Cell Biol.* **2011**, *13*, 1116–1123. [CrossRef]
47. Papadopoulos, C.; Kirchner, P.; Bug, M.; Grum, D.; Koerver, L.; Schulze, N.; Poehler, R.; Dressler, A.; Fengler, S.; Arhzaouy, K.; et al. Vcp/p97 cooperates with yod1, ubxd1 and plaa to drive clearance of ruptured lysosomes by autophagy. *EMBO J.* **2017**, *36*, 135–150. [CrossRef]
48. Bento, A.C.; Bippes, C.C.; Kohler, C.; Hemion, C.; Frank, S.; Neutzner, A. Ubxd1 is a mitochondrial recruitment factor for p97/vcp and promotes mitophagy. *Sci. Rep.* **2018**, *8*, 12415. [CrossRef]
49. Nagahama, M.; Ohnishi, M.; Kawate, Y.; Matsui, T.; Miyake, H.; Yuasa, K.; Tani, K.; Tagaya, M.; Tsuji, A. Ubxd1 is a vcp-interacting protein that is involved in er-associated degradation. *Biochem. Biophys. Res. Commun.* **2009**, *382*, 303–308. [CrossRef]
50. Ernst, R.; Mueller, B.; Ploegh, H.L.; Schlieker, C. The otubain yod1 is a deubiquitinating enzyme that associates with p97 to facilitate protein dislocation from the er. *Mol. Cell* **2009**, *36*, 28–38. [CrossRef]
51. Ewing, R.M.; Chu, P.; Elisma, F.; Li, H.; Taylor, P.; Climie, S.; McBroom-Cerajewski, L.; Robinson, M.D.; O'Connor, L.; Li, M.; et al. Large-scale mapping of human protein-protein interactions by mass spectrometry. *Mol. Syst. Biol.* **2007**, *3*, 89. [CrossRef] [PubMed]
52. Liu, X.; Salokas, K.; Tamene, F.; Jiu, Y.; Weldatsadik, R.G.; Ohman, T.; Varjosalo, M. An ap-ms- and bioid-compatible mac-tag enables comprehensive mapping of protein interactions and subcellular localizations. *Nat. Commun.* **2018**, *9*, 1188. [CrossRef] [PubMed]
53. Parag, H.A.; Raboy, B.; Kulka, R.G. Effect of heat shock on protein degradation in mammalian cells: Involvement of the ubiquitin system. *EMBO J.* **1987**, *6*, 55–61. [CrossRef] [PubMed]
54. Fujimuro, M.; Sawada, H.; Yokosawa, H. Dynamics of ubiquitin conjugation during heat-shock response revealed by using a monoclonal antibody specific to multi-ubiquitin chains. *Eur. J. Biochem.* **1997**, *249*, 427–433. [CrossRef]
55. Maxwell, B.A.; Gwon, Y.; Mishra, A.; Peng, J.; Nakamura, H.; Zhang, K.; Kim, H.J.; Taylor, J.P. Ubiquitination is essential for recovery of cellular activities after heat shock. *Science* **2021**, *372*, eabc3593. [CrossRef]
56. Friant, S.; Meier, K.D.; Riezman, H. Increased ubiquitin-dependent degradation can replace the essential requirement for heat shock protein induction. *EMBO J.* **2003**, *22*, 3783–3791. [CrossRef]
57. Elsiena Kuiper, E.F.; Gallardo, P.; Bergsma, T.; Mari, M.; Musskopf, M.K.; Kuipers, J.; Giepmans, B.N.G.; Steen, A.; Veenhoff, L.M.; Kampinga, H.H.; et al. The molecular chaperone dnajb6 provides surveillance of fg-nups and is required for interphase nuclear pore complex biogenesis. *bioRxiv* **2021**. [CrossRef]
58. Weisheit, C.E.; Dauer, W.T. A novel conditional knock-in approach defines molecular and circuit effects of the dyt1 dystonia mutation. *Hum. Mol. Genet.* **2015**, *24*, 6459–6472. [CrossRef]
59. Li, J.; Liang, C.-C.; Pappas, S.S.; Dauer, W.T. Torsinb overexpression prevents abnormal twisting in dyt1 dystonia mouse models. *eLife* **2019**, *9*, e54285. [CrossRef]

60. Goodchild, R.E.; Dauer, W.T. Mislocalization to the nuclear envelope: An effect of the dystonia-causing torsina mutation. *Proc. Natl. Acad. Sci. USA* **2004**, *101*, 847–852. [CrossRef]
61. Vander Heyden, A.B.; Naismith, T.V.; Snapp, E.L.; Hanson, P.I. Static retention of the lumenal monotopic membrane protein torsina in the endoplasmic reticulum. *EMBO J.* **2011**, *30*, 3217–3231. [CrossRef] [PubMed]
62. Nery, F.C.; Armata, I.A.; Farley, J.E.; Cho, J.A.; Yaqub, U.; Chen, P.; da Hora, C.C.; Wang, Q.; Tagaya, M.; Klein, C.; et al. Torsina participates in endoplasmic reticulum-associated degradation. *Nat. Commun.* **2011**, *2*, 393. [CrossRef] [PubMed]
63. Shin, J.Y.; Hernandez-Ono, A.; Fedotova, T.; Ostlund, C.; Lee, M.J.; Gibeley, S.B.; Liang, C.C.; Dauer, W.T.; Ginsberg, H.N.; Worman, H.J. Nuclear envelope-localized torsina-lap1 complex regulates hepatic vldl secretion and steatosis. *J. Clin. Investig.* **2019**, *130*, 4885–4900. [CrossRef] [PubMed]
64. Sasset, L.; Petris, G.; Cesaratto, F.; Burrone, O.R. The vcp/p97 and yod1 proteins have different substrate-dependent activities in endoplasmic reticulum-associated degradation (erad). *J. Biol. Chem.* **2015**, *290*, 28175–28188. [CrossRef]
65. Chen, M.; Gutierrez, G.J.; Ronai, Z.A. Ubiquitin-recognition protein ufd1 couples the endoplasmic reticulum (er) stress response to cell cycle control. *Proc. Natl. Acad. Sci. USA* **2011**, *108*, 9119–9124. [CrossRef]
66. Xu, Y.M.; Wang, H.J.; Chen, F.; Guo, W.H.; Wang, Y.Y.; Li, H.Y.; Tang, J.H.; Ding, Y.; Shen, Y.C.; Li, M.; et al. Hrd1 suppresses the growth and metastasis of breast cancer cells by promoting igf-1r degradation. *Oncotarget* **2015**, *6*, 42854–42867. [CrossRef]
67. Schindelin, J.; Arganda-Carreras, I.; Frise, E.; Kaynig, V.; Longair, M.; Pietzsch, T.; Preibisch, S.; Rueden, C.; Saalfeld, S.; Schmid, B.; et al. Fiji: An open-source platform for biological-image analysis. *Nat. Methods* **2012**, *9*, 676–682. [CrossRef]
68. Stirling, D.R.; Swain-Bowden, M.J.; Lucas, A.M.; Carpenter, A.E.; Cimini, B.A.; Goodman, A. Cellprofiler 4: Improvements in speed, utility and usability. *BMC Bioinform.* **2021**, *22*, 433. [CrossRef]

Atypical nuclear envelope condensates linked to neurological disorders reveal nucleoporin-directed chaperone activities

Sarah M Prophet[1], Anthony J Rampello[1], Robert F Niescier[1,2], Juliana E Gentile[1,2,4], Sunanda Mallik[1], Anthony J Koleske[1,2], Christian Schlieker[1,3*]

[1]Yale University, Department of Molecular Biophysics and Biochemistry, New Haven, CT, [2]Yale School of Medicine, Department of Neuroscience, New Haven, CT, [3]Yale School of Medicine, Department of Cell Biology, New Haven, CT, [4]Present address: Broad Institute of MIT and Harvard, Cambridge, MA

* Correspondence: Christian Schlieker, Department of Molecular Biophysics & Biochemistry, Yale University, 266 Whitney Avenue, P.O. Box 208114, Bass 236A, New Haven, CT 06520-8114, office phone: (203) 432-5035, office fax: (203) 432-8492, email: christian.schlieker@yale.edu

Abstract

DYT1 dystonia is a debilitating neurological movement disorder arising from mutation in the AAA+ ATPase TorsinA. The hallmark of Torsin dysfunction is nuclear envelope blebbing resulting from defects in nuclear pore complex biogenesis. Whether blebs actively contribute to disease manifestation is unknown. We report that FG-nucleoporins (FG-Nups) in the bleb lumen form aberrant condensates and contribute to DYT1 dystonia by provoking two proteotoxic insults. Short-lived ubiquitylated proteins that are normally rapidly degraded partition into the bleb lumen and become stabilized. Additionally, blebs selectively sequester a specific HSP40/HSP70 chaperone network that is modulated by the bleb component MLF2. MLF2 suppresses the ectopic accumulation of FG-Nups and modulates the selective properties and size of condensates *in vitro*. Our studies identify dual mechanisms of proteotoxicity in the context of condensate formation and establish FG-Nup-directed activities for a nuclear chaperone network.

Introduction

Torsin ATPases (Torsins) are the only members of the AAA+ protein superfamily that localize within the endoplasmic reticulum (ER) and nuclear envelope (NE) [1, 2]. TorsinA is essential for viability [3] and strictly requires regulatory cofactors to hydrolyze ATP[4]. A mutation in TorsinA that disrupts the interactions with its cofactors results in a loss of ATPase activity [5, 6] and is responsible for a debilitating neurological movement disorder called DYT1 dystonia [7]. Mutations in the Torsin activator LAP1 also give rise to dystonia and myopathies [8-10]. Thus, the Torsin system is critical for neurological function [9, 11].

While the molecular targets of Torsins and the mechanism of DYT1 dystonia onset are not understood, the hallmark phenotype observed across diverse animal and cell-based models of DYT1 dystonia is NE blebbing [3, 12-21]. NE blebs in the context of Torsin disruption are omega-shaped herniations of the inner nuclear membrane that are constricted at their base by a nuclear pore complex (NPC)-like structure and stem from defective NPC assembly [18, 22] (Extended Data Fig. 1a). Blebs are observed via distinct mechanisms of Torsin perturbation, i.e., dominant-negative alleles, Torsin-null alleles, siRNA, and in yeast harboring mutations of NPC-related proteins [23, 24]. As a consequence of NE blebbing, nuclear transport defects have been observed in models of compromised Torsin function including patient-derived iPSC neurons [12, 20, 21].

NPCs are composed of nucleoporins (Nups), several of which contain disordered phenylalanine-glycine (FG)-rich domains, which form a dense hydrogel and establish the permeability barrier characteristic of NPCs [25-28]. While small (<30 kDa) molecules can passively diffuse through this barrier [29], larger molecules require facilitated passage via nuclear transport receptors (NTRs) [30].

NE blebs arising from Torsin deficiency are enriched for FG-Nups but do not contain NTRs or bulk nuclear export cargo [18, 22]. Moreover, the poorly characterized protein myeloid leukemia factor 2 (MLF2) and K48-linked ubiquitin (Ub) chains are diagnostic constituents of the bleb lumen

[18, 20, 22] (Extended Data Fig. 1a). While Ub accumulation and defects in the ubiquitin/proteasome system have been implicated in many other neurological disorders including Huntington's and Parkinson's disease [31-33], it is unknown whether or how NE blebs contribute to DYT1 dystonia onset. Both the lack of suitable readouts and our incomplete understanding of the molecular composition of blebs represent major obstacles towards identifying their functional consequences.

In this study, we develop a virally-derived model substrate to define the bleb proteome and probe the significance of ubiquitin accumulation for DYT1 dystonia development. We find that normally short-lived proteins evade degradation once they are trapped inside blebs. Along with stabilized ubiquitylated proteins, blebs sequester a highly specific chaperone network composed of HSP40s and HSP70s. The FG-Nup Nup98 is required for blebs to form, and we demonstrate that blebs harbor an FG-rich condensate. We combine cellular and *in vitro* approaches to assign an FG-directed activity to MLF2 in complex with HSP70 and DNAJB6. Together, our results advance our understanding of cellular phase separation and define a link between PQC defects and disease etiology via pathological NE-associated condensates.

Results

Torsin deficiency stabilizes rapidly degraded proteins. To develop approaches for probing the consequences of sequestering protein into NE blebs, we examined viral proteins that have been functionally tied to nuclear transport. ORF10 from Kaposi's sarcoma-associated herpesvirus (KSHV) is produced as a full length 418-residue protein and a shorter 286-residue protein (Δ133 ORF10) via an alternative translation initiation (Fig. 1a,b). The full-length protein [34] localizes diffusely within the nucleoplasm in wild type (WT) and TorsinKO HeLa cells (Fig. 1c). However, Δ133 ORF10 becomes tightly sequestered into NE foci that strictly co-localize with K48-Ub in TorsinKO cells (Fig. 1c). Recruitment to these foci strictly depends on ubiquitylation as fusing a deubiquitylating (DUB) domain [35] to Δ133 ORF10 prevents NE sequestration (Extended Data Fig. 1b). Because Δ133 ORF10 remains diffusely nucleoplasmic in WT cells (Fig. 1c) and

associates with more K48-Ub in TorsinKO compared to WT cells (Fig. 1d), we establish Δ133 ORF10 as the only known protein that localizes to blebs in a ubiquitin-dependent manner.

As Δ133 ORF10 is less abundant and associated with lower levels of K48-Ub in WT cells compared to TorsinKO cells (Fig. 1d), we hypothesized that Δ133 ORF10 is normally a short-lived protein. Indeed, we observed its half-life in WT cells to be approximately 45 minutes (Fig. 1e,f). In TorsinKO cells, Δ133 ORF10 is stabilized and exists with a half-life of four hours (Fig. 1e,f). This reveals an unexpected proteotoxic property of NE blebs.

Blebs are enriched for a specific chaperone network. The absence of a comprehensive, bleb-specific proteome is a major limitation in understanding the molecular underpinnings of NE bleb formation. We fused the engineered ascorbate peroxidase APEX2 [36, 37] to MLF2-HA and performed a biotin-based proximity labeling reaction (Fig. 2a). To control the MLF2-APEX2-HA protein level, we placed its expression under a doxycycline (Dox)-inducible promoter (Fig. 2b). The presence of biotin conjugates within blebs after the APEX reaction was verified by immunofluorescence (IF) (Fig. 2c). The biotin-conjugating activity of APEX2 was confirmed via immunoblotting (Fig. 2d). After performing the APEX2 reaction, NE fractions were biochemically separated from WT and TorsinKO cells. Biotinylated proteins were enriched via streptavidin-coated beads and identified by mass spectrometry (LC-MS/MS) (Fig. 2e, Supplemental Table 1). In parallel, we performed an immunoprecipitation (IP) using Δ133 ORF10-HA followed by LC-MS/MS (Fig. 2e, Supplemental Table 2). This allowed for a direct comparison of the bleb proteome from two independent approaches with our previously published dataset of immunoprecipitated K48-Ub from NE fractions [22]. From these three datasets, we considered proteins with a ≥1.5-fold enrichment of spectral counts in TorsinKO samples compared to WT (Fig. 2e).

Only three proteins were consistently enriched across all datasets in samples from TorsinKO cells—MLF2, HSPA1A, and HSC70 (Fig. 2e). HSPA1A and HSC70 are the canonical HSP70 members in mammalian cells, mediating a range of essential processes [38]. This

functional diversity is achieved, at least in part, by interactions with J-domain proteins (HSP40s) [39]. Thus, we asked whether the HSP40s identified in the MLF2-APEX2 and K48-Ub datasets may also be enriched in blebs.

HSP70s and HSP40s are sequestered into NE blebs. We performed a co-IP with ∆133 ORF10 and found it to stably interact with DNAJB6 exclusively in TorsinKO cells (Fig. 2f). Next, we determined whether HSPA1A, HSC70, DNAJB6, and DNAJB2 localized to blebs at endogenous expression levels. In TorsinKO cells, these chaperones redistribute from diffuse cytosolic/nucleoplasmic distributions to foci that decorate the nuclear rim (Fig. 3a, Extended Data Fig. 2a). By overexpressing a dominant-negative TorsinA-EQ construct, we also found that chaperones localize to blebs in the human neuroblastoma cell line SH-SY5Y (Extended Data Fig. 2b).

We additionally performed immunogold labeling and examined the ultrastructure of the NE with electron microscopy (EM) (Fig. 3b,c). While we did not detect DNAJB6 or HSPA1A at mature NPCs, DNAJB6 and HSPA1A localize within the bleb lumen (Fig. 3b,c). Thus, we conclude that multiple members of the HSP70 and HSP40 families become tightly sequestered into the bleb lumen in Torsin-deficient cells.

Neurons lacking TorsinA function sequester chaperones. As DYT1 dystonia is a neurological disease, we investigated whether the sequestration of chaperones occurs in neurons with compromised Torsin function. In mouse models of DYT1 dystonia, ≥80% of central nervous system nuclei exhibit NE blebs in eight-day-old mice [16]. This number decreases when expression of TorsinB begins after about 14 days [16]. We therefore cultured primary murine hippocampal neurons and transfected GFP with or without the dominant-negative TorsinA-EQ construct after four days *in vitro* (DIV4). Cells were processed for IF on DIV7 to recapitulate the

peak blebbing phenotype reported in conditional TorsinKO mice [16]. GFP was used to distinguish neurons from other cell types in the primary cultures.

In neurons with functional Torsins, the chaperones are diffuse throughout the cytosol/nucleoplasm (Fig. 3d-g). Upon expression of TorsinA-EQ, these chaperones become sequestered into blebs (Fig. 3d-g). MLF2-HA is also sequestered into blebs in Torsin-deficient neurons when overexpressed (Extended Data Fig. 2c). Thus, the sequestration of highly abundant and essential molecular chaperones into blebs is a conserved and general consequence of Torsin dysfunction.

MLF2 recruits DNAJB6 to blebs. To understand the relationship between MLF2 and chaperones, we depleted MLF2 from TorsinKO cells. Upon MLF2 knockdown, K48-Ub and HSPA1A remained efficiently sequestered into NE foci but DNAJB6 was no longer recruited to blebs (Fig. 4a). While the recruitment of HSPA1A to blebs was independent of MLF2, the small molecule VER-155008, which approximates the ADP-bound state of HSP70 [40], strongly promoted the recruitment of K48-Ub to blebs (Extended data 3a,b).

Next, we performed a radioimmunoprecipitation of endogenous HSPA1A from WT and TorsinKO cells under non-targeting or siMLF2 conditions (Fig. 4b). Two major co-immunoprecipitating bands were highly enriched in the TorsinKO siNT condition (Fig. 4b). The most prominent band around 28 kDa disappeared when MLF2 was knocked down, suggesting that HSPA1A interacts with significantly more MLF2 in TorsinKO cells than in WT (Fig. 4b). Another band unique to the TorsinKO siNT condition migrated at the expected molecular mass of DNAJB6 (27 kDa) and co-immunoprecipitates with HSPA1A exclusively in TorsinKO cells in an MLF2-dependent manner (Fig. 4b).

To test if this protein was DNAJB6, we performed both a DNAJB6 knockdown and a RE-IP wherein the HSPA1A co-immunoprecipitating proteins were dissociated and subjected to another IP using an antibody against DNAJB6 (Fig. 4c). When DNAJB6 was depleted by RNAi,

the band migrating around 27 kDa no longer co-immunoprecipitated with HSPA1A (Fig. 4c). Unexpectedly, less MLF2 co-immunoprecipitated with HSPA1A when DNAJB6 was depleted (Fig. 4c). Upon RE-IP, a single band migrating around 27 kDa was clearly detectable from TorsinKO cells (Fig.4c). We further confirmed this interaction by traditional co-IP (Fig. 4d). The recruitment of DNAJB6 to blebs strongly depended on the S/T-rich region within DNJAB6 and not the G/F-rich region (Extended Data Fig. 3c,d). Lastly, we confirmed the identity of the 27 kDa band by mass spectrometry as DNAJB6 (Extended Data Fig. 3e). We conclude that MLF2 recruits DNAJB6 to blebs where these proteins stably interact with HSPA1A.

Sequestering chaperones may contribute to proteotoxicity. DNAJB6 prevents the formation of toxic inclusions including polyglutamine (poly-Q) expansions [41-43]. Thus, we determined if this funciton is affected by sequestering DNAJB6 into blebs. In TorsinKO/MLF2 KO cells, DNAJB6 is recruited to poly-Q aggregates (Fig. 4e,f). However, upon re-introducing MLF2-HA via transient transfection, DNAJB6 is sequestered into blebs and away from the poly-Q aggregate (Fig. 4e,f). This titration of DNAJB6 out of an aggregate-prone client underscores the pronounced proteotoxic potential of NE blebs with MLF2 being a critical modulator of this property.

Sequestering protein into NE blebs requires Nup98. While analyzing the MLF2-APEX2 MS datasets, we noticed that specific Nups including Nup98 were enriched in samples from TorsinKO cells (Fig. 5a) [44]. Since the only protein known to localize to blebs in a K48-Ub-dependent manner is KSHV ORF10 (Fig. 1), which interacts with Nup98 [34], we prioritized our analysis on Nup98.

Depleting Nup98 provoked the formation of cytosolic granules composed of K48-Ub and FG-Nups to form in TorsinKO cells (Fig. 5b, Extended Data Fig. 4a). This phenotype can be rescued by an siRNA-resistant Nup98 construct but not by Nup96, which is derived from a Nup98-96 precursor protein through proteolytic cleavage [45] (Extended Data Fig. 4b-e). We also

examined whether other bleb components became incorporated into these cytosolic granules. Both MLF2-GFP and DNAJB6 also localize to these cytosolic puncta (Fig. 5c) while HSPA1A and HSC70 did not (Extended Data Fig. 4f). While we cannot rule out all possibilities of non-specific effects, knockdown of Nup98 did not significantly perturb nucleo/cytosolic transport (Extended Data Fig. 4g,h) Together, we conclude that the FG-Nup Nup98 is required for the NE bleb sequestration of granules composed of K48-Ub, MLF2, FG-Nups, and chaperones.

Overexpressing MLF2 decreases FG-Nup mislocalization. When MLF2-GFP was overexpressed in Nup98-depleted TorsinKO cells, we noticed a significant decrease in the amount of FG-Nup incorporation into the cytosolic granule (Fig. 5d,e). We calculated the nuclear/whole cell ratio of nucleoporins in TorsinKO cells under siNT, siNup98, or siNup98 + MLF2-FLAG (Fig. 5e). When Nup98 is depleted, significant FG-Nup mislocalization occurs and the nuclear/whole cell nucleoporin ratio decreases (Fig. 5e). However, when MLF2-FLAG is overexpressed in Nup98-depleted cells, the nuclear/whole cell nucleoporin ratio significantly increases (Fig. 5e). Thus, MLF2 may possess an FG-Nup directed activity.

Blebs share properties with condensates. The cytosolic granules that form upon siNup98 in TorsinKO cells were often spherical (Fig. 5b-d), prompting us to ask whether they may represent condensates. One strategy to probe the nature of such structures is to determine their sensitivity to 1,6-hexanediol, an alcohol that interrupts weak hydrophobic contacts and dissolves many phase separated condensates while preserving the integrity of the nuclear membrane (Extended Data Fig. 5e) [46, 47]. When exposed to 5% 1,6-hexanediol, the K48-Ub and MLF2-GFP granules typically observed in TorsinKO cells under siNup98 conditions were dissolved (Fig. 5f,g). This suggests that these cytosolic granules are indeed condensates potentially driven by FG-Nups.

The functional yeast ortholog of Nup98, Nup116, serves as “Velcro” to recruit other FG-Nups during NPC assembly [48]. We hypothesized that Nup98 may direct FG-Nups to blebs.

When we treat TorsinKO cells with 1,6-hexanediol, K48-Ub and MLF2-HA are released from blebs despite the NE remaining intact (Fig. 5h,i). To rule out that blebs contain terminally aggregated protein, we overexpressed polyQ-97-GFP and found the aggregates to be resistant to 1,6-hexanediol treatment (Extended Data Fig. 5a,b). Furthermore, the K48-Ub and MLF2 sequestered inside blebs was not dissociated by 2,5-hexanediol (Extended Data Fig. 5c) [49]. We note that the NPC permeability barrier established by FG-Nups was, as expected [46], partially broken down by 1,6-hexanediol (Extended Data Fig. 5d).

MLF2 and DNAJB6b immerse into FG-rich phases *in vitro*. MLF2 has a strikingly high methionine and arginine content (Extended Data Fig. 6a), two residues that specifically facilitate interactions with FG-domains [50]. Thus, the recruitment of MLF2 to blebs could rely on an FG-driven condensate. To address this, we purified FG-domains from the *Homo sapiens* Nup98, *Saccharomyces cerevisiae* Nup116, and *Tetrahymena thermophila* MacNup98A. Under denaturing conditions, these FG-domains do not phase separate [51]. However, upon dilution into buffer without denaturants, these FG-domains form condensates exhibiting selective permeability [50, 51] (Fig. 6a). We formed FG-rich phases and validated their selectivity with purified GFP derivatives 3B7C-GFP and sinGFP4a [50] (Fig. 6a). 3B7C-GFP behaves like an NTR while sinGFP4a is excluded from the phases [50] (Fig. 6a).

In Torsin-deficient cells, MLF2 localizes to FG-rich blebs where it interacts with chaperones (Fig. 4b-d). HSP70s represent the most abundant of these (Fig. 4b,c). Thus, to recapitulate the bleb lumen environment *in vitro*, we purified the MLF2:HSP70 complex from mammalian cells (Extended Data Fig. 6b,c) and tested the ability for MLF2 to immerse into FG-rich condensates (Fig. 6a). We tagged MLF2 with a C-terminal Atto488 label and found it immersed into ScNup116 and TtMacNup98A phases but remained mostly at the surface of HsNup98 condensates (Fig. 6a). To exclude the possibility that HSP70 brings MLF2:HSP70 into the phase, we purified and Atto488 tagged HSPA1A (Fig. 6b). Unlike DNAJB6b-Atto488, which

we find to immerse into FG condensates, HSPA1A-Atto488 is nearly completely excluded (Fig. 6b). Thus, HSP70 is unlikely to be the major factor driving MLF2:HSP70 into Nup phases. Taken together, we conclude that MLF2 and DNAJB6b interact with phylogenetically diverse FG-domains.

Condensates have distinct properties when formed with MLF2. FG-rich condensates formed in the presence of MLF2:HSP70 were significantly larger compared to other conditions (Fig. 6a). To quantify this effect, we performed dynamic light scattering (DLS) to obtain the distribution of apparent radii for ScNup116 condensates under different conditions. When solutions containing MLF2:HSP70, DNAJB6b, or denatured Nup116 were analyzed by DLS, small condensates (<10 nm radius) corresponding to protein monomers were detected (Fig. 6c). Diluting ScNup116 into non-denaturing buffer caused significantly larger condensates (≥1,000 nm radius) to be detected as condensation occurred (Fig. 6d).

When ScNup116 condensates were formed in the presence of DNAJB6b or HSPA1A, we observed condensates with a similar size distribution compared to ScNup116 alone (Fig. 6d). However, when the ScNup116 condensates were formed in the presence of MLF2:HSP70, a pronounced shift towards larger condensate sizes occurred (Fig. 6d). This suggests that MLF2:HSP70 possesses an FG-Nup directed activity.

DNAJB6b and MLF2:HSP70 compete with an NTR-like molecule. An important consequence of DNAJB6b or MLF2:HSP70 interacting with FG-rich condensates is that they prevent the full partition of 3B7C-GFP into the phase (Extended Data Fig. 6d). This is not the case when condensates are formed in the presence of HSPA1A, which is excluded from the phase (Fig. 6b, Extended Data Fig. 6d). While this may result from an excluded volume effect or from competition for binding sites in FG domains, this observation may explain why blebs are completely devoid of NTRs despite harboring FG-Nups (Supplemental Tables 1,2) [18, 22].

Chaperones preserve FG-Nup condensate integrity over time. After three hours in solution, ScNup116 and TtMacNup98A condensates largely disassociate (Fig. 6e,g, Extended Data Fig. 7a,b). In the presence of MLF2:HSP70, however, the condensates shrink but remain intact (Fig. 6e, Extended Data Fig. 7b). When WT DNAJB6b is included with MLF2:HSP70, ScNup116 and TtMacNup98A condensates remain largely unchanged after three hours (Fig. 6e,h). In contrast, when the H31Q-DNAJB6b mutant is included, which cannot interact with HSP70, the FG-rich condensates are strongly disassociated (Fig. 6f, Extended Data Fig. 7c). This illustrates a dominant-negative FG-directed activity for H31Q-DNAJB6b (Fig. 6e,f). While the WT DNAJB6b:HSP70 complex preserves small clusters of condensates, this was not as uniform or penetrant as the effect by the complete MLF2:HSP70:DNAJB6b complex (Fig. 6f-h, Extended Data Fig. 7c). Taken together, these data suggest that the MLF2:HSP70 complex maintains FG-rich condensates over time, an activity that is enhanced by DNAJB6b.

The MLF2:HSP70 complex reduces FG-Nup amyloid formation. The ScNup116 FG domain is known to form cross-β amyloid-like structures [51, 52]. Initially, ScNup116 does not form amyloids as the condensates are readily reversable (Extended Data Fig. 7d). The transition to amyloids is detectable by the dye Thioflavin-T (ThT), which fluoresces upon interacting with amyloids (Extended Data Fig. 7e). We monitored ThT fluorescence of solutions containing ScNup116 plus HSPA1A, DNAJB6b, or MLF2:HSP70 (Extended Data Fig. 7f,g). While neither HSPA1A nor DNAJB6b affected ScNup116 amyloid formation, MLF2:HSP70 reduced it by approximately half in an ATP-dependent manner even at a sub-stoichiometric concentration (Extended Data Fig. 7f). We found that the DNAJB6b-HSP70 complex has a similar ATP-dependent, sub-stoichiometric ability to reduce amyloid formation (Extended Data Fig. 7g). Amyloid formation was most potently suppressed in the presence of ATP upon inclusion of MLF2,

HSPA1A, and DNAJB6 (Extended Data Fig. 7g). These data reveal an additional FG-Nup directed activity of the chaperone network identified herein.

Discussion

In this study, we developed a virally-derived model substrate (Δ133 ORF10, Fig. 1) to explore the molecular composition and cellular consequences of NE herniations that arise in disease models of primary dystonia. While NE blebs are striking morphological features in dystonia model systems and found in other experimental settings [53], it has generally been unclear whether NE blebs contribute to disease development. Using Δ133 ORF10 and the APEX-derivatized MLF2 in a comparative proteomics approach, we found that blebs are highly enriched for the FG-Nup Nup98 and specific members of the HSP40 and HSP70 chaperone family (Fig. 2). In cells with perturbed Torsin function, these chaperones become tightly sequestered within the lumen of NE blebs and are titrated away from their normal subcellular localization (Fig. 3). Importantly, this sequestration also occurs in primary neurons with perturbed Torsin function (Fig. 3). This raises the question of what mechanisms are at work to cause this unusual sequestration.

We demonstrate that NE blebs contain FG-rich condensates (Fig. 5) that impose two proteotoxic challenges: an unprecedented degree of chaperone sequestration that is typically only observed upon overexpression of disease alleles, and a profound stabilization of normally short-lived proteins (Fig. 1e,f). We furthermore find that MLF2 affects FG-domain condensation (Fig. 5d,f, Fig. 6, Extended Data Fig. 7). Our observation that MLF2 expression results in a near-complete re-distribution of DNAJB6–a critical factor for suppressing proteotoxic aggregation [41, 43] – from poly-Q inclusions to NE blebs (Fig. 4e,f) establishes MLF2 as an important player in protein homeostasis. Taken together, we uncover a direct proteotoxic contribution of blebs to DYT1 dystonia pathology and a role for MLF2, HSPA1A, and DNAJB6 in the formation and maintenance of FG-rich phases.

While NTRs function as FG-Nup-directed chaperones during postmitotic NPC assembly [54], interphase NPC biogenesis follows a distinct insertion pathway [55]. We demonstrate that MLF2 overexpression prevents the ectopic accumulation of FG-Nups upon Nup98 depletion (Fig. 5d,e). It is therefore tempting to speculate that non-NTR chaperones like MLF2 and DNAJB6

function during interphase NPC biogenesis to prevent premature FG-Nup assembly. Indeed, Kuiper et al. have independently assigned DNAJB6 to a role in NPC biogenesis [56]. *In vitro*, we find that MLF2:HSP70 and DNAJB6 prevent the full partition of NTR-like molecules into FG-Nup phases (Extended Data Fig. 6d). While this may be explained by excluded volume effects or a competition mechanism, either scenario would result in fewer NTR-FG domain interactions, consistent with our observation that bulk nuclear transport cargo is excluded from FG-rich NE blebs [18, 22].

We previously reported that MLF2-GFP accumulates at sites of NE developing membrane curvature in Torsin-deficient cells [22]. This clustering of MLF2 juxtaposed against the curved NE may represent nucleation events of FG-Nups undergoing condensation at sites of *de novo* interphase NPC assembly. This *in vivo* role for MLF2 would reflect the activity we report *in vitro* (Fig. 6c-h, Extended Data Fig. 7).

Our proteomic experiments reveal a specific enrichment of class B HSP40s inside blebs. While future work will be required to understand whether an active exclusion of other HSP40 classes exists, we propose that DNAJB2 and DNAJB6 are recruited by the specific properties of these HSP40s. Future studies are warranted to understand whether MLF2 interacts with other HSP40 classes, and if other HSP40s can immerse into condensates as exemplified here for DNAJB6 (Fig. 6b).

The observation that mutations in ER/NE-luminal Torsin ATPases give rise to an indirect proteotoxic mechanism across compartmental borders is unexpected. This feature adds a unique disease mechanism to the growing list of movement disorders with functional ties between liquid-liquid phase separation, nuclear transport machinery, and proteotoxicity [57-59]. Our finding that NE blebs exert a twofold proteotoxicity also represents a distinct pathological mechanism from the documented nuclear transport defects that arise in Torsin-deficient cells due to compromised NPC assembly [12, 20-22] (Extended Data Fig. 8).

We propose that this dual proteotoxicity mechanism contributes to DYT1 dystonia's unusual disease manifestation. Unlike other congenital movement disorders, DYT1 dystonia is characterized by a limited window of onset. After the age of 30, carriers of the DYT1 mutation will never develop the disease [60]. Furthermore, the disease displays a reduced penetration as only one third of all mutation carriers develop DYT1 dystonia [11]. These features may be explained by the fact that blebs are transient structures that resolve in model organisms after TorsinB is upregulated [16, 61]. Thus, the proteotoxicity imposed by blebs is confined to a specific window in life—likely closing before the age of 30. We propose that sequestered chaperones and accumulated short-lived proteins confer this window of vulnerability and generate a high but potentially manageable degree of proteotoxic stress. Further insult on the PQC machinery that may normally be inconsequential could cause severe problems in these pre-sensitized cells. This model describes a stochastic and previously underappreciated influence on disease manifestation (Extended Data Fig. 8). While additional studies will be required to test these ideas, our data provide a strong motivation to investigate pharmacological modulators of the cellular PQC system for DYT1 dystonia prevention and management.

Acknowledgements

This work is supported by NIH R01GM114401 (CS), DOD PR200788 (CS), NIH 5T32GM007223-44 (SMP), NIH F31NS120528 (SMP), NIH R56MH122449 (AJK), NIH R01MH115939 (AJK), NIH NS105640 (AJK), NIH F31MH116571 (JEG) and the Dystonia Medical Research Foundation (CS and AJR). The mass spectrometers and accompanying biotechnology tools at the Keck MS & Proteomics Resource at Yale University were funded in part by the Yale School of Medicine and by the Office of the Director, National Institutes of Health (S10OD02365101A1, S10OD019967, and S10OD018034). We thank Dirk Görlich and members of his laboratory for sharing reagents. We thank the Yale Keck Biophysical Resource Center, Morven Graham, and the Yale Center for Cellular and Molecular Imaging. We also thank the MS & Proteomics Resource at Yale University for providing the necessary mass spectrometers and the accompany biotechnology tools funded in part by the Yale School of Medicine and by the Office of The Director, National Institutes of Health. The funders had no role in study design, data collection and analysis, decision to publish, or preparation of the manuscript.

Author contributions

SMP, AJR, JEG, RFN, SM, AJK, and CS conceptualized and designed experiments. SMP, AJR, JEG, RFN, and SM performed experiments. SMP, AJR, JEG, RFN, SM, AJK, and CS analyzed and interpreted data. SMP and CS wrote the original manuscript. SMP, AJR, JEG, RFN, AJK, and CS edited the manuscript.

Competing interests statement

The authors declare no competing interests.

Methods

This research complies with all relevant ethical regulations. All experiments using animal models were approved by the Yale University School of Medicine Institutional Animal Care and Use Committee as described in protocol 2022-07912.

Antibodies and reagents

All cell lines, bacterial strains, antibodies, reagents, and oligonucleotides used in this study can be found in Supplemental tables 5-8.

Cell culture and cell lines

HeLa, SH-SY5Y, and HEK293T cells were maintained in Dulbecco's modified Eagle's medium (DMEM) supplemented with 10% v/v FBS (Thermo Fisher Scientific) and 100 U/mL of penicillin-streptomycin (Thermo Fisher Scientific). Cells were routinely checked for mycoplasma and determined to be free of contamination through the absence of extranuclear Hoechst 33342 (Life Technologies) staining.

Expi293 suspension cells were cultured at 37ºC in flat-bottom shaking flasks in preformulated Expi293 Expression Media (Gibco, A1435102) in an 8% CO_2 atmosphere.

To generate stable HeLa cell lines expressing MLF2-APEX2-HA, 6 µg was transiently transfected into HEK293T cells along with 2 µg of MMLV gag/pol and 1 µg of the viral envelope protein VSV-G. After 72 hours of expression, the supernatant was collected and filtered through a 0.45 µm filter before storage at -80°C. HeLa cells were seeded in 6-well plates and transduced with 100 µL viral supernatant plus 4 µg/mL polybrene reagent (Sigma-Aldrich). After 24 hours, media was switched to contain 1 µg/mL of puromycin (Sigma-Aldrich). Antibiotic selection was performed for 7 days before the dox-inducible MLF2-APEX2-HA expression was verified.

Plasmids, transient RNAi knockdowns, and transient transfections

KSHV ORF10-HA was synthesized by Genscript into the pcDNA3.1 vector. ∆133 ORF10-HA was cloned from the full lenth cDNA into pcDNA3.1. Plasmids containing the deubiquitylating enzyme M48 [35] were a gift from Hidde L. Ploegh (Whitehead Institute for Biomedical Research, Cambridge, MA). MLF2-HA and MLF2-GFP were cloned into pcDNA3.1 or pEGFP-N1 using standard molecular cloning techniques. polyQ-72-GFP and polyQ-97-GFP were a gift from Susan Lindquist (Addgene plasmid # 1179; http://n2t.net/addgene:1179; RRID:Addgene_1179, Addgene plasmid # 1180; http://n2t.net/addgene:1180; RRID:Addgene_1180) [62]. These polyQ constructs were subcloned into pcDNA3.1 using standard cloning techniques.

MLF2-APEX2-HA was cloned into the pRetroX-Tight-Pur vector from pcDNA3.1 using standard cloning techniques. mito-V5-APEX2 was a gift from Alice Ting (Addgene plasmid # 72480; http://n2t.net/addgene:72480; RRID:Addgene_72480) [36].

DNAJB6b-ΔG/F-HA and DNAJB6b-ΔG/F-S/T-HA were synthesized by Genscript into the pcDNA3.1 vector. The G/F-rich region was defined as G72-G131 and the S/T-rich region as S132-T195. All phenylalanine residues within these regions were mutated to alanine to generate the DNAJB6b mutants.

pCMV-PV-NES-GFP was a gift from Anton Bennett (Addgene plasmid # 17301; http://n2t.net/addgene:17301; RRID:Addgene_17301) [63].

The plasmids containing His-tagged 3B7C-GFP, sinGFP4a, HsNup98, TtMacNup98A, and ScNup116 FG domains were gifts from Dirk Görlich (Max Planck Institute for Biophysical Chemistry, Göttingen, Germany) [50, 51].

MLF2-LPEXTG-Tev-MBP-His-FLAG, DNAJB6b-LPETG-His and HSPA1A-LPETG-His were synthesized by Genscript into pcDNA3.1 (for the MLF2 construct) or pET11a (DNAJB6b and HSPA1A constructs). The LPETG motif was included as a sortase enzyme recognition motif for tagging with the Atto488 dye.

Nontargeting RNAi and RNAi targeting MLF2, DNAJB6, and Nup98 were performed with SMARTpool oligos from Horizon Discovery. Knockdown efficiency was validated by quantitative PCR (qPCR) using iQ SYBR Green mix with a CFX Real-Time PCR 639 Detection System (Bio-Rad). For each knockdown, we employed the comparative Ct method using the internal control transcript RPL32 [22]. All primers were synthesized by Integrated DNA Technologies.

All plasmid transfections were performed with Lipfectamine 2000 (Invitrogen) according to manufacturer's instructions and allowed to express for 24 hours prior to analyses. All RNAi knockdowns were performed with Lipfectamine RNAiMAX (Invitrogen) according to manufacturer's instructions and allowed to incubate for 48 hours before analyses.

CRISPR/Cas9 generation of MLF2 knockout

To generate MLF2 KO HeLa cells, we employed the CRISPR/Cas9 system [64] as previously implemented [65]. Briefly, a guide RNA targeting MLF2 was cloned into the px459 vector and transfected into HeLa cells. pSpCas9(BB)-2A-Puro (px459) V2.0 was a gift from Feng Zhang (Addgene plasmid # 62988 ; http://n2t.net/addgene:62988 ; RRID:Addgene_62988) [66]. The transfected cells underwent antibiotic selection for 48 hours via treatment with 0.4 μg/mL puromycin (Thermo Fisher Scientific). After selection, cells were seeded at a low density such that single-cell colonies could be isolated after 10 days in culture. These colonies were expanded and screened for MLF2 knockout by genotyping PCR [65].

Hippocampal cultures, transfection, and immunofluorescence

Hippocampal cultures were performed using seven mixed sex BALB/c P0 pups in accordance with IACUC protocol number 2022-07912 (Yale University School of Medicine IACUC). Hypothermia was induced in pups, followed by decapitation and hippocampal dissection. Hippocampi were dissociated using 200 units Papain (Worthington LS003124, 200 U) and were plated on 14 mm poly-D-lysine coated coverslips in a 24 well dish at a density of 150,000 cells/well. Neurons were transfected at DIV 4 with 1 µL per reaction of Lipofectamine 2000 (Thermo Fisher Scientific) at a concentration of 0.6 µg per plasmid, for a total of 1.8 µg of DNA. Neurons were fixed at DIV 7 with 4% v/v paraformaldehyde (PFA) in PBS at room temperature for 15 minutes, permeabilized with 0.1% v/v Triton-X for 15 minutes, blocked with 1% w/v BSA for one hour, and stained with primary antibodies in blocking buffer overnight at 4°C (1:1000 rat HA, 1:200 rabbit TorsinA). Following the primary stain, coverslips were washed with PBST three times for 5 minutes, followed by a secondary antibody stain in blocking buffer for 1 hour at room temperature (1:1000 rat Alexa 568 and rabbit 633). Coverslips were washed with PBST three times for 5 minutes, stained with DAPI for 10 minutes at room temperature, washed with PBST three times for 5 minutes, and mounted in Aqua-Mount (Lerner Laboratories).

Immunofluorescence and confocal microscopy

HeLa and SH-SY5Y cells were grown on coverslips and prepared for IF by fixing in 4% v/v PFA (Thermo Fisher Scientific), permeabilized in 0.1% v/v Triton X-100 (Sigma-Aldrich) for 10 minutes, then blocked in 4% w/v bovine serum albumin (BSA). Primary antibodies were diluted into 4% w/v BSA and incubated with coverslips for 45 minutes at RT. After extensive washing with PBS, fluorescent secondary antibodies were diluted in 4% w/v BSA and incubated with coverslips for 45 minutes. Cells were stained with Hoechst 33342 (Life Technologies) before mounting onto slides with Fluoromount-G (Southern Biotech).

For hexanediol experiments, cells were incubated for five minutes with complete DMEM containing 5% w/v hexanediol (Millipore) before fixing in 4% v/v PFA and processing for IF as described above. VER-155008 was dissolved in DMSO at a stock concentration of 10 mM and used at a final concentration of 20 μM for 24 hours prior to fixation for IF.

Phase separated condensates were imaged by spotting a 10 μL volume of the indicated conditions onto a glass bottom dish (WillCo Wells). To visualize effects of protein on Nups after three hours, FG phases were formed in supplemented TBS (50 mM Tris (pH 7.5), 150 mM NaCl, 2 mM DTT, 10 mM $Mg(CH_3COO)_2$, 10 mM $K(CH_3COO)_2$, 4 mM creatine phosphate, 0.25 μL creatine kinase, 2 mM ATP). Where indicated, ATP was omitted from the supplemented TBS (the ATP regenerating system remained). Incubation took place at 30ºC.

All images were collected on an LSM 880 laser scanning confocal microscope (Zeiss) with a C Plan-Apochromat 63×/1.40 oil DIC M27 objective using ZEN v2.1 & v3.4 software (Zeiss).

Spectroscopic measurements of Nup solutions

Turbidity of Nup solutions was measured at an excitation and emission wavelength of 550 nm (Synergy Mx, BioTek Instruments, Inc).

To monitor ScNup116 amyloid formation, Nups were diluted into supplemented TBS with the indicated proteins. Solutions were brought to 2 μM ThT. Bottom reads of ThT fluorescence (excitation 440 nm, emission 480 nm) were captured every two minutes at 30ºC for 24 hours (Synergy Mx, BioTek Instruments, Inc).

Cycloheximide chase

WT and TorsinKO cells were plated in a 10 cm dish and transfected with Δ133 ORF10-HA. After 24 hours of expression, each cell line was trypsinized and split into two tubes. Tubes were incubated at 37°C with gentle shaking and treated with either DMSO or 100 μg/mL CHX and

aliquots were taken at 0, 1, 2, 3, or 4 hours post treatment. Cells were collected via centrifugation and subjected to immunoblot for analyses.

Immunoprecipitation, mass spectrometry preparation, and immunoblot analysis

For native IP experiments, cells were transfected with the indicated constructs 24 hours before harvesting. Cells were lysed in NET buffer (150 mM NaCl, 50 mM Tris pH 7.4, 0.5% v/v NP-40) supplemented with EDTA-free protease inhibitor cocktail (Roche) and 5 mM NEM (Sigma-Aldrich). Immunoprecipitation was conducted with pre-cleared lysates on anti-HA affinity matrix (Roche), magnetic beads conjugated to streptavidin, or magnetic protein G beads (Pierce) non-covalently coupled to anti-HSPA1A. Stable interactions were eluted for immunoblot analyses in 30 µL of 2x SDS reducing buffer and heated at 70°C for five minutes. For mass spectrometry applications, protein complexes were briefly run into SDS-PAGE gels, stained with SimplyBlue Safe Stain (Thermo Fisher Scientific) before bands of 2-4 mm were extracted. Gel bands were submitted to the MS & Proteomics Resource at the Yale University Keck Biotechnology Laboratory.

Radioimmunoprecipitations were carried out in as described previously [4, 67]. Briefly, metabolically labeled cells were grown in complete DMEM containing 150 µCi/mL ^{35}S-Cys/Met labeling mix (PerkinElmer) for 16 hours prior to lysis in NET buffer. Co-eluting protein were detected by autoradiography and imaged on a Typhoon laser-scanning platform (Cytiva).

Immunoblotting was carried out with IP eluates or cell lysates in supplemented NET buffer. Equal micrograms of protein were resolved in SDS-PAGE gels (Bio-Rad) and transferred onto PVDF membranes (Bio-Rad). Membranes were blocked in 5% w/v milk in PBS + 0.1% v/v Tween-20 (Sigma-Aldrich). Primary and HRP-conjugated secondary antibodies were diluted in blocking buffer. Blots were visualized by chemiluminescence on a ChemiDoc Gel Imaging System (Bio-Rad).

APEX2 reaction and NE enrichment

To induce the expression of MLF2-APEX2-HA, cells were treated with 500 µg/mL dox for 24 hours. After 24 hours, cells were incubated for 30 minutes with complete DMEM containing 500 µM biotin phenol. For the APEX2 reaction, cells were treated with 1 mM H_2O_2 for one minute before quenching by washing the plates three times with quenching buffer (PBS, pH 7.4, 0.5 mM $MgCl_2$, 1 mM $CaCl_2$, 5 mM Trolox, 10 mM sodium ascorbate, 10 mM sodium azide). Cells were collected and enriched for NE fractions as described previously [22, 68]. Briefly, cells were gently pelleted in buffer containing 250 mM sucrose and homogenized via trituration through a 25-guage needle. The homogenates were layered onto a 0.9 M sucrose buffer and spun down. The pellets (membrane fractions and nuclei) were solubilized overnight in buffer without sucrose containing benzonase, heparin, NEM, and protease inhibitors. The solubilized nuclei were spun at 15,000 x g for 45 minutes and the supernatant was collected as the nucleoplasm and pellet as the NE/ER enriched fraction. The ER/NE fraction was solubilized in 8 M urea and equal amounts of protein were loaded onto streptavidin beads for capture of biotinylated protein, which were analyzed by immunoblot or mass spectrometry.

Transmission electron microscopy and immunogold labeling

Electron microscopy (EM) and immunogold labeling was performed as previously described [18, 22] at the Yale School of Medicine's Center for Cellular and Molecular Imaging. Briefly, cells were fixed by high-pressure freezing (Leica EM HPM100) and freeze substitution (Leica AFS) was carried out at 2,000 pounds/square inch in 0.1% w/v uranyl acetate/acetone. Samples were infiltrated into Lowicryl HM20 resin (Electron Microscopy Science) and sectioned onto Formvar/carbon-coated nickel grids for immunolabeling.

Samples were blocked in 1% w/v fish skin gelatin, then incubated with primary antibodies diluted 1:50 in blocking buffer. 10 nm protein A-gold particles (Utrecht Medical Center) were used to detect the primary antibodies and grids were stained with 2% w/v uranyl acetate and lead citrate.

Images were captured with an FEI Tecnai Biotwin TEM at 80Kv equipped with a Morada CCD and iTEM (Olympus) software.

Recombinant protein expression and purification

HsNup98, TtMacNup98A, and ScNup116 [50, 51] were purified from BL21(DE3) *E. coli* strains under denaturing conditions by virtue of an N-terminal His_{18} tag. Cell pellets containing the FG domains were resuspended in denaturing lysis buffer (8 M urea, 150 mM NaCl, 50 mM Tris (pH 8), 20 mM imidazole, 10 mM β-me, 2 mM PMSF). Solubilized His-tagged Nups were complexed with Ni-NTA agarose (Qiagen) at 4ºC for 16 hours before the columns were extensively washed at room temperature (6 M urea, 150 mM NaCl, 50 mM Tris (pH 8), 25 mM imidazole, 10 mM β-me). Protein was eluted in room temperature elution buffer (6 M urea, 150 mM NaCl, 50 mM Tris (pH 8), 400 mM imidazole, 10 mM β-me) and dialyzed overnight at 4°C into UTS buffer (2 M urea, 150 mM NaCl, 50 mM Tris (pH 7.4)). Finally, the dialyzed Nup was concentrated to 500 μM using a Macrosep 10,000 MWCO centrifugation unit (Pall Corporation).

Phase separated condensates were formed by diluting 500 μM Nup stock solutions in denaturing UTS buffer into tris-buffered saline (TBS; 50 mM Tris (pH 7.4), 150 mM NaCl) to a final concentration of 10 μM [51].

His-tagged GFP variants were purified as previously described [50]. BL21(DE3) [50, 69] cell pellets containing His-*Brachypodium distachyon* (bd)-SUMO-sinGFP4a or His-bdSUMO-3B7C-GFP[50, 69] were resuspended in resuspension buffer (50 mM Tris (pH 7.5), 150 mM NaCl, 10 mM β-Me, 20 mM imidazole, 1 mM PMSF) and passed through the French Press. His-tagged proteins were bound to Ni-NTA agarose (Qiagen) for 1 hour at 4°C before washing in resuspension buffer. GFP constructs were eluted in resuspension buffer containing 400 mM

imidazole, then concentrated with a Macrosep 10,000 MWCO centrifugation unit (Pall Corporation). Final concentrates were buffer-exchanged into TBS.

DNAJB6b-LPETG-His_{10} was purified as previously described [70]. BL21(DE3) cell pellets were resuspended in resuspension buffer (100 mM Tris (pH 8), 150 mM KCl, 10 mM β-Me, 1 mM PMSF) and were passed through the French Press DNAJB6b-LPETG-His_{10} was solubilized from inclusion bodies in pellet buffer (100 mM Tris (pH 8), 8 M urea, 150 mM KCl, 20 mM imidazole, 10 mM β-Me, 1 mM PMSF). DNAJB6b-LPETG-His_{10} was allowed to bind Ni-NTA agarose (Qiagen) for 1 hour at 4°C. The matrix was washed (100 mM Tris (pH 8), 8 M urea, 150 mM KCl, 20 mM imidazole, 10 mM β-Me) and DNAJB6-LPETG-His_{10} was eluted in elution buffer (100 mM Tris (pH 8), 150 mM KCl, 10 mM β-Me, 350 mM imidazole). The protein was dialyzed overnight into final buffer (50 mM Tris (pH 7.5), 150 mM KCl) and concentrated with a Macrosep 10,000 MWCO centrifugation unit (Pall Corporation).

HSPA1A-LPETG-His_{10}-FLAG was purified from BL21(DE3) cells resuspended in resuspension buffer (100 mM HEPES (pH 8), 500 mM NaCl, 10% v/v glycerol, 10 mM β-Me, 20 mM imidazole, 1 mM PMSF) and passed through the French Press The supernatant was applied to Ni-NTA agarose (Qiagen) for 1 hour at 4ºC. The matrix was washed (30 mM HEPES (pH 7.4), 500 mM NaCl, 10% v/v glycerol, 20 mM imidazole, 10 mM β-Me) and protein was eluted in wash buffer with 400 mM imidazole. Protein was dialyzed overnight into TBS and concentrated as described above.

The MLF2-LPETG-TEV-MBP-His-FLAG:HSP70 complex was purified from a mammalian Expi293 suspension system. Cells were harvested after 72 hours of expression and pellets were lysed in ice cold lysis buffer (50 mM Tris (pH 7.5), 150 mM NaCl, 1% w/v DDM, 10% v/v glycerol, protease inhibitor tablet (Roche)). Clarified supernatant was applied to anti-FLAG M2 Affinity Gel

(Sigma-Aldrich) and allowed to bind overnight at 4°C. The matrix was washed (50 mM Tris (pH 7.5), 150 mM NaCl, 0.05% w/v DDM), then washed with buffer minus detergent. Protein was eluted in final buffer (50 mM Tris (pH 7.5), 150 mM NaCl, 0.3 mg/mL FLAG peptide) for 1 hour at 4°C. TEV enzyme (New England BioLabs) was added to the elution and the mixture was dialyzed overnight into TBS. The resulting MLF2:HSP70 complex was concentrated as described above.

Atto-tagging via the sortase reaction

To produce Atto488-tagged MLF2, DNAJB6b, and HSPA1A, constructs were purified with an LPETG sortase recognition sequence between the C-terminal end and the downstream purification tag. This motif is recognized by the transpeptidase sortase, which catalyzes a reaction wherein a molecule harboring a poly-glycine label is attached to the LPETG sequence [71]. Reactions were carried out using purified MLF2-LPETG, DNAJB6b-LPETG, or HSPA1A-LPETG and the Sortag-IT™ ATTO 488 Labeling Kit (Active Motif) according to manufacturer's instructions. After the sortase reaction, free dye was removed from the Atto-tagged proteins by washing extensively with TBS in Amicon Ultra-0.5 mL Centrifugal Filters (MilliporeSigma), then running through a PD MiniTrap desalting column (Cytiva).

Dynamic light scattering

DLS was used to assess the size distribution of FG-rich condensates forming the in presence or absence of MLF2:HSP70. Measurements were taken on a DynaPro Titan DLS instrument (Wyatt Technologies) at 25°C and data were analyzed using DYNAMICS software (Wyatt Technologies). 10 µL reactions of 10 µM ScNup116 in TBS containing no additional protein, 5 µM MLF2:HSP70, 5 µM HSPA1A, or 5 µM DNAJB6b were allowed to form for one minute before diluting 1:10 in TBS. 30 µL of this dilution was transferred to a quartz cuvette and datasets of 100 measurements of five-second acquisition times were collected.

Image processing

The number of immunogold beads against HSPA1A or DNAJB6 was manually counted for 400 μm^2 centered around the NE from WT or TorsinKO cells (Fig. 3c). The number of immunogold beads was quantified for a square of 2 µm by 2 µm with the NE in the middle. This value was obtained for 100 2x2 µm squares centered around the NE.

The ratio of DNAJB6 within polyQ aggregates compared to the whole cell was calculated using Fiji Software [72] (Fig. 4f). The DNAJB6 antibody signal intensity was obtained by defining a region of interest (ROI) within the polyQ aggregate (Q), then of the whole cell (W). The ratio of Q/W was calculated for at least eight cells/condition.

The rescue effect of MLF2 on FG-Nup mislocalization (Fig. 5e) was determined for 94 cells/condition. The nucleoporin (Mab414 antibody) signal intensity in the whole cell and the nucleus was quantified using Fiji by selecting these as ROIs. From these values, the ratio of nuclear Mab414 intensity to whole cell intensity was calculated.

The presence of cytosolic granules under siNup98 conditions (Fig. 5g, Extended Data Fig. 4c) was determined by visualizing the presence or absence of cytosolic K48-Ub deposits for 300 cells/condition.

To quantify the number of NE-associated K48-Ub foci in TorsinKO cells treated with 1,6-hexanediol (Fig. 5i), the nucleus was selected in Fiji as the region of interest (ROI) and the number of foci was quantified as previously performed [18, 22]. The “Find Maxima” function was employed with a noise tolerance of 10. Foci were quantified for 100 cells/condition.

The nuclear to cytoplasmic (N/C) ratio of the Ran GTPase under siNT or siNup98 was quantified using CellProfiler software [73] (Extended Data Fig. 4h). Briefly, the Ran IF signal was quantified

within cell regions co-localizing or not co-localizing with DAPI stain to define the nuclear and cytoplasmic regions, respectively. These values were used to calculate the N/C ratio for 85 cells/condition.

The 3B7C-GFP signal intensity was determined in Fiji using the measure function (Extended Data Fig. 6d). The center of Nup condensates was selected as an ROI, then the average GFP signal intensity was measured for 100 condensates/condition.

Statistics and reproducibility

All data were considered representative by repeating experiments at least three times with similar results or using three independent samples for analysis. Datasets were tested for normality using the Shapiro-Wilk test. If found to be normally distributed, datasets were analyzed using a two-tailed unpaired *t*-test. Datasets not normally distributed were analyzed with a two-tailed unpaired Mann-Whitney test. GraphPad Prism 9.4.0 was used for all statistical analyses. *P* values <0.05 were considered significant. Data are displayed with the mean value indicated and error bars showing the standard deviation (SD). No statistical method was used to predetermine sample size. No data were excluded from the analyses. The Investigators were not blinded to allocation during experiments and outcome assessment. The experiments were not randomized.

Data availability statement

Mass spectrometry datasets are uploaded to the massIVE database (Supplemental Table 1 accession MSV000090177. Supplemental Table 2 accession number MSV000090186. Supplemental Table 3 accession number MSV000090187. Supplemental Table 4 accession number MSV000090188). The mass spectrometry proteomics data have been deposited to the ProteomeXchange Consortium via the PRIDE partner repository with the following accession numbers: Supplemental Table 1, PXD036262. Supplemental Table 2, PXD036264. Supplemental Table 3, PXD036266. Supplemental Table 4, PXD036267. Source data for all graphical

representations and unprocessed blot images are provided. All other data supporting the findings of this study are available from the corresponding author on reasonable request.

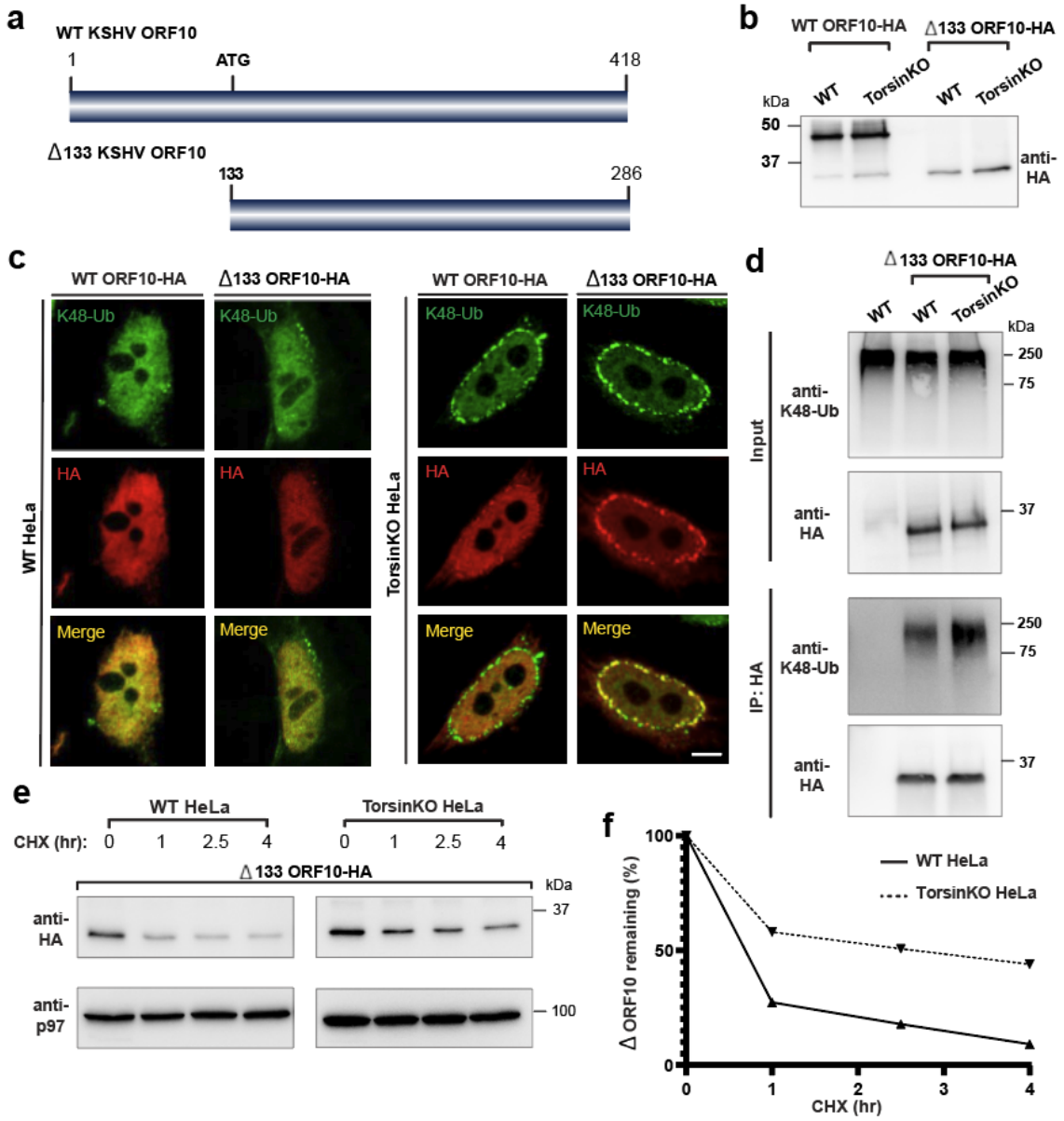

Figure 1. **NE herniations arising from Torsin ATPase deficiency sequester and stabilize short-lived protein. a**, Schematic model of the ORF10 protein from KSHV. KSHV ORF10 contains an internal start codon at residue 133 that produces Δ133 ORF10. **b**, Immunoblot demonstrating expression of Δ133 ORF10-HA in WT and TorsinKO HeLa cells 24 hours post transfection. Note that ORF10-HA is produced as a major full-length protein a lower abundance

Δ133 product. **c**, Representative IF images of full length and Δ133 ORF10-HA in WT and TorsinKO cells. Scale bar, 5 μm. **d**, Anti-HA immunoprecipitation (IP) from WT or TorsinKO cells expressing Δ133 ORF10-HA. The IP was probed with antibodies against K48-Ub and HA. Note that Δ133 ORF10-HA is associated with more K48-Ub in TorsinKO than WT cells. **e**, A cycloheximide (CHX) chase over four hours in WT and TorsinKO cells expressing Δ133 ORF10-HA. Cells were treated with 100 μg/mL of CHX at 37°C for the indicated timepoints. p97 serves as a loading control. **f**, Relative percentage of Δ133 ORF10-HA obtained in (**e**) was determined via densitometry by comparing to the abundance at time = 0. All data were standardized to p97 levels. Source numerical data and unprocessed blots are available in source data.

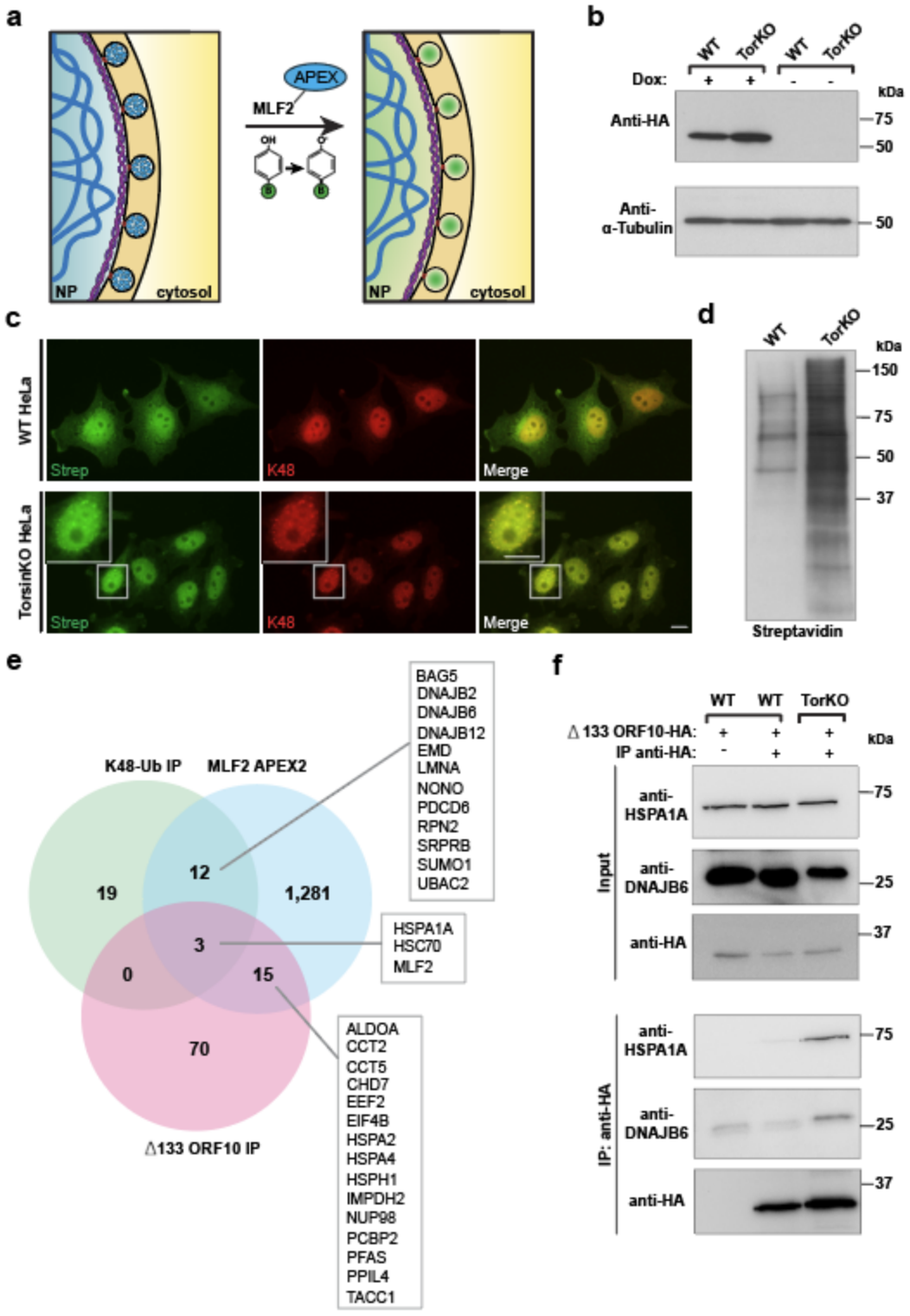

Figure 2. A comparative proteomics approach reveals NE blebs in Torsin-deficient cells are enriched for a highly specific chaperone network. a, A schematic illustration of the

APEX2 reaction strategy to identify bleb protein contents. Left panel, the MLF2- APEX2-HA fusion protein (blue) localizes within the bleb lumen. Right panel, after incubation with 500 μM of biotin-phenol, cells were treated with 1 mM H_2O_2. Upon exposure to H_2O_2, APEX2 oxidizes biotin phenol to form highly reactive biotin radicals that covalently label protein within a ~20 nm radius (ref. [74]) (green cloud). NP, nucleoplasm. **b**, The expression of MLF2-APEX2-HA was engineered in WT and TorsinKO cells to be under doxycycline (Dox) induction. Cells were treated with Dox for 24 hours before immunoblotting. **c**, Representative IF images of WT and TorsinKO cells after the APEX2 reaction. Note the enrichment of biotin conjugates in blebs of TorsinKO cells compared to the diffuse nuclear signal in WT cells. Strep (green) indicates fluorescently conjugated streptavidin signal and K48-Ub (red) indicate NE blebs. Scale bar, 10 μm. **d**, Immunoblot of biochemically enriched NE fractions from WT and TorsinKO cells after the MLF2- APEX2 reaction as described in (**c**). **e**, Candidate proteins potentially enriched in blebs were identified by mass spectrometry (MS). These were defined as proteins with spectral counts ≥1.5-fold enriched in APEX2 reactions carried out in TorsinKO cells compared to WT. The number of candidates identified for each of the three MS datasets are displayed as numbers within the Venn diagram. Hits overlapping between datasets are listed in alphabetical order. See Supplemental Tables 1,2 for complete datasets. **f**, To validate MS findings, the stable interaction between Δ133 ORF10-HA and HSPA1A or DNAJB6 was interrogated by co-IP. These interactions are unique to TorsinKO cells, consistent with the findings by comparative MS in panel (**e**). Unprocessed blots are available in source data.

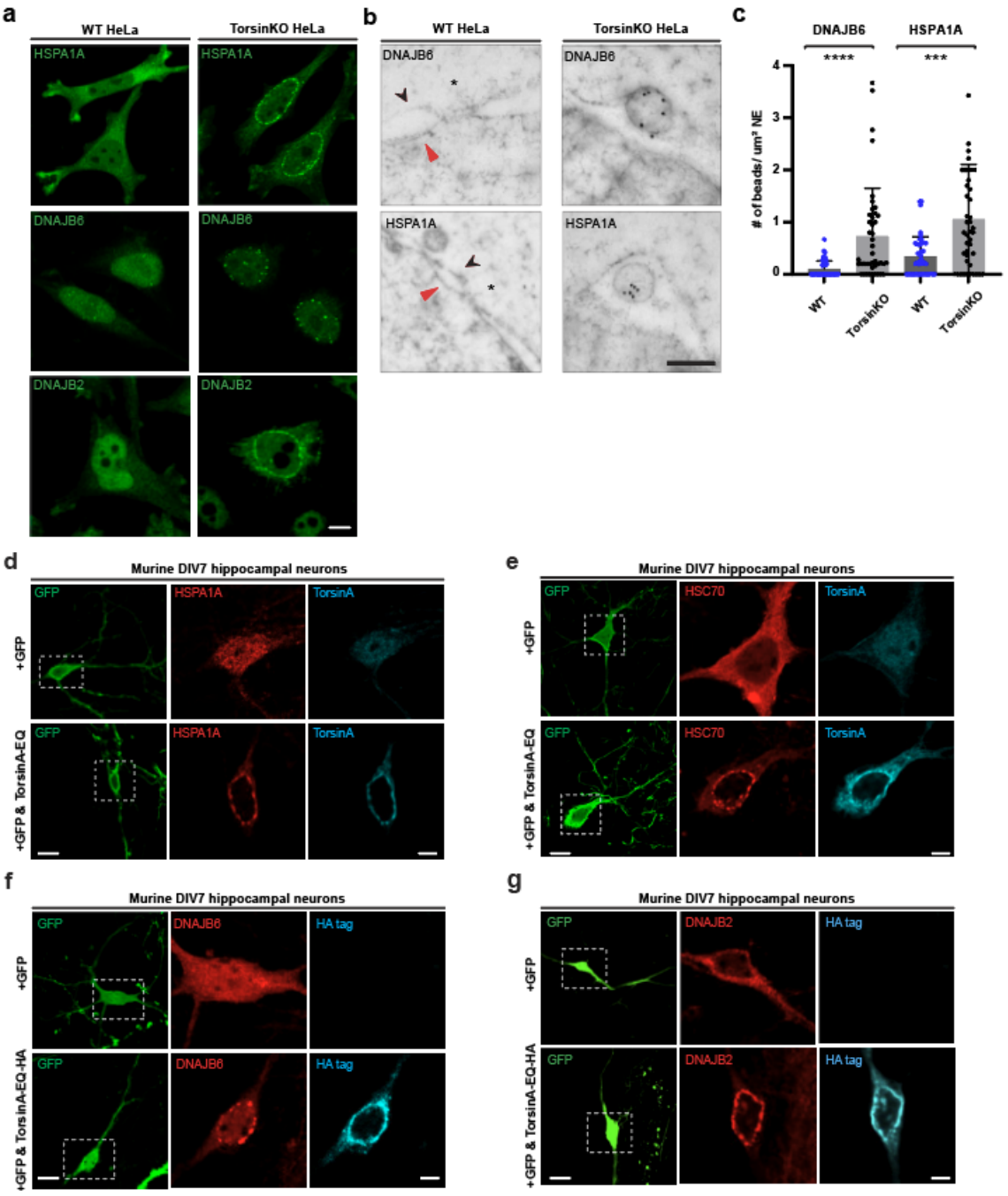

Figure 3. Highly abundant molecular chaperones are sequestered into NE blebs of tissue culture cells and primary mouse neurons with compromised TorsinA function. a, Antibodies against endogenous HSPA1A, DNAJB6, and DNAJB2 (green) reveal that chaperones from the HSP70 and HSP40 families become tightly sequestered into NE blebs upon Torsin deficiency. Scale bar, 5 μm. **b**, EM ultrastructure of the NE from WT or TorsinKO

cells labeled with immunogold beads conjugated to anti-DNAJB6 (top) or anti-HSPA1A (bottom). Black arrowhead, outer nuclear membrane. Red arrowhead, inner nuclear membrane. Asterisk, NPC. Scale bar, 250 nm. **c**, The number of DNAJB6 or HSPA1A immunogold beads per μm^2 centered around the NE (DNAJB6, WT n=50 micrographs, TorsinKO n=43 micrographs. HSPA1A, WT n=45 micrographs, TorsinKO n=43 micrographs. 400 μm^2 of NE was quantified/condition). Error bars, SD. Statistical analyses were performed using a two-tailed unpaired Mann-Whitney test where **** indicates $p < 0.0001$ and *** $p = 0.0002$. **d-g**, Murine DIV4 hippocampal neurons were transfected with GFP and empty vector (top row of all panels) or a dominant-negative TorsinA-EQ construct (bottom row of all panels). Constructs were allowed to express for 72 hours before processing the DIV7 cultures for IF. GFP expression was used to distinguish neurons from other cell types in the heterogeneous primary cell culture. Localization of the chaperones shown in panels (**d-g**) was probed using antibodies against the indicated endogenous chaperone (red). Untagged TorsinA-EQ was transfected in panels (**d**) and (**e**) and detected with a TorsinA antibody (cyan). TorsinA-EQ-HA was transfected in panels (**f**) and (**g**) and detected with an anti-HA antibody (cyan). Scale bar, 20 μm for unmagnified images, 5 μm for magnified images. Source numerical data are available in source data.

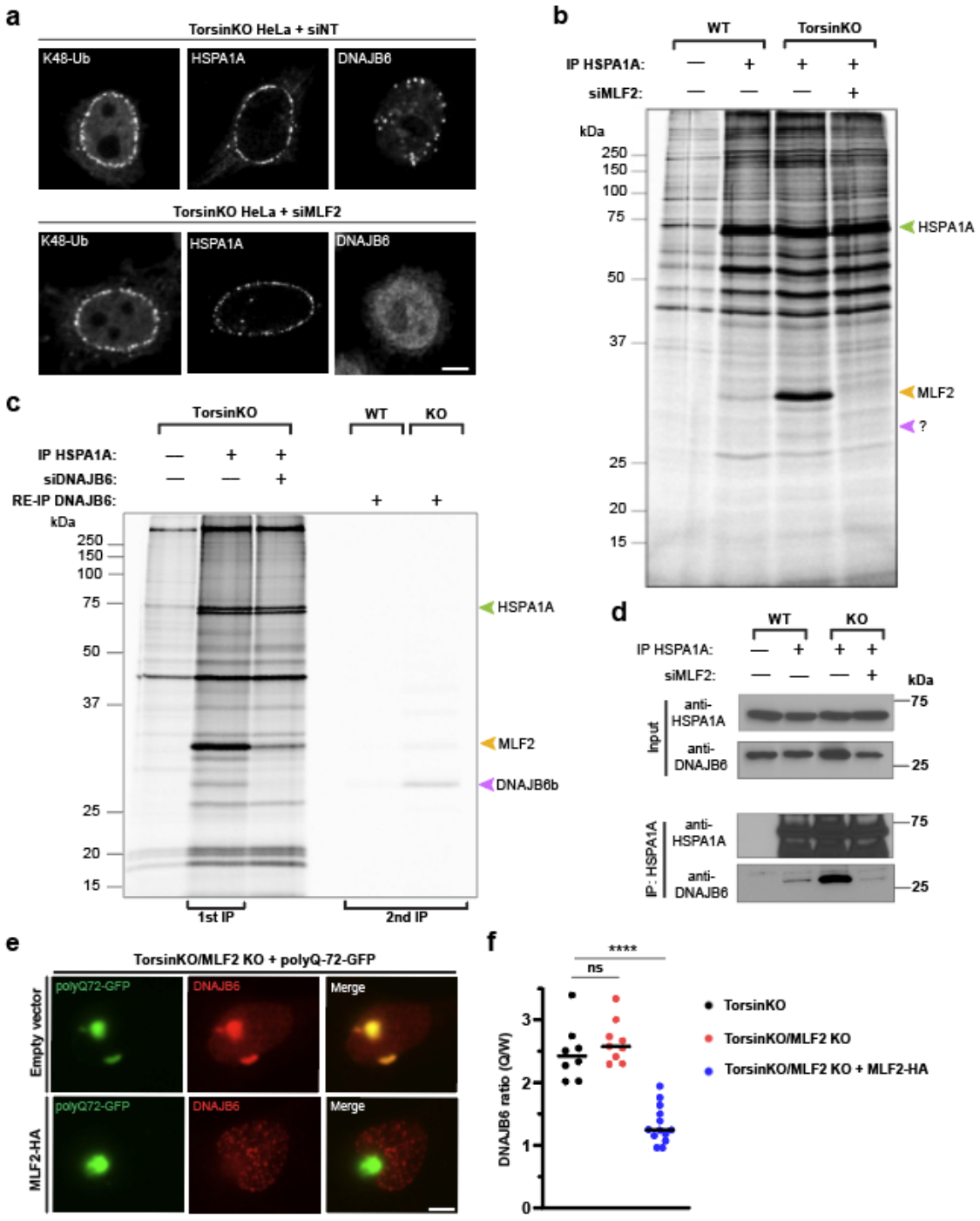

Figure 4. MLF2 is required for DNAJB6 to localize to NE blebs in Torsin-deficient cells. a, Representative IF images of chaperone localization upon knocking down MLF2 for 48 hours. Scale bar, 5 μm. **b**, WT and TorsinKO cells were metabolically labeled overnight with 150 μCi/mL ^{35}S-Cys/Met and treated with a nontargeting or MLF2-targetting siRNA for 48 hours.

HSPA1A was immunoprecipitated and stably associated proteins were detected by autoradiography. Green arrowhead, HSPA1A. Yellow arrowhead, MLF2. Purple arrowhead, unknown protein. **c**, Lanes 1-3, metabolically labeled TorsinKO cells were treated with a nontargeting or siRNA targeting DNAJB6 for 48 hours. HSPA1A was immunoprecipitated and co-eluting proteins were visualized by autoradiography. Lanes 4-5, metabolically labeled WT or TorsinKO cells under nontargeting siRNA were subjected to an HSPA1A IP, then disassociated and subjected to a second IP against DNAJB6 (RE-IP). **d**, HSPA1A was immunoprecipitated from TorsinKO and WT HeLa cells under siNT or siMLF2 conditions. **e**, A “tug of war” IF experiment showing that overexpression of MLF2-HA in TorsinKO/MLF2 KO cells titrates DNAJB6 out of polyQ72-GFP aggregates and into blebs. Representative IF images of TorsinKO/MLF2KO cells transfected with polyQ72-GFP alone (left column) or in combination with MLF2-HA (right column). Note that the HA channel is not shown. Scale bar, 5 μm. **f**, The ratio of DNAJB6 fluorescence signal inside polyQ72-GFP foci (Q) compared to whole cell (W) was calculated for at least eight cells/condition. Bars over datapoints indicate the mean ratio. Statistical analysis was performed using a two-tailed unpaired Mann-Whitney test where **** indicates $p < 0.0001$. ns, not significant. Source numerical data and unprocessed blots are available in source data.

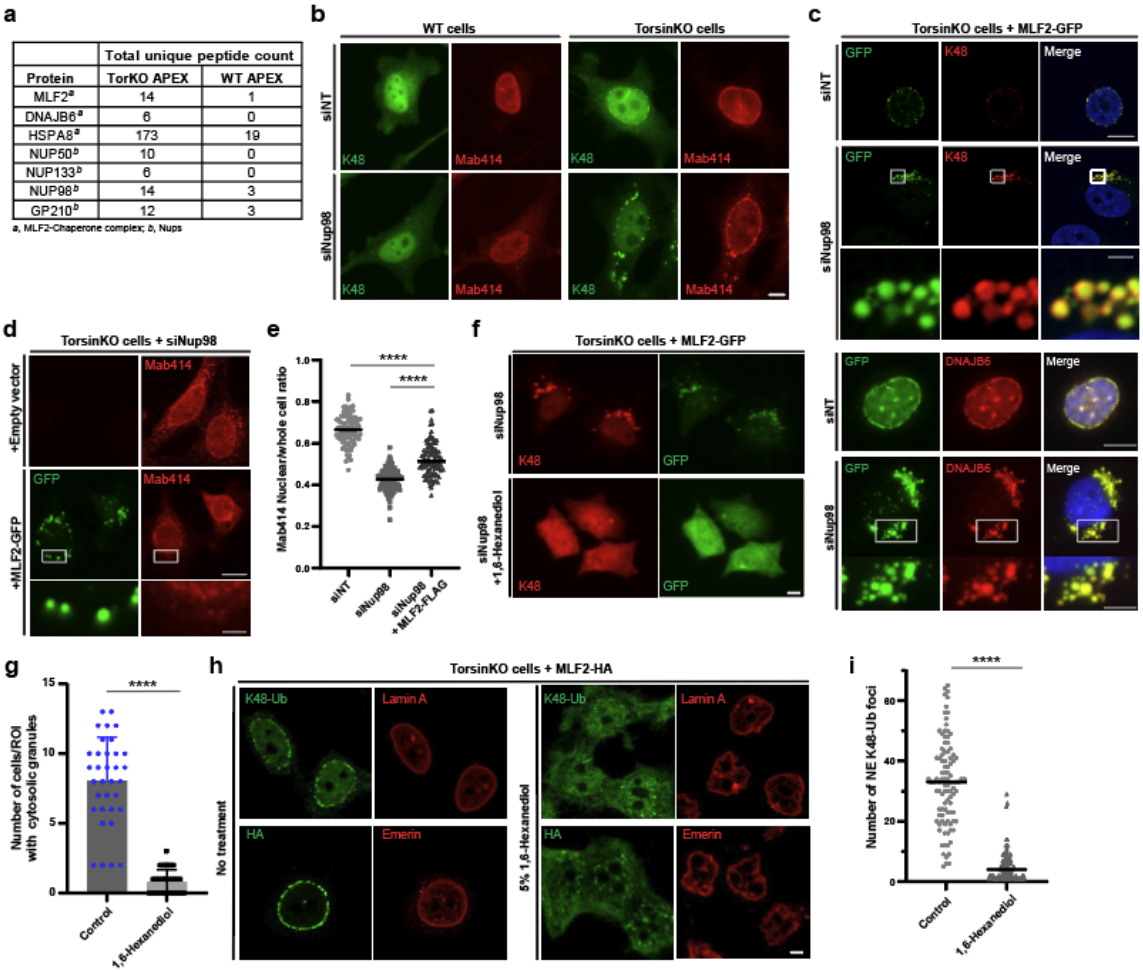

Figure 5. Nup98 is required for the sequestration into NE blebs harboring condensates composed of K48-Ub, FG-nucleoporins, MLF2, and chaperones. a, The APEX2 MS strategy described in (figure **2a**) reveals an enrichment of chaperones and nucleoporins interacting with MLF2 in TorsinKO cells. **b**, Representative IF images of WT and TorsinKO cells under siNup98 conditions. In TorsinKO cells, cytosolic granules enriched for K48-Ub and FG-Nups (Mab414, red) form upon siNup98. Note the normal NE accumulation of K48-Ub in TorsinKO cells is abolished under siNup98. Scale bar, 5 μm. **c**, Representative IF images of TorsinKO cells expressing MLF2-GFP under siNup98 conditions. MLF2-GFP (top panels) localizes to the cytosolic granules containing K48-Ub that arise upon Nup98 depletion in TorsinKO cells. DNAJB6 (bottom panels) is also recruited to the cytosolic granules. 1x images scale bar, 10 μm.

8x magnification scale bar, 1.25 μm. **d**, Representative IF images of the effect on the FG-Nup accumulation in cytosolic granules upon overexpression of MLF2-GFP under siNup98 conditions. 1x images scale bar, 10 μm. 8x magnification scale bar, 1.25 μm. **e**, The ratio of nuclear to whole cell nucleoporin (Mab414) signal was determined for 94 cells/condition. Bars over datapoints indicate the mean ratio. Expressing MLF2-FLAG significantly decreases the amount of cytosolic FG-Nup mislocalization upon siNup98. **f**, Representative IF images of TorsinKO cells expressing MLF2-GFP under siNup98 conditions in the absence or presence of 5% 1,6-hexanediol for five minutes. Scale bar, 5 μm. **g**, The presence of cytosolic K48-Ub granules upon Nup98 depletion was assessed for 300 cells/condition (≥35 regions of interest (ROI) quantified/condition). Error bar, SD. **h**, Representative IF images of TorsinKO cells expressing MLF2-HA in the absence (left columns) or presence (right columns) of 5% 1,6-hexanediol for five minutes. The intact NE is indicated by laminA (top panels) and emerin (bottom panels). Scale bar, 5 μm. **i**, The number of K48-Ub foci around the NE rim was determined for 100 cells/condition. Bars over datapoints indicate the mean number of K48-Ub foci. For all panels, statistical analyses were performed using a two-tailed unpaired Mann-Whitney test. **** indicates $p < 0.0001$. Source numerical data are available in source data.

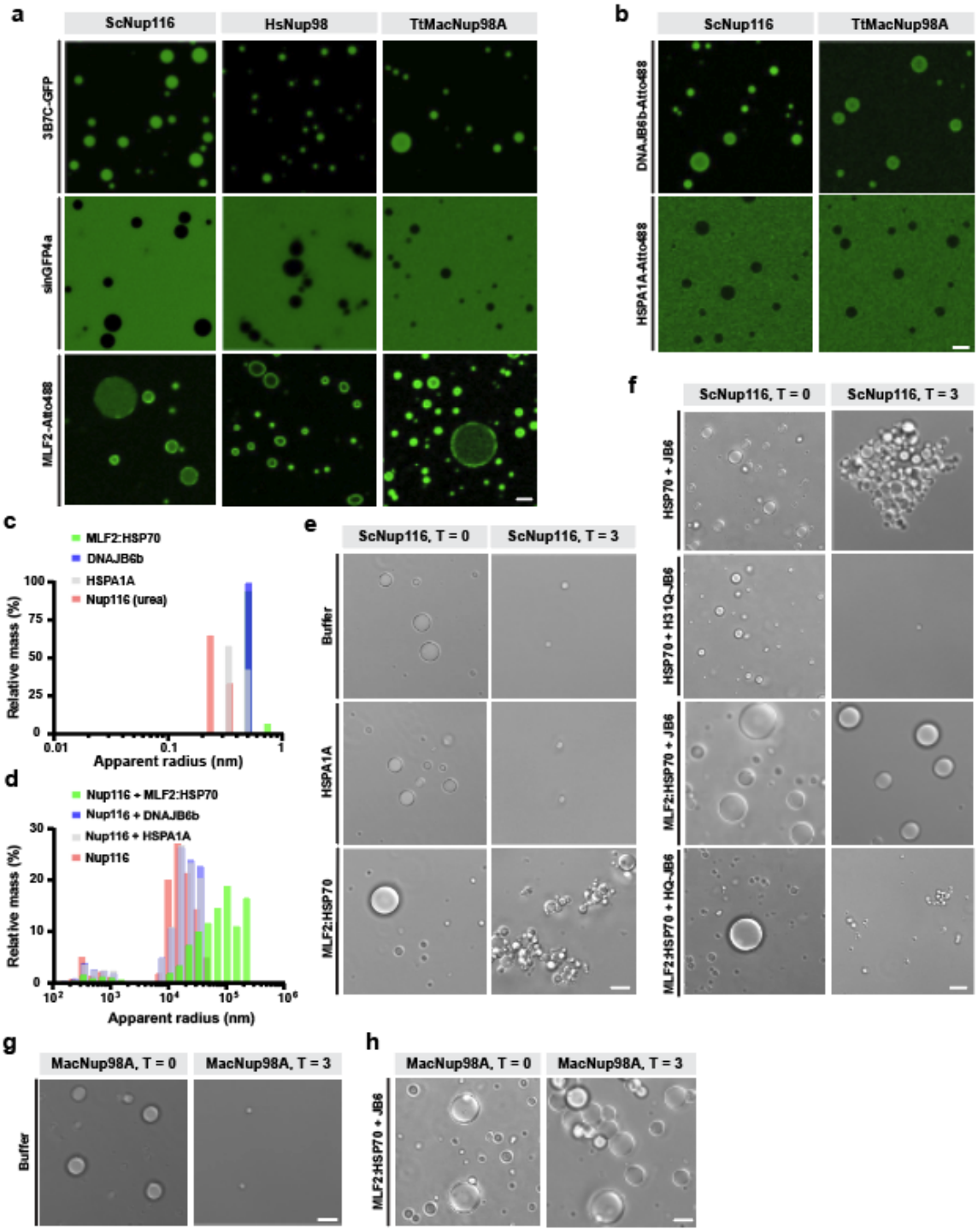

Figure 6. MLF2 interacts with FG-rich phases and preserves condensate integrity over time with HSP70 and DNAJB6. a, Atto488-tagged MLF2 interacts with phylogenetically diverse FG-Nups. Purified, label-free ScNup116, HsNup98, or TtMacNup98A FG-domains were diluted

from 500 μM stocks in 2 M urea to 10 μM in tris-buffered saline (TBS) to form condensates. Condensates were formed at room temperature in TBS containing 5 μM 3B7C-GFP, sinGFP4a, or MLF2-Atto488. **b**, HSPA1A-Atto488 is excluded from ScNup116 and TtMacNup98A condensates while DNAJB6b-Atto488 readily immerses into FG-rich phases. **c**, Solutions of 5 μM MLF2:HSP70, DNAJB6b, HSPA1A, or urea-denatured ScNup116 were analyzed by dynamic light scattering (DLS). Datasets of 100 reads with five-second acquisition times were collected for each condition. **d**, Solutions of 10 μM ScNup116 were formed in TBS with no additional protein (pink), 5 μM DNAJB6b (blue), 5 μM HSPA1A (grey), or 5 μM MLF2:HSP70 (green). Condensate size distributions were analyzed by DLS as described above. **e**, Phase contrast images of 10 μM ScNup116 condensates formed in the presence of 5 μM HSPA1A or 5 μM MLF2:HSP70. Images were taken immediately after condensates formation (T = 0) or after three hours of incubation at 30ºC (T = 3) in the presence of ATP. Note that the buffer condition is also shown in Extended Data Fig. 7a. **f**, Phase contrast images of 10 μM ScNup116 condensates formed in the presence of 5 μM HSPA1A or 5 μM of MLF2:HSP70 and 2.5 μM DNAJB6b constructs. Note the H31Q-DNAJB6b mutant cannot interact with HSP70. Images were taken at timepoints described in panel (**e**). **g**, Phase contrast images of 10 μM ThMacNup98A condensates immediately following formation or after three hours of incubation as described above. Note that the buffer condition is also shown in Extended Data Fig. 7b. **h**, Images of 10 μM ThMacNup98A condensates formed in the presence of 5 μM MLF2:HSP70 and 2.5 μM DNAJB6b at the zero timepoint or after three hours of incubation. Note that this condition is also shown in Extended Data Fig. 7c. Scale bar, 5 μm for all panels. Source numerical data are available in source data.

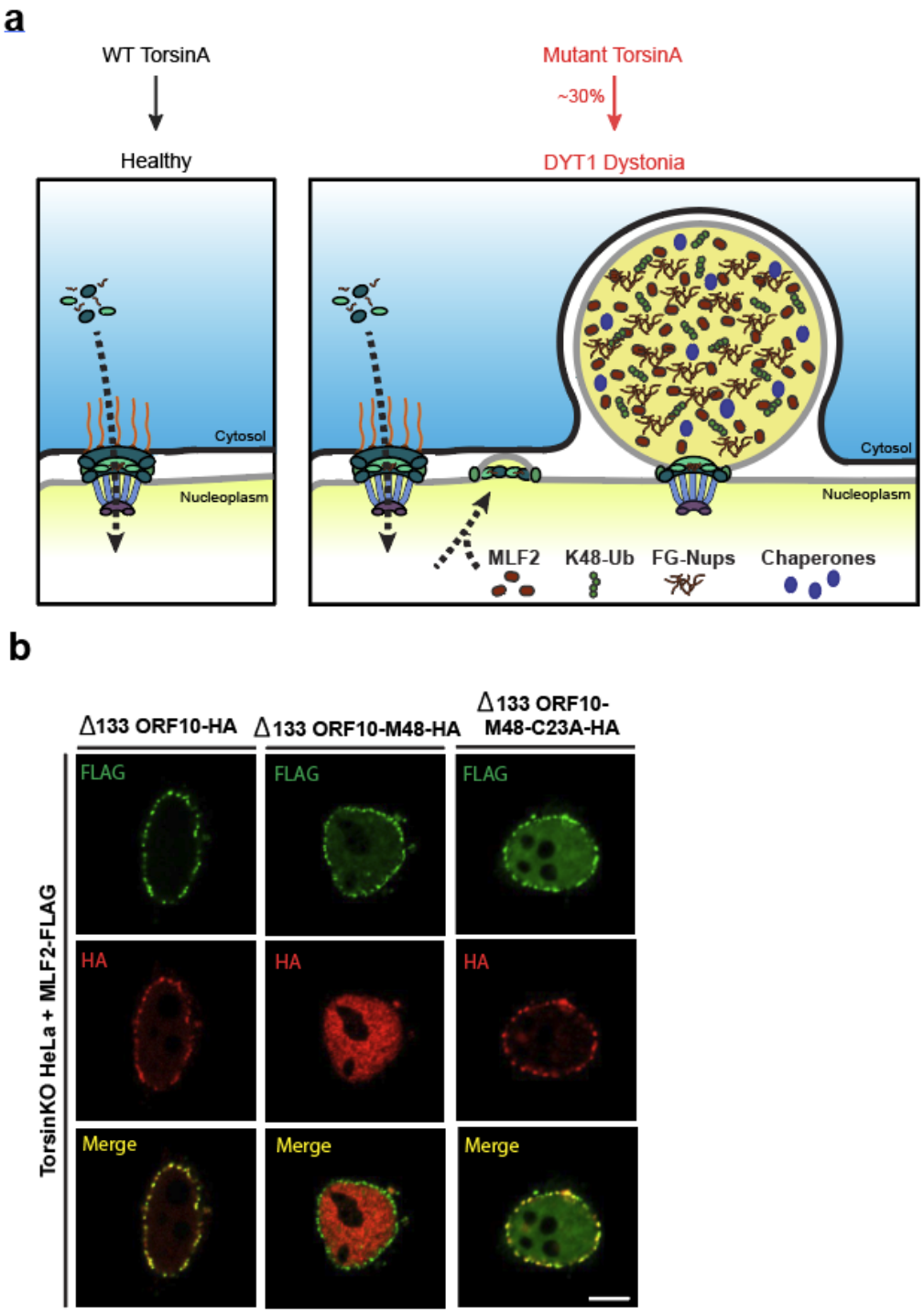

Extended data 1. NE blebs recruit Δ133 ORF10 in a ubiquitin-dependent manner. a, Schematic illustration of the NE blebs that form upon Torsin deficiency. In cells with mutant TorsinA, NPC biogenesis is compromised and a subset of nascent NPCs are arrested (ref. [22]). These arrested NPCs form blebs that are enriched for K48-linked ubiquitin (K48-Ub), FG-

nucleoporins (FG-Nups), myeloid leukemia factor 2 (MLF2), and a specific chaperone network. The inner nuclear membrane (INM) is depicted in gray, outer nuclear membrane in black. **b**, Representative IF images of TorsinKO cells expressing MLF2-FLAG and ∆133 ORF10-HA fusion constructs. ∆133 ORF10 was fused to the cytomegalovirus deubiquitinase (DUB) domain, M48 (ref. [75]). M48 is a highly active DUB domain that efficiently removes ubiquitin conjugates (ref. [22, 35]). A C23A mutation renders the DUB domain catalytically inactive (ref. [75]). Scale bar, 5 μm.

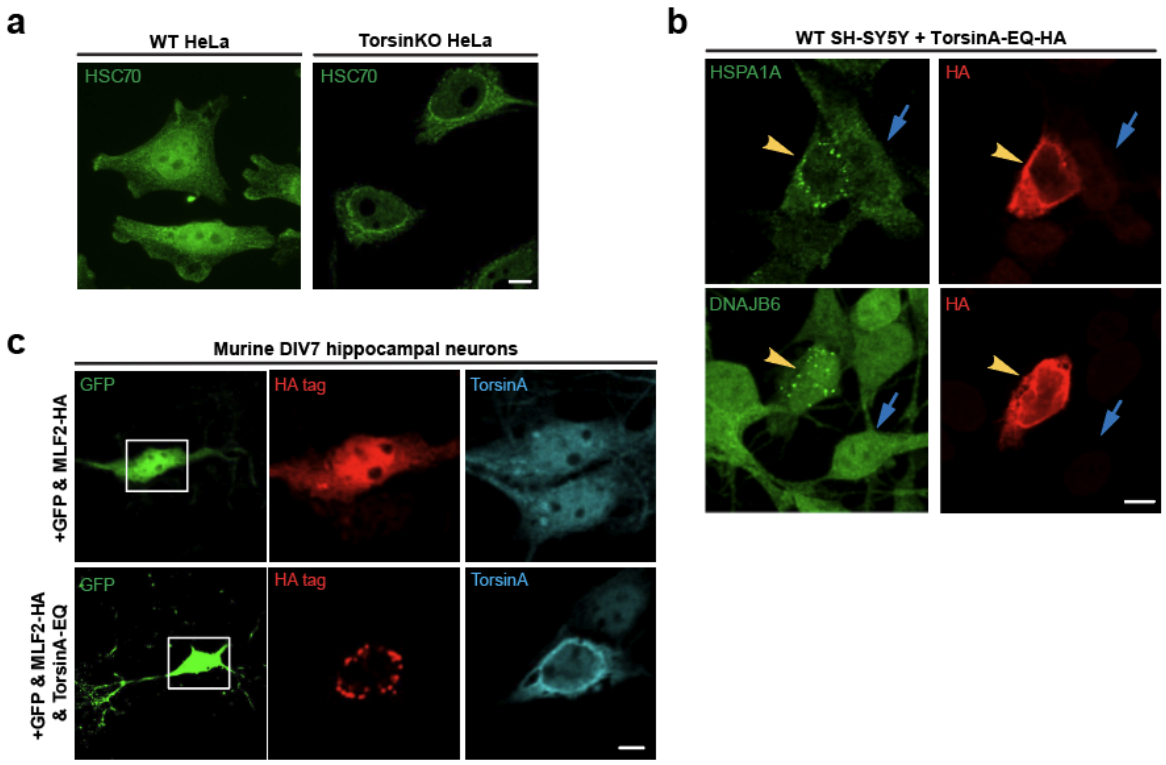

Extended data 2. Additional abundant molecular chaperones are sequestered into NE blebs of tissue culture cells and primary mouse neurons. a, Representative image of endogenous HSC70 in WT and TorsinKO HeLa cells. Note that HSC70 re-localizes from diffusely throughout the cell to nuclear rim foci in TorsinKO cells. **b**, SH-SY5Y cells expressing a dominant-negative TorsinA construct, TorsinA-EQ-HA, sequester HSPA1A and DNAJB6 into NE blebs. Yellow arrowhead, transfected cell. Blue arrow, untransfected cell. Endogenous chaperones (green) form foci around the nuclear rim upon TorsinA-EQ-HA (red) expression. **c**, Murine DIV4 hippocampal neurons were transfected with GFP and either MLF2-HA alone or in combination with a dominant-negative TorsinA-EQ construct. Constructs were allowed to express for 72 hours before processing the DIV7 cultures for IF. Note that GFP expression was used to distinguish neurons from other cell types in the heterogeneous primary cell culture. Scale bar, 5 μm.

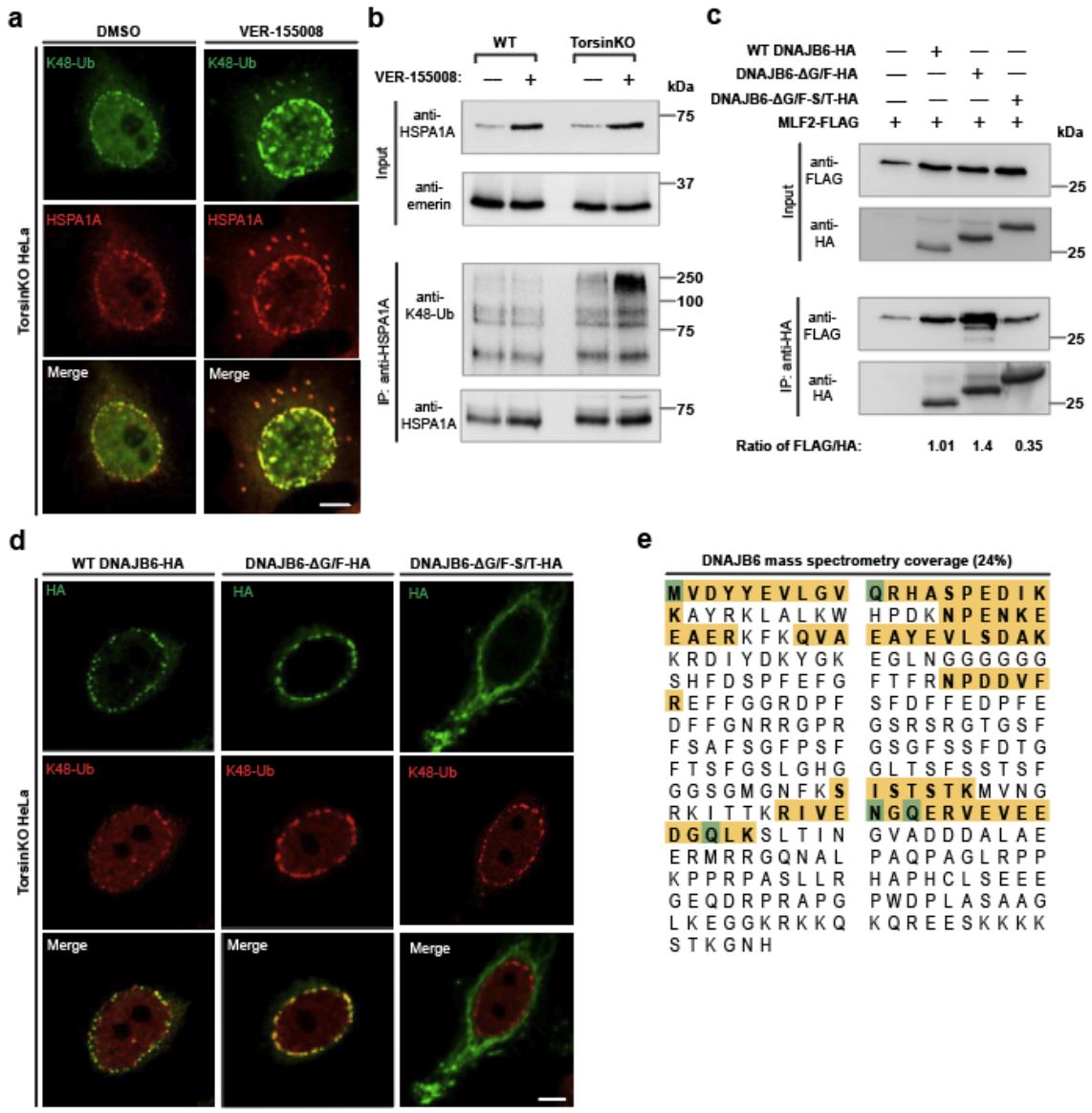

Extended data 3. Chaperones are recruited to blebs by different mechanisms. a, Representative IF images of TorsinKO cells treated with DMSO or VER-155008 for 24 hours. VER-155008 is a small molecule inhibitor of HSP70 ATPase activity, which targets the HSP70 ATP binding pocket and approximates an ADP-bound state (ref. [40]). This compound causes elevated HSPA1A expression and more K48-Ub to accumulate in blebs. Scale bar, 5 μm. **b**, An IP of HSPA1A from biochemically enriched ER/NE fractions from WT or TorsinKO cells treated with DMSO or VER-155008. **c**, A co-IP of MLF2-FLAG with HA-tagged DNAJB6 constructs lacking functional G/F-rich or S/T-rich regions in TorsinKO cells. ΔG/F indicates all

phenylalanine residues have been mutated to alanine within the G/F-rich region, and ΔG/F-S/T indicates the mutation of the phenylalanine residues within the G/F- and S/T-rich regions. Note that DNAJB6-ΔG/F-S/T-HA retrieves significantly less MLF2-FLAG, suggesting that the S/T-rich region strongly promotes its interaction with MLF2 and recruitment to blebs. **d**, Representative IF images of the DNAJB6 constructs described in panel (**c**) in TorsinKO cells. Note that interfering with the S/T-rich region, but not the G/F-rich region, prevents DNAJB6 from reaching the bleb. Scale bar, 5 μm. **e**, DNAJB6 peptides identified by mass spectrometry from an IP of HSPA1A from TorsinKO cells (see figure 4b-d). Peptides identified by mass spectrometry are highlighted in yellow and post-translationally modified residues are rendered in green. While an IP of HSPA1A from TorsinKO cells identified DNAJB6 with 24% coverage, no DNAJB6 peptides were identified in the HSPA1A IP from WT HeLa cells. See Supplemental Table 3 for complete dataset. Unprocessed blots are available in source data.

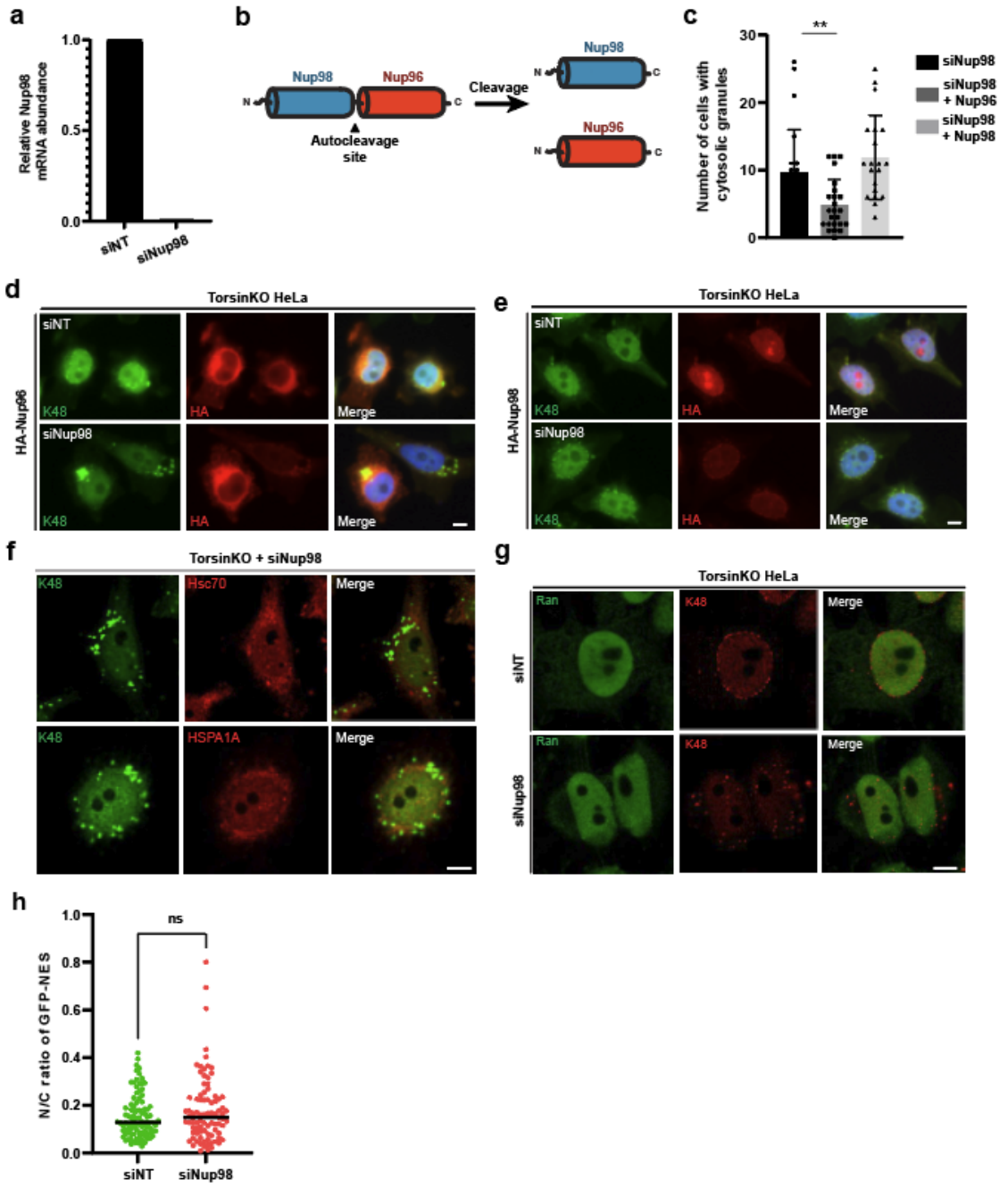

Extended data 4. Validation of Nup98 knockdown and effect on nuclear transport. a, qPCR validation of Nup98 depletion upon 48 hours of 50 nM siRNA treatment. Relative Nup98 transcript levels are normalized to RPL32. **b**, Nup98 and Nup96 are translated as a single precursor protein that undergoes an autocleavage event to produce the two individual proteins (ref. [45]). Thus, RNAi knockdown of Nup98 results in the simultaneous depletion of Nup96. **c-e**,

To distinguish which protein knockdown produces the cytosolic granules in TorsinKO cells, HA-tagged Nup98 or Nup96 was assessed for the ability to rescue the phenotype under knockdown conditions. **c**, Quantification of the rescue affect when HA-Nup96 or HA-Nup98 are expressed. The presence of cytosolic inclusions was assessed for 300 cells/condition in ≥20 ROIs. Error bar, SD. Statistical analysis was performed using a two-tailed unpaired Mann-Whitney test. ** indicates $p = 0.0013$. **d**, Representative IF images of TorsinKO cells expressing HA-Nup96 or HA-Nup98 (**e**) under nontargeting or siNup98-96 conditions. Results are quantified in panel (**c**). **f**, Representative IF images of endogenous Hsc70 and HSPA1A in TorsinKO cells upon Nup98 depletion. Note that these HSP70 members are not recruited to the cytosolic granules. **g**, Representative IF images of the Ran GTPase in TorsinKO cells under 48 hours of siNT or siNup98 conditions. **h**, The nuclear to cytoplasmic ratio was calculated for GFP-NES in TorsinKO cells under siNT (n = 94) or siNup98 (n = 87) conditions. The ratio was calculated using CellProfiler software (ref. [73]). Statistical analysis was performed using a two-tailed unpaired Mann-Whitney test. Ns, not significant. Scale bar, 5 μm for all panels. Source numerical data are available in source data.

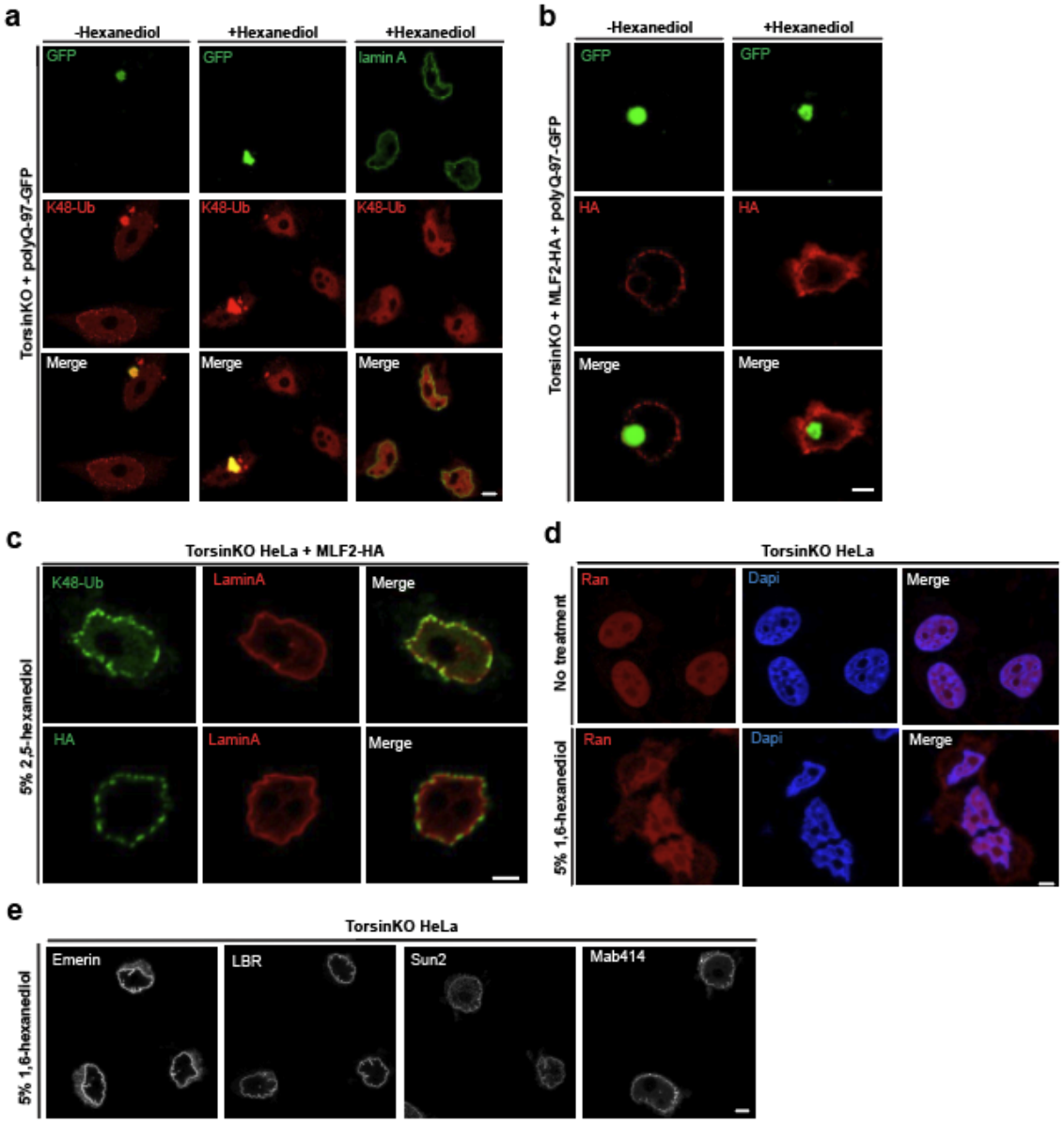

Extended data 5. The effects of 5% 1,6-hexanediol on NE integrity and bleb sensitivity to 2,5-hexanediol. **a**, Representative IF images of TorsinKO cells expressing polyQ-97-GFP under normal IF conditions or exposed to 5% 1,6-hexanediol for five minutes prior to fixation. Note that the K48-Ub inside polyQ aggregates is not dissolved by 1,6-hexanediol but the K48-Ub inside blebs is sensitive to this alcohol. Lamin A staining demonstrates this 5% 1,6-hexanediol treatment does not break down NE membranes (see also panel (**e**)). **b**, Representative IF images of TorsinKO cells expressing polyQ-97-GFP and MLF2-HA treated

with 5% 1,6-hexanediol for five minutes. A five-minute treatment with 5% 1,6-hexanediol does not dissolve polyQ aggregates but can selectively dissolve the contents of blebs. **c**, Treatment with the related alcohol 5% w/v 2,5-hexanediol for five minutes does not dissolve the K48-Ub or MLF2-HA sequestered inside blebs. **d**, Representative IF images of Ran in TorsinKO cells under normal IF conditions or after treatment with 5% 1,6-hexanediol for five minutes. Although the NE membranes are not disassembled by a 5% 1,6-hexanediol, the permeability barrier established by NPCs is lost. 1,6-hexanediol is known to disrupt the hydrophobic contacts required for the cohesion of FG-Nups within the central channel of the NPC (ref. [51]). **e**, Representative IF images of TorsinKO cells treated with 5% w/v 1,6-hexanediol for five minutes prior to fixation. This treatment does not compromise the integrity of the NE as determined by staining for multiple inner nuclear membrane proteins. Scale bar, 5 μm for all panels.

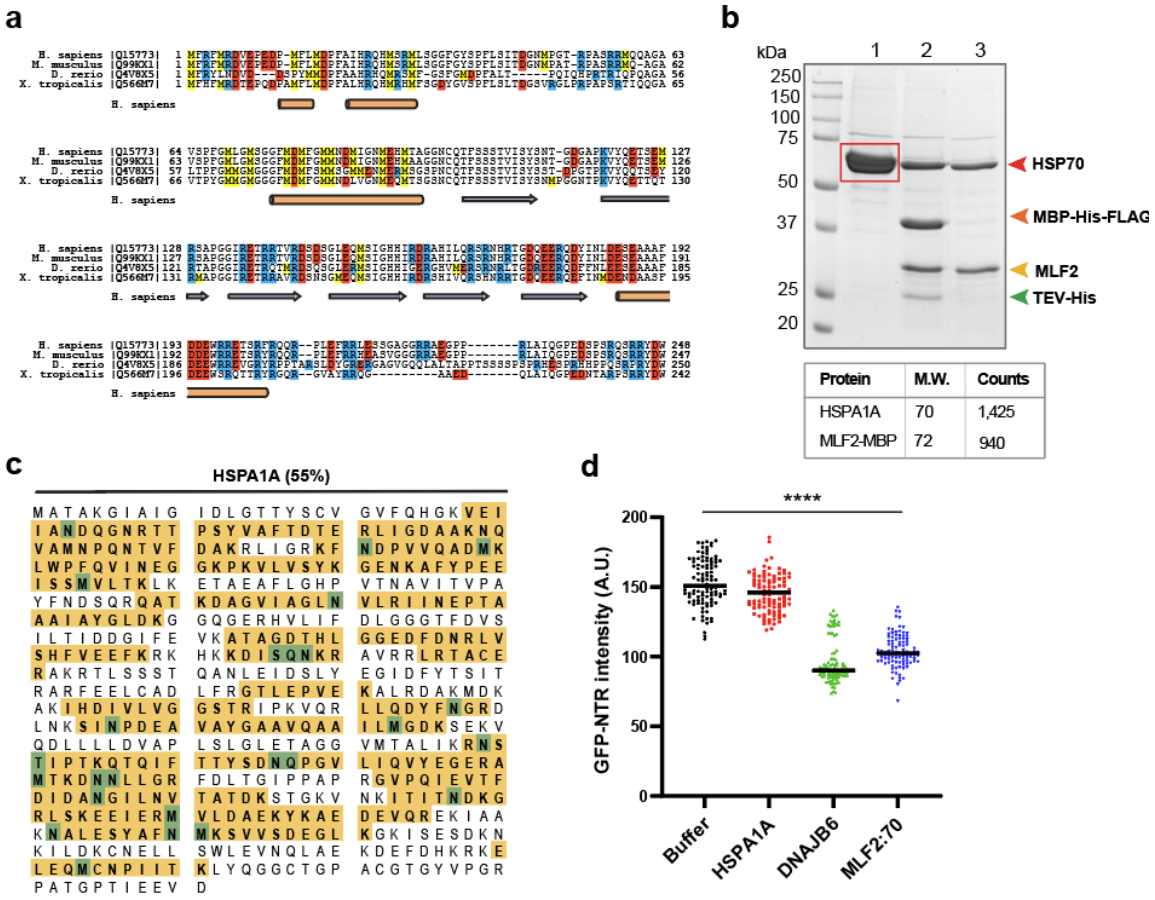

Extended data 6. MLF2 is a methionine/arginine rich protein and associates with HSPA1A. a, Multiple sequence alignment of MLF2 homologs from *Xenopus tropicalis*, *Danio rerio*, *Mus musculus*, and *Homo sapiens*. MLF2 is a methionine- and arginine-rich protein with a high degree of conservation. Methionine residues are highlighted in yellow boxes, arginine in blue, and positively charged residues in red. Orange cylinders indicate alpha helices predicted by AlphaFold [76] and blue arrows represent predicted beta sheets. **b**, MLF2 purified from Expi293F cells associates with HSPA1A. MLF2 was expressed as a maltose binding protein (MBP) fusion and affinity purified by virtue of FLAG- and His-tags. Lane 1, anti-FLAG resin elution composed of MLF2-Tev-MBP-His-FLAG and associating protein. Red box, gel section analyzed by mass spectrometry. Lane 2, incubation with Tev-His cleaved MBP-His from MLF2. Lane 3, Ni-NTA flowthrough in which MBP-His and Tev-His are removed. Mass spectrometry of the gel segment indicated in lane 1 confirmed the identity of the associating protein as HSPA1A. **c**, Mass spectrometry analysis of the co-purifying protein from panel (**b**) revealed 55% coverage of HSPA1A. Identified peptides mapping to HSPA1A are in yellow, post-translationally modified residues in green. See Supplemental Table 4 for complete dataset. **d**, 10 μM TtMacNup98A condensates were formed in the presence of 5 μM 3B7C-GFP plus 10 μM HSPA1A, DNAJB6Bb, or MLF2:HSP70. 3B7C-GFP signal intensity was measured in the center of 100 condensates/condition. Bars over datapoints indicate the mean intensity value. Statistical analysis was performed using a two-tailed unpaired Mann-Whitney test comparing buffer or HSPA1A conditions to DNAJB6b or MLF2:HSP70. **** indicates $p < 0.0001$. Source numerical data and unprocessed blots are available in source data.

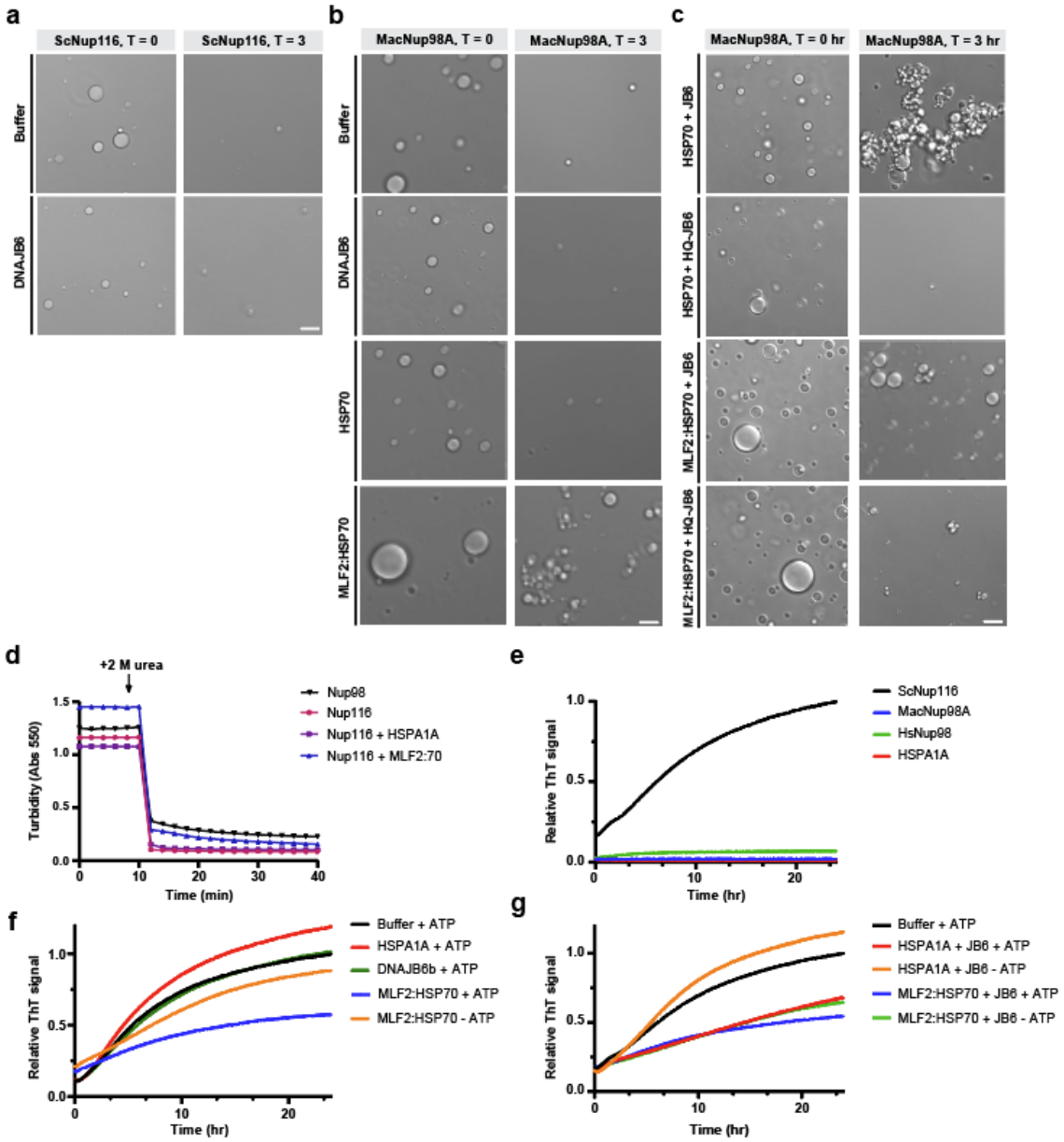

Extended data 7. MLF2 in complex with HSP70 and DNAJB6 preserves FG-rich condensate integrity over time. a, Phase contrast images of 10 μM ScNup116 condensates formed in the presence of 2.5 μM DNAJB6b. Images were taken immediately after condensate formation (T = 0) or after three hours of incubation at 30ºC (T = 3) in the presence of ATP. Note the buffer condition is also shown in Fig. 6e. **b**, Phase contrast images of 10 μM TtMacNup98A condensates formed in the presence of 2.5 μM DNAJB6b, 5 μM HSPA1A, or 5 μM MLF2:HSP70. Images were taken at the timepoints described in panel (**a**). **c**, Images of 10 μM

TtMacNup98A condensates formed in the presence of 5 μM HSPA1A plus 2.5 μM of the indicated DNAJB6b construct or 5 μM of the MLF2:HSP70 complex with 2.5 μM H31Q-DNAJB6b. Images were taken at the timepoints described in panel (**a**). Note the buffer condition is also shown in Fig. 6g. **d**, The turbidity of 10 μM ScNup116 or HsNup98 solutions in the absence or presence of 5 μM HSPA1A or the MLF2:HSP70 complex. Upon addition of 2 M urea, the condensates fully reverse and the solution loses turbidity as assessed by monitoring absorbance at 550 nm. **e**, 10 μM of ScNup116, TtMacNup98A, HsNup98, or 5 μM HSPA1A was incubated with 5 μM Thioflavin T (ThT) for 24 hours at 30ºC. ThT fluorescence (excitation 440 nm, emission 480 nm) was monitored to detect amyloid formation. All reactions contained 2 mM ATP and an ATP regenerating system. ThT signals for all conditions were normalized to the ScNup116 maximum value. **f**, 10 μM of ScNup116 was monitored for amyloid formation as described above in buffer containing 5 μM HSPA1A, 2.5 μM DNAJB6b, or 5 μM of the MLF2:HSP70 complex. Where indicated, 2 mM ATP was included or omitted. **g**, ScNup116 amyloid formation was observed under conditions with 5 μM HSP70 or the MLF2:HSP70 complex plus 2.5 μM DNAJB6b. Where indicated, 2 mM ATP was included or omitted. ThT conditions were as described for panel (**e**). Scale bar 5 μM for all panels. Source numerical data are available in source data.

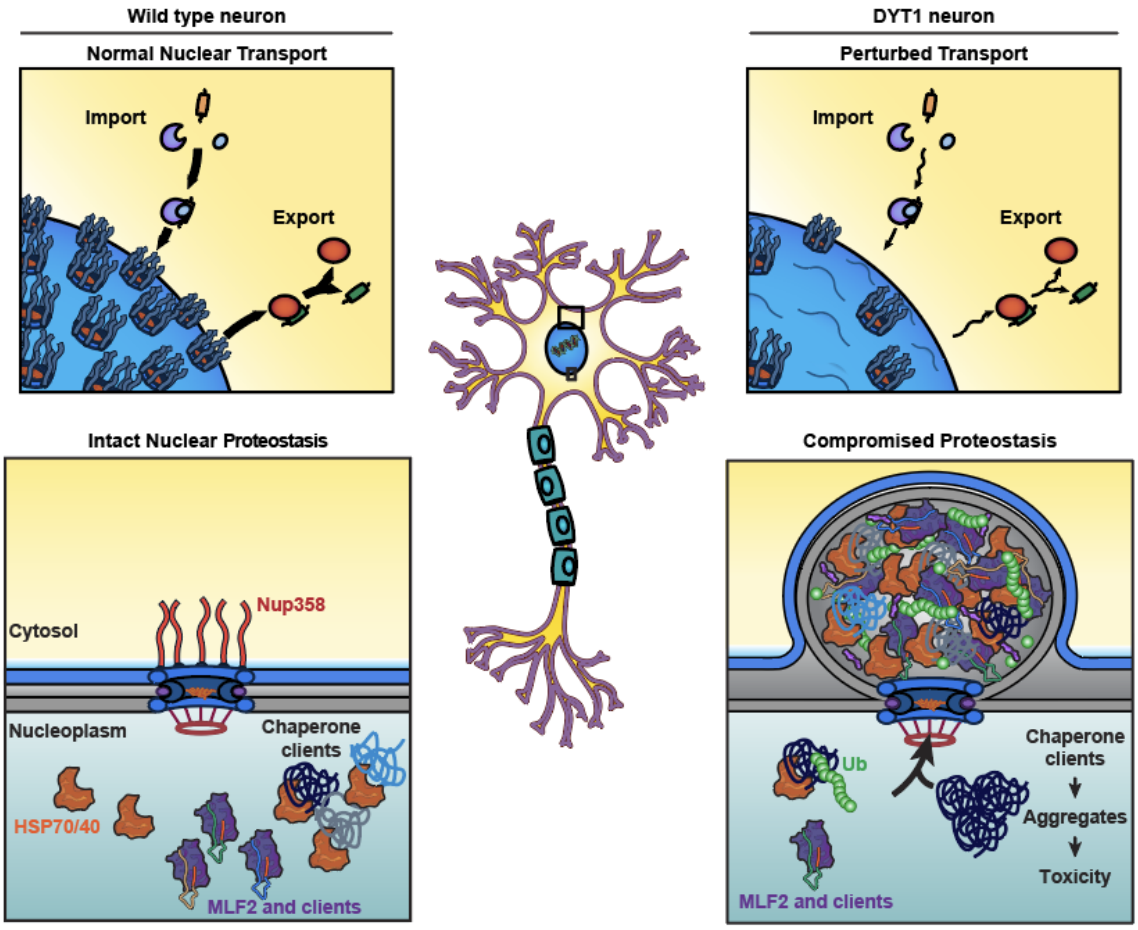

Extended data 8. A dual proteotoxicity mechanism contributes to DYT1 Dystonia onset. Schematic model for how proteotoxicity may accumulate in Torsin-deficient cells. In wild type neurons, NPC biogenesis is unperturbed and chaperones are free to interact with clients. In DYT1 dystonia neurons, nuclear transport is perturbed due to defective NPC biogenesis. As FG-Nup containing blebs form instead of mature NPCs, they sequester proteins normally destined for degradation, chaperones, and MLF2. When essential chaperones are sequestered away from clients in Torsin-deficient cells, proteotoxic species may be allowed to form and persist to a greater extent than in cells with normal chaperone availability, sensitizing cellular proteostasis towards additional insults.

References

1. Khan, Y.A., K.I. White, and A.T. Brunger, *The AAA+ superfamily: a review of the structural and mechanistic principles of these molecular machines.* Crit Rev Biochem Mol Biol, 2021: p. 1-32.

2. Rose, A.E., R.S. Brown, and C. Schlieker, *Torsins: not your typical AAA+ ATPases.* Crit Rev Biochem Mol Biol, 2015. **50**(6): p. 532-49.

3. Goodchild, R.E., C.E. Kim, and W.T. Dauer, *Loss of the dystonia-associated protein torsinA selectively disrupts the neuronal nuclear envelope.* Neuron, 2005. **48**(6): p. 923-32.

4. Zhao, C., et al., *Regulation of Torsin ATPases by LAP1 and LULL1.* Proc Natl Acad Sci U S A, 2013. **110**(17): p. E1545-54.

5. Demircioglu, F.E., et al., *Structures of TorsinA and its disease-mutant complexed with an activator reveal the molecular basis for primary dystonia.* Elife, 2016. **5**.

6. Brown, R.S., et al., *The mechanism of Torsin ATPase activation.* Proc Natl Acad Sci U S A, 2014. **111**(45): p. E4822-31.

7. Ozelius, L.J., et al., *The early-onset torsion dystonia gene (DYT1) encodes an ATP-binding protein.* Nat Genet, 1997. **17**(1): p. 40-8.

8. Fichtman, B., et al., *Combined loss of LAP1B and LAP1C results in an early onset multisystemic nuclear envelopathy.* Nat Commun, 2019. **10**(1): p. 605.

9. Rampello, A.J., S.M. Prophet, and C. Schlieker, *The Role of Torsin AAA+ Proteins in Preserving Nuclear Envelope Integrity and Safeguarding Against Disease.* Biomolecules, 2020. **10**(3).

10. Shin, J.Y. and H.J. Worman, *Molecular Pathology of Laminopathies.* Annu Rev Pathol, 2021.

11. Gonzalez-Alegre, P., *Advances in molecular and cell biology of dystonia: Focus on torsinA.* Neurobiol Dis, 2019. **127**: p. 233-241.

12. VanGompel, M.J., et al., *A novel function for the Caenorhabditis elegans torsin OOC-5 in nucleoporin localization and nuclear import.* Mol Biol Cell, 2015. **26**(9): p. 1752-63.

13. Jokhi, V., et al., *Torsin mediates primary envelopment of large ribonucleoprotein granules at the nuclear envelope.* Cell Rep, 2013. **3**(4): p. 988-95.

14. Kim, C.E., et al., *A molecular mechanism underlying the neural-specific defect in torsinA mutant mice.* Proc Natl Acad Sci U S A, 2010. **107**(21): p. 9861-6.

15. Liang, C.C., et al., *TorsinA hypofunction causes abnormal twisting movements and sensorimotor circuit neurodegeneration.* J Clin Invest, 2014. **124**(7): p. 3080-92.

16. Tanabe, L.M., C.C. Liang, and W.T. Dauer, *Neuronal Nuclear Membrane Budding Occurs during a Developmental Window Modulated by Torsin Paralogs.* Cell Rep, 2016. **16**(12): p. 3322-3333.

17. Naismith, T.V., et al., *TorsinA in the nuclear envelope.* Proc Natl Acad Sci U S A, 2004. **101**(20): p. 7612-7.

18. Laudermilch, E., et al., *Dissecting Torsin/cofactor function at the nuclear envelope: a genetic study.* Mol Biol Cell, 2016. **27**(25): p. 3964-3971.

19. Jacquemyn, J., et al., *Torsin and NEP1R1-CTDNEP1 phosphatase affect interphase nuclear pore complex insertion by lipid-dependent and lipid-independent mechanisms.* EMBO J, 2021. **40**(17): p. e106914.

20. Pappas, S.S., et al., *TorsinA dysfunction causes persistent neuronal nuclear pore defects.* Hum Mol Genet, 2018. **27**(3): p. 407-420.

21. Ding, B., et al., *Disease Modeling with Human Neurons Reveals LMNB1 Dysregulation Underlying DYT1 Dystonia.* J Neurosci, 2021. **41**(9): p. 2024-2038.

22. Rampello, A.J., et al., *Torsin ATPase deficiency leads to defects in nuclear pore biogenesis and sequestration of MLF2.* The Journal of Cell Biology, 2020. **219**(6).

23. Wente, S.R. and G. Blobel, *A temperature-sensitive NUP116 null mutant forms a nuclear envelope seal over the yeast nuclear pore complex thereby blocking nucleocytoplasmic traffic.* J Cell Biol, 1993. **123**(2): p. 275-84.

24. Zhang, W., et al., *Brr6 and Brl1 locate to nuclear pore complex assembly sites to promote their biogenesis.* J Cell Biol, 2018. **217**(3): p. 877-894.

25. Ribbeck, K. and D. Gorlich, *Kinetic analysis of translocation through nuclear pore complexes.* EMBO J, 2001. **20**(6): p. 1320-30.

26. Frey, S. and D. Gorlich, *A saturated FG-repeat hydrogel can reproduce the permeability properties of nuclear pore complexes.* Cell, 2007. **130**(3): p. 512-23.

27. Hulsmann, B.B., A.A. Labokha, and D. Gorlich, *The permeability of reconstituted nuclear pores provides direct evidence for the selective phase model.* Cell, 2012. **150**(4): p. 738-51.

28. Schmidt, H.B. and D. Gorlich, *Transport Selectivity of Nuclear Pores, Phase Separation, and Membraneless Organelles.* Trends Biochem Sci, 2016. **41**(1): p. 46-61.

29. Bonner, W.M., *Protein migration into nuclei. I. Frog oocyte nuclei in vivo accumulate microinjected histones, allow entry to small proteins, and exclude large proteins.* J Cell Biol, 1975. **64**(2): p. 421-30.

30. Gorlich, D. and U. Kutay, *Transport between the cell nucleus and the cytoplasm.* Annu Rev Cell Dev Biol, 1999. **15**: p. 607-60.

31. Labbadia, J. and R.I. Morimoto, *The biology of proteostasis in aging and disease.* Annu Rev Biochem, 2015. **84**: p. 435-64.

32. Sweeney, P., et al., *Protein misfolding in neurodegenerative diseases: implications and strategies.* Transl Neurodegener, 2017. **6**: p. 6.

33. Le Guerroue, F. and R.J. Youle, *Ubiquitin signaling in neurodegenerative diseases: an autophagy and proteasome perspective.* Cell Death Differ, 2021. **28**(2): p. 439-454.

34. Gong, D., et al., *A Herpesvirus Protein Selectively Inhibits Cellular mRNA Nuclear Export.* Cell Host Microbe, 2016. **20**(5): p. 642-653.

35. Schlieker, C., et al., *Structure of a herpesvirus-encoded cysteine protease reveals a unique class of deubiquitinating enzymes.* Mol Cell, 2007. **25**(5): p. 677-87.

36. Lam, S.S., et al., *Directed evolution of APEX2 for electron microscopy and proximity labeling.* Nat Methods, 2015. **12**(1): p. 51-4.

37. Hung, V., et al., *Spatially resolved proteomic mapping in living cells with the engineered peroxidase APEX2.* Nat Protoc, 2016. **11**(3): p. 456-75.

38. Rosenzweig, R., et al., *The Hsp70 chaperone network.* Nat Rev Mol Cell Biol, 2019. **20**(11): p. 665-680.

39. Dekker, S.L., H.H. Kampinga, and S. Bergink, *DNAJs: more than substrate delivery to HSPA.* Front Mol Biosci, 2015. **2**: p. 35.

40. Li, X., et al., *Targeting Allosteric Control Mechanisms in Heat Shock Protein 70 (Hsp70).* Curr Top Med Chem, 2016. **16**(25): p. 2729-40.

41. Thiruvalluvan, A., et al., *DNAJB6, a Key Factor in Neuronal Sensitivity to Amyloidogenesis.* Mol Cell, 2020. **78**(2): p. 346-358 e9.

42. Kakkar, V., et al., *Versatile members of the DNAJ family show Hsp70 dependent anti-aggregation activity on RING1 mutant parkin C289G.* Sci Rep, 2016. **6**: p. 34830.

43. Hageman, J., et al., *A DNAJB chaperone subfamily with HDAC-dependent activities suppresses toxic protein aggregation.* Mol Cell, 2010. **37**(3): p. 355-69.

44. Lin, D.H. and A. Hoelz, *The Structure of the Nuclear Pore Complex (An Update).* Annu Rev Biochem, 2019. **88**: p. 725-783.

45. Fontoura, B.M., G. Blobel, and M.J. Matunis, *A conserved biogenesis pathway for nucleoporins: proteolytic processing of a 186-kilodalton precursor generates Nup98 and the novel nucleoporin, Nup96.* J Cell Biol, 1999. **144**(6): p. 1097-112.

46. Ribbeck, K. and D. Gorlich, *The permeability barrier of nuclear pore complexes appears to operate via hydrophobic exclusion.* EMBO J, 2002. **21**(11): p. 2664-71.

47. Shulga, N. and D.S. Goldfarb, *Binding dynamics of structural nucleoporins govern nuclear pore complex permeability and may mediate channel gating.* Mol Cell Biol, 2003. **23**(2): p. 534-42.

48. Onischenko, E., et al., *Natively Unfolded FG Repeats Stabilize the Structure of the Nuclear Pore Complex.* Cell, 2017. **171**(4): p. 904-917 e19.

49. Lin, Y., et al., *Toxic PR Poly-Dipeptides Encoded by the C9orf72 Repeat Expansion Target LC Domain Polymers.* Cell, 2016. **167**(3): p. 789-802 e12.

50. Frey, S., et al., *Surface Properties Determining Passage Rates of Proteins through Nuclear Pores.* Cell, 2018. **174**(1): p. 202-217 e9.

51. Schmidt, H.B. and D. Gorlich, *Nup98 FG domains from diverse species spontaneously phase-separate into particles with nuclear pore-like permselectivity.* Elife, 2015. **4**.

52. Ng, S.C., T. Guttler, and D. Gorlich, *Recapitulation of selective nuclear import and export with a perfectly repeated 12mer GLFG peptide.* Nat Commun, 2021. **12**(1): p. 4047.

53. Thaller, D.J. and C. Patrick Lusk, *Fantastic nuclear envelope herniations and where to find them.* Biochem Soc Trans, 2018. **46**(4): p. 877-889.

54. Walther, T.C., et al., *RanGTP mediates nuclear pore complex assembly.* Nature, 2003. **424**(6949): p. 689-94.

55. Otsuka, S., et al., *Nuclear pore assembly proceeds by an inside-out extrusion of the nuclear envelope.* Elife, 2016. **5**.

56. Kuiper, E.F., et al., *The molecular chaperone DNAJB6 provides surveillance of FG-Nups and is required for interphase nuclear pore complex biogenesis.* Nat Cell Biol, 2022.

57. Alberti, S. and D. Dormann, *Liquid-Liquid Phase Separation in Disease.* Annu Rev Genet, 2019. **53**: p. 171-194.

58. Hofweber, M., et al., *Phase Separation of FUS Is Suppressed by Its Nuclear Import Receptor and Arginine Methylation.* Cell, 2018. **173**(3): p. 706-719 e13.

59. Guo, L., et al., *Nuclear-Import Receptors Reverse Aberrant Phase Transitions of RNA-Binding Proteins with Prion-like Domains.* Cell, 2018. **173**(3): p. 677-692 e20.

60. Tanabe, L.M., et al., *Primary dystonia: molecules and mechanisms.* Nat Rev Neurol, 2009. **5**(11): p. 598-609.

61. Li, J., et al., *TorsinB overexpression prevents abnormal twisting in DYT1 dystonia mouse models.* eLife, 2019. **9:e54285**.

62. Krobitsch, S. and S. Lindquist, *Aggregation of huntingtin in yeast varies with the length of the polyglutamine expansion and the expression of chaperone proteins.* Proc Natl Acad Sci U S A, 2000. **97**(4): p. 1589-94.

63. Pusl, T., et al., *Epidermal growth factor-mediated activation of the ETS domain transcription factor Elk-1 requires nuclear calcium.* J Biol Chem, 2002. **277**(30): p. 27517-27.

64. Ran, F.A., et al., *Genome engineering using the CRISPR-Cas9 system.* Nat. Protocols, 2013. **8**(11): p. 2281-2308.

65. Turner, E.M., et al., *The Torsin Activator LULL1 Is Required for Efficient Growth of Herpes Simplex Virus 1.* J Virol, 2015. **89**(16): p. 8444-52.

66. Ran, F.A., et al., *Genome engineering using the CRISPR-Cas9 system.* Nat Protoc, 2013. **8**(11): p. 2281-2308.

67. Zhao, C., et al., *Site-specific Proteolysis Mobilizes TorsinA from the Membrane of the Endoplasmic Reticulum (ER) in Response to ER Stress and B Cell Stimulation.* J Biol Chem, 2016. **291**(18): p. 9469-81.

68. Tsai, P.L., C. Zhao, and C. Schlieker, *Methodologies to monitor protein turnover at the inner nuclear membrane.* Methods Enzymol, 2019. **619**: p. 47-69.

69. Frey, S. and D. Gorlich, *A new set of highly efficient, tag-cleaving proteases for purifying recombinant proteins.* J Chromatogr A, 2014. **1337**: p. 95-105.

70. Mansson, C., et al., *DNAJB6 is a peptide-binding chaperone which can suppress amyloid fibrillation of polyglutamine peptides at substoichiometric molar ratios.* Cell Stress Chaperones, 2014. **19**(2): p. 227-39.

71. Pishesha, N., J.R. Ingram, and H.L. Ploegh, *Sortase A: A Model for Transpeptidation and Its Biological Applications.* Annu Rev Cell Dev Biol, 2018. **34**: p. 163-188.

72. Schindelin, J., et al., *Fiji: an open-source platform for biological-image analysis.* Nat Methods, 2012. **9**(7): p. 676-82.

73. Stirling, D.R., et al., *CellProfiler 4: improvements in speed, utility and usability.* BMC Bioinformatics, 2021. **22**(1): p. 433.

74. Rhee, H.W., et al., *Proteomic mapping of mitochondria in living cells via spatially restricted enzymatic tagging.* Science, 2013. **339**(6125): p. 1328-1331.

75. Schlieker, C., et al., *A deubiquitinating activity is conserved in the large tegument protein of the herpesviridae.* J Virol, 2005. **79**(24): p. 15582-5.

76. Varadi, M., et al., *AlphaFold Protein Structure Database: massively expanding the structural coverage of protein-sequence space with high-accuracy models.* Nucleic Acids Res, 2022. **50**(D1): p. D439-D444.